A Stochastic Study of Temporally Resolved Neuronal Growth

Matthew R. Wiens

Table of Contents

1. **Introduction**

The neuron forms the basis for the nervous system. It consists of three main components, the soma (cell body), dendrites and an axon. The dendrites are short, branching structures that receive stimuli from other neurons. Axons are much longer structures, with secondary components, which form synapses with other neurons. The neurons transmit electrical signals (action potentials), along axons and across synapses to other neurons. The mechanisms in which neurons search for and find other neurons are still not well understood, and here a framework is developed to elucidate some factors which influence growth.

The primary structure controlling the growth of the axon is the growth cone, a motile structure at the end of a growing axon. Within the growth cone, the cytoskeletal components determine the two primary regions of the growth cone. In the region near the forward edge of the growth cone, F-actin dominates as the cytoskeletal polymer. The F-actin forms long bundles which give rise to the finger-like appearance of the filopodia, and is in a loosely aggregated network in the lamellipodium between the filopodia [1]. In the axon and the inner portion of the growth cone, microtubules of tubulin, dominate the cytoskeleton. The microtubules also form stable bundles within the axon shaft. Some microtubules (dynamic microtubules), extend into the filopodia, but the majority terminate in the interior of the growth cone, forming a semicircular arc. The transition between the two regions is not discrete, but rather there is a transition zone between F-actin dominated areas and the microtubule bundles [2].

Important factors controlling growth include chemical gradients, mechanical properties, and electric forces. Chemical gradients on the surface have been the traditional way to influence neuronal growth, both through attractive (e.g. netrins) and repellant (e.g. ephrins) molecules [2]. On a larger scale, there are four major phenomena that drive directionality in neuronal growth. First, a portion of the veil between filopodia expands, and drives growth in that direction. Second, the filopodia extends in response to guidance cues, and the opposite filopodia retract, directing growth in the direction of extension. Thirdly, growing axons can branch, and if one the branches is subsequently pruned, growth is directed in the non-pruned direction. Lastly, the axon can branch, not at the growth cone, but closer to the soma, and from there, the original direction is pruned, and the new branch becomes the primary path [3].

The cytoskeletal polymers drive growth through differences in the rates of polymerization at the leading and trailing edges of each filament. One basic proposed model is like a car, where a “clutch” is engaged, and the growth cone moves forward. In all cases, actin continuously undergoes a process known as “actin treadmilling”, where F-actin is constantly polymerized at the leading edge, and depolymerized in the central region of the growth cone. In this process, the F-actin undergoes retrograde flow, so that the overall position of the polymer

stays constant. The "clutch" is engaged by anchoring the F-actin and halting the retrograde flow [4] . Microtubules also explore the growth cone, responding to signals, in particular following F-actin extension, thereby extending the axon [5].

A variety of stochastic models have been applied to axonal growth. Because of the complexity of the growth and the number of possible parameters, models may not attempt to describe all the possible factors, but rather look at the aggregate in a phenomenological approach. One such approach is modeling the growth cone as a random walker. The simplest random walk is on a 1-D lattice, where the walker moves 1 unit left or right with equal probability. Such a model leads to two important results. First, the probability of the walker being at a particular location follows as binomial distribution, which in the limit as time goes to infinity, is approximated by a normal distribution, centered at zero. Second, the mean squared displacement increases linearly with time [6]. Such models can be generalized to include non-uniform time steps, waiting times, differential weights and probabilities of each direction, higher dimensions, etc. Such changes in the model affect the resulting probability distribution and other statistical properties of the random walk. For example, in some cases the variance of the probability distribution may be infinite and the central limit theorem will not apply, leading to different predicted behavior.

Another style of model uses takes the continuous time analogue of the random walk. In such models, differential equations for the velocity typically arise, such as the Langevin equation:

$$\frac{dv}{dt} = -\gamma(v - v_s) + \eta(t), \tag{1.1}$$

where $\eta(t)$ is a stochastic random variable, which includes the randomness in the system, v_s is the stationary velocity, and γ describes the tendency for the velocity to stay constant [3]. To extend the Langevin equation to two dimensions, it can be parameterized as follows in polar coordinates:

$$\begin{aligned} \frac{dv_x}{dt} &= -\gamma v_x + \eta_v(t)Cos(\eta_\Theta(t)) \\ \frac{dv_y}{dt} &= -\gamma v_y + \eta_v(t)Sin(\eta_\Theta(t)). \end{aligned} \tag{1.2}$$

Such a model is one of a driven car, where the speed and angle are independent [7].

In such models, as those described above, a Fokker-Planck equation naturally arises. From the models, one can consider a probability distribution, $(\boldsymbol{s}, t)$, which is the probability of being in state ***s***, at a given time t. This probability distribution naturally evolves in time from some initial condition. This is easy to see in the 1-D lattice walk case, where at t=0, the probability of being at the origin is 1, and decreases to some steady-state value depending on other parameters. To describe the time evolution of the probability distribution, a Fokker-Planck equation is often used. In its most general form, the Fokker-Planck equation, given drift force ***u*** and diffusion matrix **D,** is [6]

$$\frac{\partial p}{\partial t} = -\nabla \cdot (\boldsymbol{u}\, p) + \nabla \cdot (\boldsymbol{D}\, \nabla p). \tag{1.3}$$

More specifically, in one dimension rewritten with an effective potential *U(θ)*, the Fokker-Planck equation becomes [8]:

$$\frac{\partial P(\theta,\, t)}{\partial t} = \frac{\partial}{\partial \theta}[V'(\theta) P(\theta,\, t)] + D\frac{\partial^2 P(\theta,\, t)}{\partial \theta^2}. \tag{1.4}$$

As a linear partial differential equation, the Fokker-Planck equation is analytically solvable in certain circumstances. In the above equation, the effective potential, *V*, represents extracellular forces and other deterministic mechanisms that drive neuron growth. The diffusion term, *D*, which is often taken as constant, incorporates the inherent randomness of neuronal growth. Considering the probability distribution, the potential governs how the center of the distribution changes over time, while the diffusion term describes the spread of the distribution.

Using time-lapse videos of growing neurons, the Fokker-Planck formalism is applied to neuronal growth. The speed of axonal elongation is found to have a Laplace distribution, corresponding to a V-shaped potential in velocity space, which indicates more complex process than simple diffusion. The Fokker-Planck model is also applicable to non-uniform, directional surfaces. Neurons grown on polychloro-p-xylylene (nano-PPX) have been described with a Langevin equation and associated Fokker-Planck equation, capturing the effect of seeding density on anisotropy from directional surfaces [9]. Using polydimethylsiloxane (PDMS) surfaces with slight differences in topography, the coupling between surface topography and anisotropy of growth is further explored using the Fokker-Planck formalism.

The approaches described above treat neuron growth with a phenomenological approach, but other models hypothesize an underlying mechanism which is used to create a model. Such mechanisms include tension [10], polymerization of microtubules [11], and membrane receptors

[12]. Such models treat neuronal growth as a response to other cues, to try and elucidate the effects of particular factors on the growth cone.

2. Neuronal Structure

2.1 Morphology of a Neuron

The neuron is the basic function unit of the nervous system by transmitting electrical signals through the body. The signals are propagated through a change in voltage of the cell membrane, which is then passed across the synapse between the axons and dendrites. Wiring such a system does not occur accidentally, but rather the growing neurons follow guidance cues and general instructions to form connections with other neurons.

The nervous system divides into two primary classes of cells: neurons (nerve cells) and glial cells. Of these, the neurons transmit the action potential, and are of particular interest. Neurons typically have four distinct morphological regions: the cell body (soma), dendrites, an axons, and pre-synaptic terminals. The cell body is the center of the cell, with dendrites and the axon branching off from it. The dendrites branch out in a tree-like structure, terminating in postsynaptic dendrites. Axons, which can be orders of magnitude longer than dendrites, may branch, and terminate in the presynaptic terminal, across the synaptic cleft from another neuron's dendrite. Also, the myelin sheathes the axon is not generated by the neuron, but rather by the glial cells, and myelin is not found on all axons.

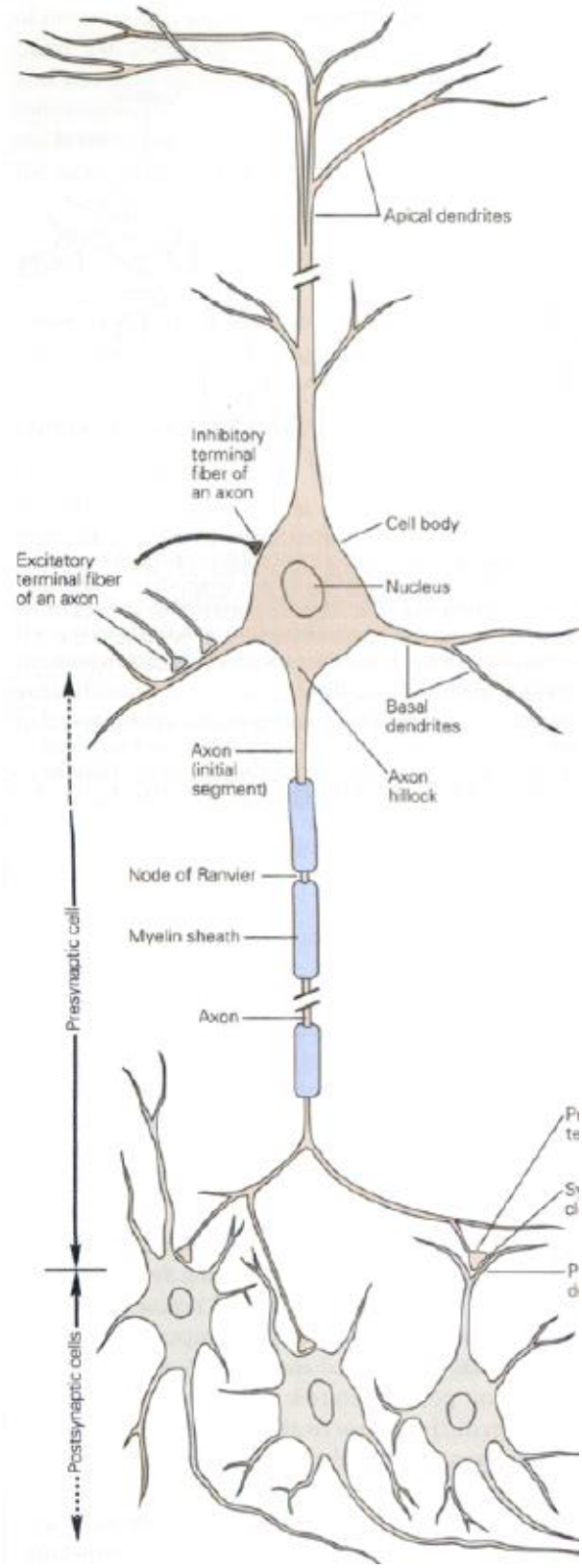

Fig 2.1 Major features of a neuron from a vertebrate [13].

Glial cells are generally seen as supporting cells, and not actively involved in the transmission of electrical signals. However they serve important functions in the overall nervous system in many ways. First, glial cells provide external structure to the brain and nervous system, and also physically divide groups of neurons. Second, two specific types of glial cells, the oligodendrocyte and the Schwann cell form myelin in the central and peripheral nervous system, respectively by wrapping the axon and improving conductivity. Third, glial cells repair damage by removing debris after injury or cell death. Fourth, they buffer K^+ ion concentration and remove transmitters from synaptic clefts. Fifth, during growth, glial cells guide the growth of axons, migration of the cell body, and the formation of the blood-brain barrier.

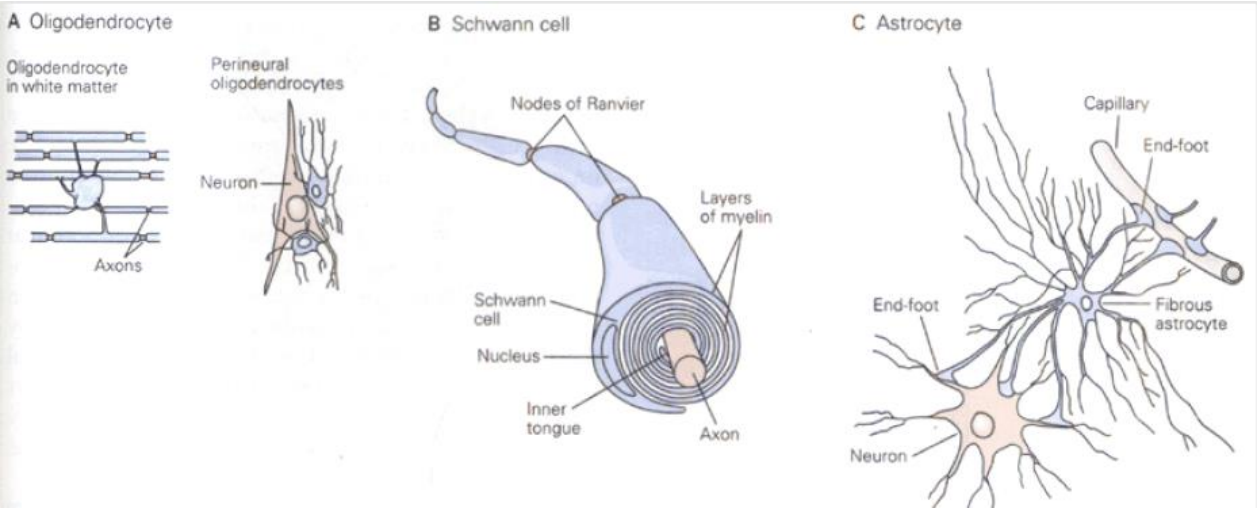

Fig 2.2 The main types of glial cells. [13]

As previously discussed, the oligodendrocytes and Schwann cells are involved in the myelination of axons. Astrocytes are the most numerous glial cell, and serve a variety of purposes. They are irregularly shaped, often in a star-like shape and may extend long projections, such as in the optic nerve.

Moving back to the neurons, one finds that the cell body in neurons is quite similar to other cell types. Like other cells, the soma contains the nucleus, which holds the DNA, and functions in the same way as in normal cells (except in some invertebrates) [14]. However, because of the neuron's specialization, the genome is regulated in a way different than other types of cells so that proteins specific to neuronal cells are expressed. The neuron is enclosed in a membrane, which is a phospholipid bilayer. The bilayer creates a barrier, preventing the inside of the cell from diffusing into the extracellular space and insulating the cell by preventing the movement of charged ions. The membrane also has various channels that mediate the movement of ions, molecules and proteins in and out of the cell. To maintain the membrane potential, neurons expend more energy than other types of cells, and therefore have an increase in the quantity of mitochondria. The neuron, like other cells, also has smooth and rough endoplasmic

reticulum, the Golgi complex, lysosomes for instance. However, neurons have a particularly dense rough endoplasmic reticulum, called the Nissl substance.

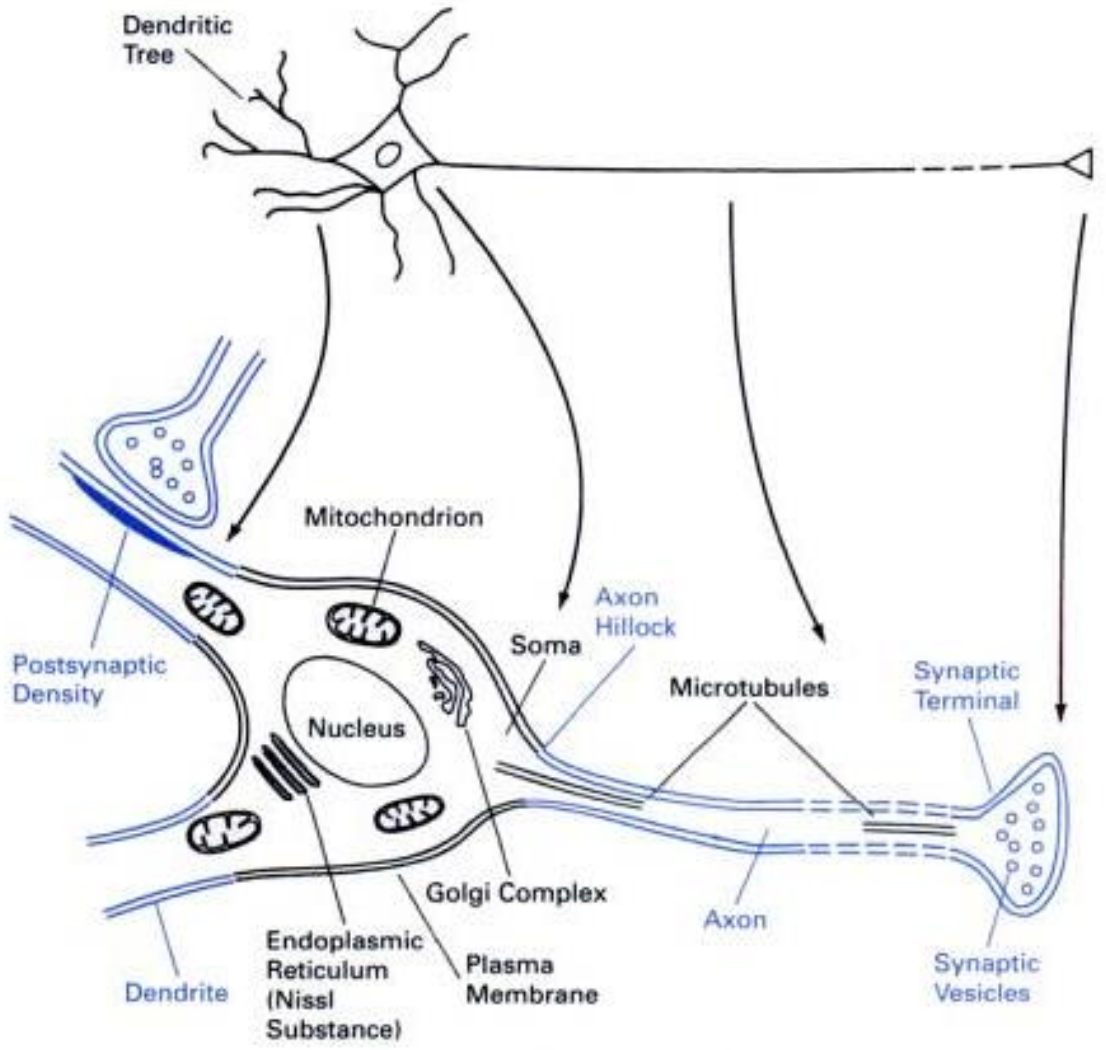

Fig 2.3 Diagram of the soma of a typical neuron [14]

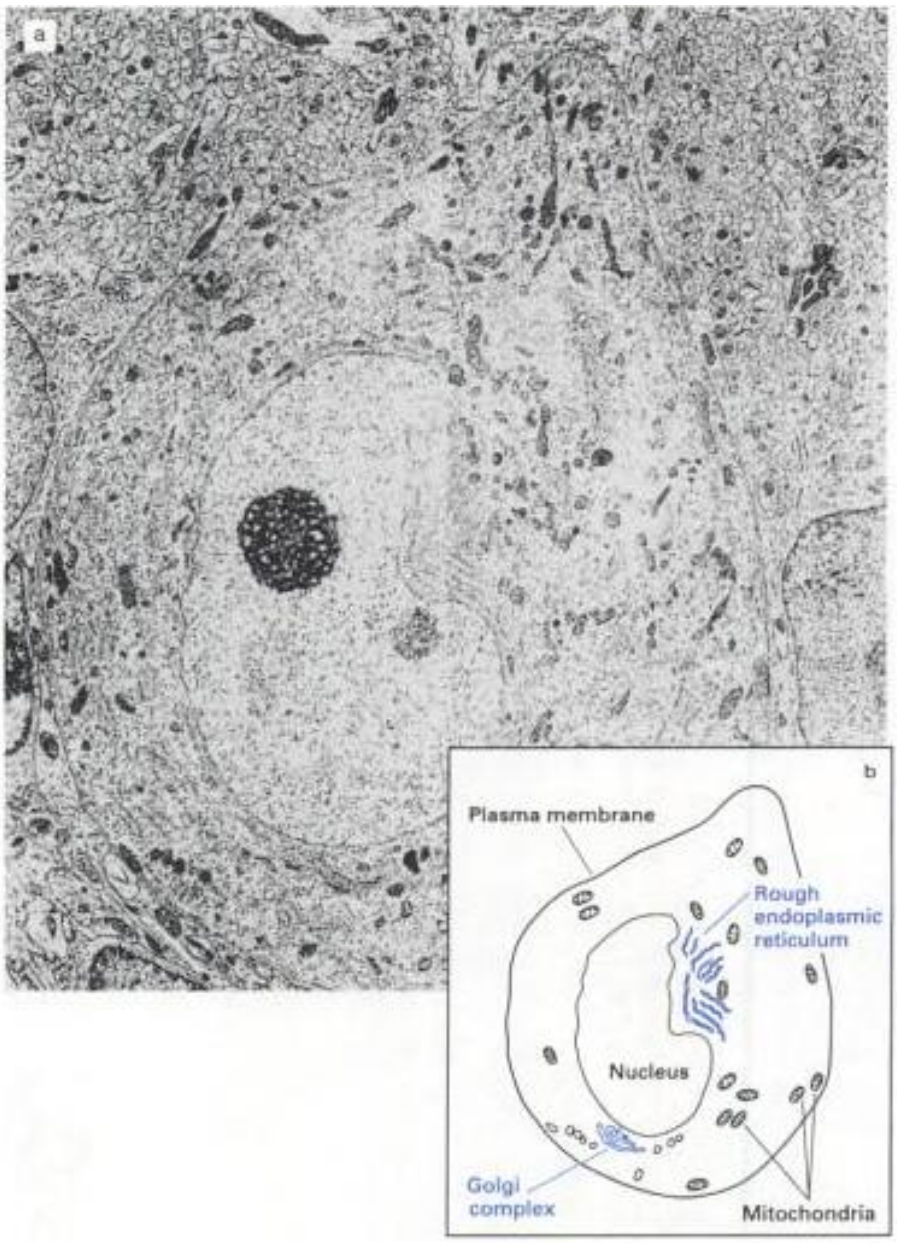

Fig 2.4 (a) Electron transmission micrograph of a cross-section of a Purkinje cell of a cerebellum, a typical neuron
(b) Schematic of the micrograph, showing visible organelles [15]

The cytoskeleton of the neuron and other complex features are also important for the functionality of the cell. The cytoskeleton, like other cells, is a heterogeneous network of microfilaments, neurofilaments and microtubules. The function of microfilaments is similar to that of muscles, as in both situations the microfilaments are composed of actin and myosin. Microtubules play an important role in cell mobility and mitosis, in addition to being the primary

component of axons and dendrites. Microtubules are polymerized from α – and β- tubulin using GTP (Guanosine Triphosphate) and promoted by microtubule-associated proteins (MAPs). MAPs are not homogenous, but generally anchor microtubules to cytoskeletal components or the cell membrane. Because the axons and dendrites are rich in microtubules, the axons and dendrites also are dense in MAPs, as shown in the figure below:

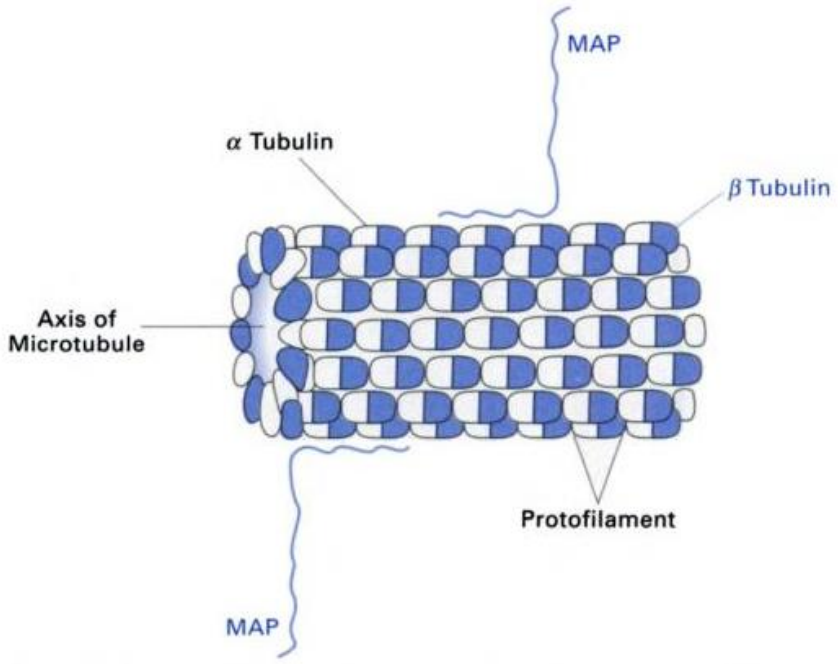

Fig 2.5 The structure of a microtubule with Tubulin and MAPs [14]

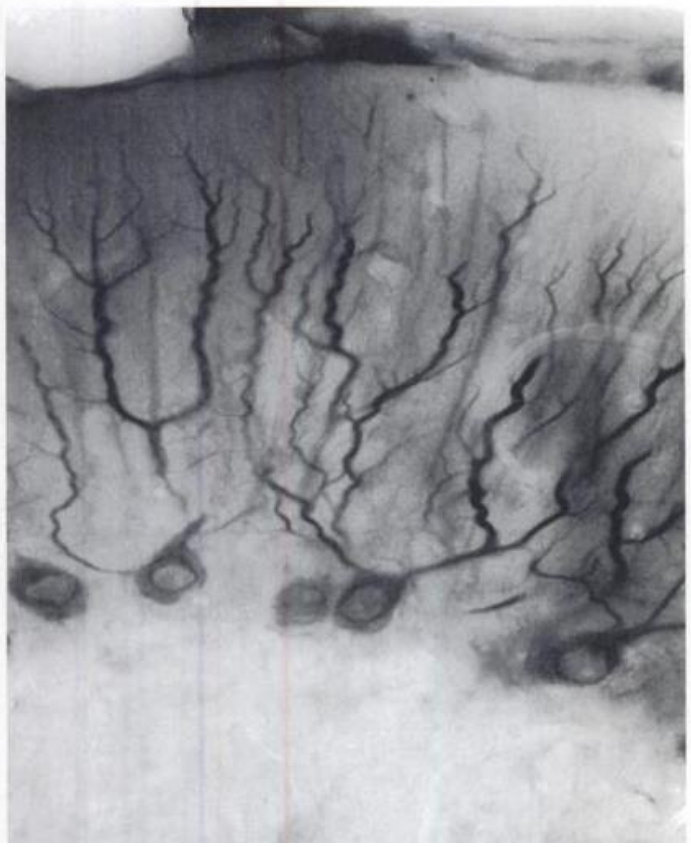

Fig 2.6 Localization of MAPs, highlighting the growing axons in Purkinje cells [14]

Another important function specific to neurons is axonal transport. Many important cell functions, such as protein synthesis, are localized to the soma. Therefore, the neuron must have mechanisms to transport proteins and other cellular components along the axon and dendrites. Based on experimental observation, transport rates along axons are not uniform; rates can vary from the order of tenths of meters per day to millimeters per day. While the mechanisms of transport are not fully understood, there are likely two primary mechanisms: transport facilitated by microtubules and transport via vesicle. For transport, molecular motors drive axonal transport and other cell movement. In many cases, myosin serves as the basis for the motors, but axonal transport is driven by kinesin. Kinesin drives motion by binding with the cytoskeleton and vesicles and hydrolyzing ATP to create relative motion [14].

2.2 Action Potential, Voltage Spikes, and the Hodgkin-Huxley Model

The structure of the neuron allows for the transmission of electric signals, the action potential, through and across neurons. The membrane and the channels in the membrane control the potential inside the axon, normally maintaining a resting potential of -60 to -70 mV, where the potential outside the cell is defined to be zero. When the potential increases towards zero, the neuron is said to be depolarized, and a decrease in potential is hyperpolarization of the

neuron. When the neuron reaches a critical threshold of depolarization, the neuron fires and briefly has a positive potential before returning to the resting state.

The potential is generated by several types of ions, primarily Na^+, Cl^-, and K^+. Each ion has an associated potential, and the equilibrium is determined from the Nernst Equation. However, the forces on each type of ion are determined by the overall electric potential across the membrane and the concentration gradient for the particular ion. For example, in the case of Na^+ and K^+, imagine that the neuron is in equilibrium. Then for sodium ions, there is a resting membrane potential of -75mV, so sodium will move to depolarize the cell. However, this moves the state away from the potassium equilibrium, causing potassium ions to counteract the depolarizing effect of sodium ions. The voltage equilibrium will be maintained, but the concentrations of the ions will change. To counteract this effect, the sodium-potassium pump removes 3 Na^+ ions from the cell while bringing in 2 K^+ ions and using ATP. The sodium-potassium pump allows for the cell to maintain constant voltage.

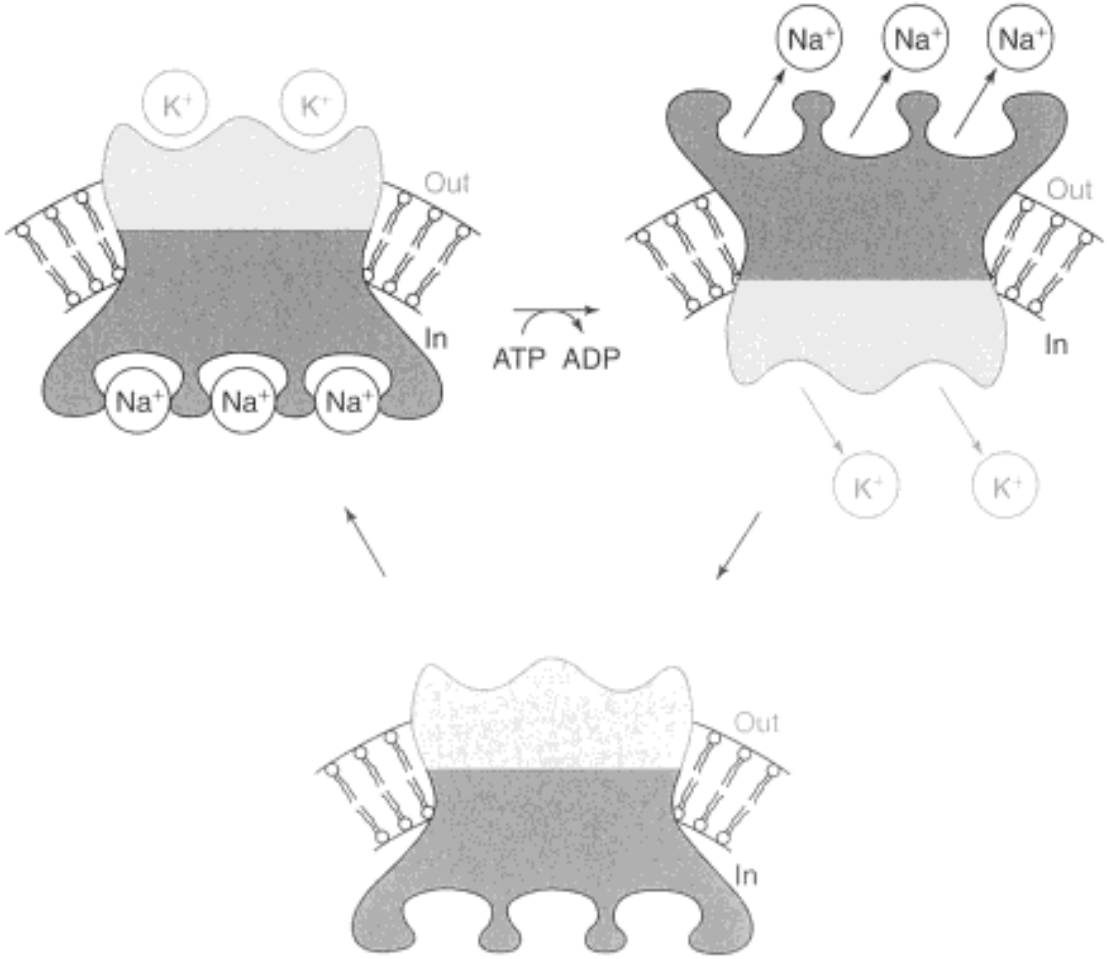

Fig 2.7 Sodium-Potassium pump, which is a protein, sodium-potassium-ATPase. The pump uses energy stored in ATP to move ions across the membrane [16]

An action potential is generated when the charge equilibrium is disturbed. When the neuron is sufficiently depolarized, the sodium channels open, allowing further sodium to enter the cell. With the positive feedback, the sodium influx is stronger than the ability of the sodium-potassium pumps to restore the concentrations, and the cell is rapidly driven to the sodium resting potential of +55 mV. However, the depolarization slowly closes the sodium channels, eventually stopping the possible rapid influx of sodium into the axon. Second, potassium channels open and positively charged potassium begins to rapidly leave the axon, and continues until the axon returns to its resting membrane potential.

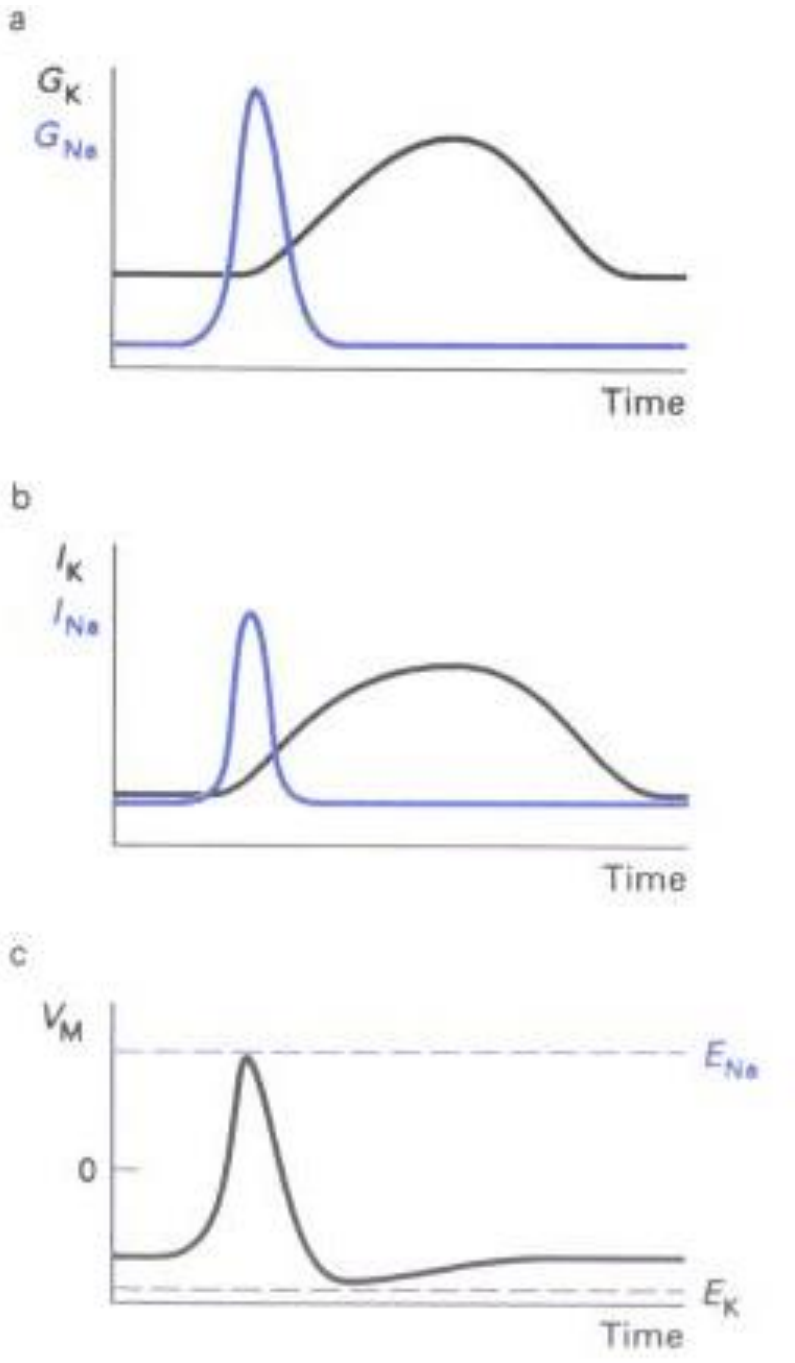

Fig 2.8 (a, b) The conductance and the current of the membrane during an action potential. (c) The membrane voltage. The membrane depolarizes during the spike, goes into a hyperpolarized state, and finally returns to the resting voltage [16]

The action potential has long been a subject of modeling. One classic model is the Hodgkin-Huxley formalism, which relates the membrane channels and the membrane voltage. The Hodgkin-Huxley model makes several simplifying assumptions; in particular, it treats the axons

as a single compartment, with the same membrane voltage everywhere. It is useful to treat the membrane as a capacitor, with channels that transmit a current (charged ions passing through the membrane), and an external current. From basic circuit properties, one derives the following equation:

$$c_m \frac{dV}{dt} = -i_m + \frac{I_e}{A} \tag{2.1}$$

In (2.1), c_m is capacitance per unit area, V the membrane voltage, i_m the current per unit area across the membrane, I_e the external current, and A the area of the membrane.

The Hodgkin-Huxley model links the membrane current to the sodium and potassium channels in the membrane. The channels are not always open, but a percent of the channels are open depending on the membrane voltage. In the Hodgkin-Huxley formalism, for a channel to be open, a number of subgates must open independently. So if there are k subgates that must open, and open with a probability n, which depends on the voltage, the probability of the channel being open is

$$P_K = n^k. \tag{2.2}$$

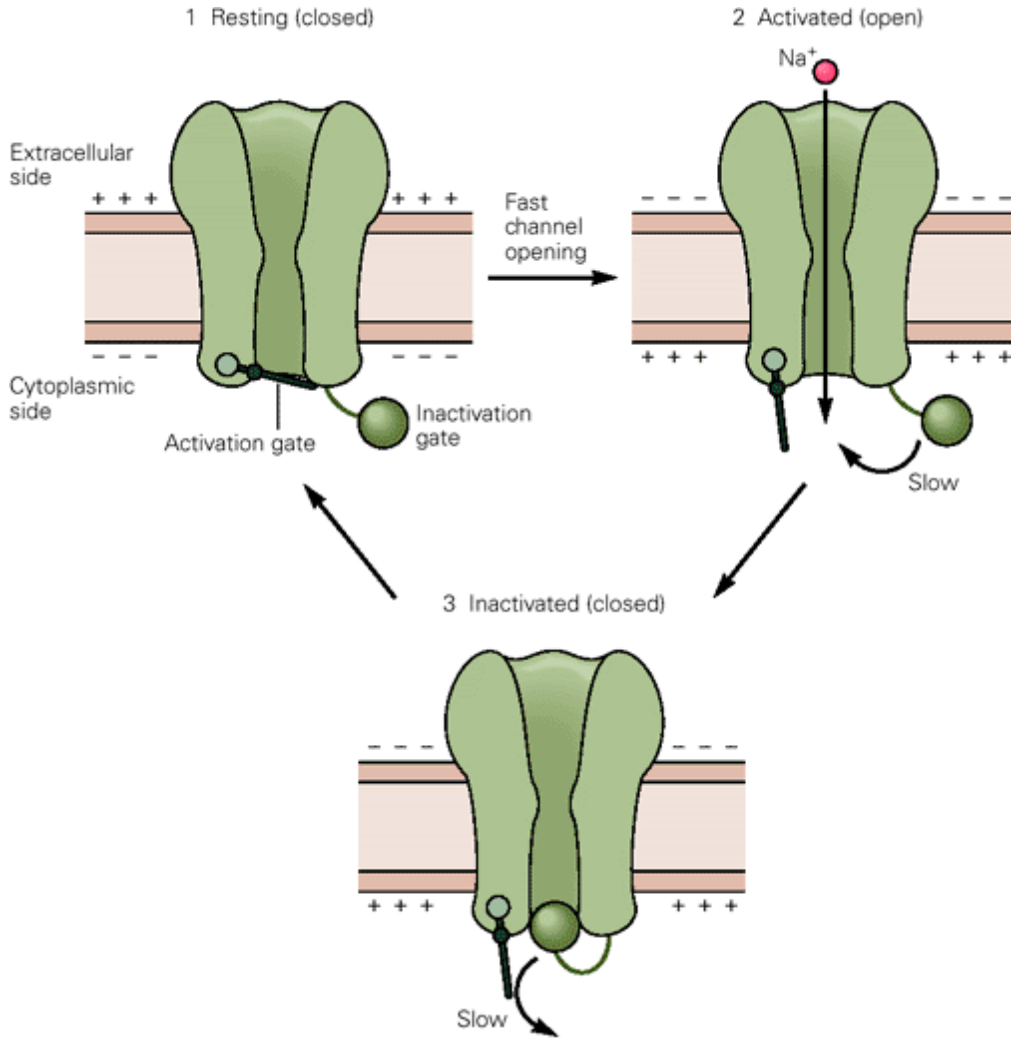

Fig 2.9 The proposed Sodium channel in the Hodgkin-Huxley model. In the resting state, the channel is closed. When the axon depolarizes, the activation gate opens, and Na^+ flows through the channel. Slightly later, the inactivation gates close, closing the channel. As the neuron repolarizes, the gates reconfigure to the resting state. [13]

The integer k, for a given channel, is chosen based on fitting the data and the structure of the channel. In Hodgkin and Huxley's time, the structure of the channel was unknown, and they chose k =4 for potassium, which turned out to match the structure of the channel. The sodium channels behave is a similar fashion, except that there are 3 gates that must be open, i.e. activation gates with probability of being open *m*, and one inactivation gate with probability of being closed of h. Collectively, n, m, and h are termed gating variables. So the probability of the channel being open is,

$$P_{Na} = m^3 h \tag{2.3}$$

The subunits open and close in a stochastic manner, with the opening and closing rates depending on the voltage, quantified with α(V) as the opening rate, and β(V) is the closing rate. If *n* is the probability of a subgate being open, and α is the transition probability of going from closed to open then the overall probability of any gate going from closed to open is $\alpha_n(V)\ (1 - n)$. Conversely, the probability of a subgate going from open to closed is $\beta_n(V)n$. Therefore, one can calculate the rate of change of the probability of a subunit being open:

$$\frac{dn}{dt} = \alpha_n(V)(1 - n) - \beta_n(V)n \tag{2.4}$$

The functional form of α and β can be determined from experiment, but a thermodynamic argument also gives an approximate expression. Each transition, α, requires some thermal energy and require the movement of charge across the membrane potential, requires an energy proportional to qV. Then, there is some probability that the energy of thermal fluctuations will be sufficient to cross the energy barrier, which is proportional to the Boltzmann factor. Combining these arguments, one gets a function for α, with constants A and B:

$$\alpha_n(V) = A \exp(-p\ B\ V/(k_B T)) \tag{2.5}$$

A similar function is expected for β, but with different constants.

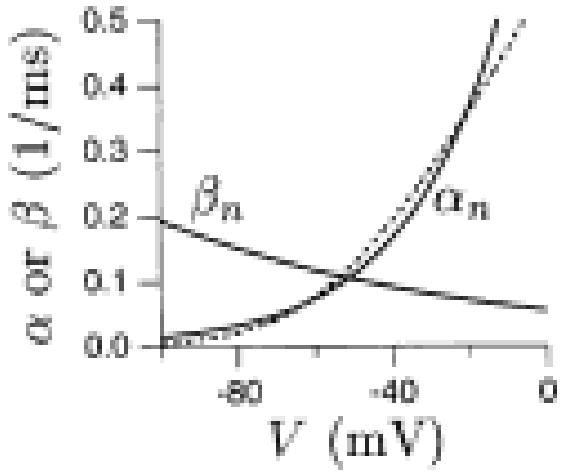

Fig 2.10 The predicted values of α and β, the transition probabilities in the Hodgkin-Huxley formalism in solid lines. The dashed line is the experimentally derived function for α. [17]

The Hodgkin-Huxley model uses the gates to model the current density across the membrane. In combination with the description of the membrane as a capacitor, the Hodgkin-Huxley model can be presented. The variables g are maximum conductance, E_i are the equilibrium voltages for each ion and a leak term, L, which encompasses other ions not specifically included in the model:

$$
\begin{aligned}
i = \ & \overline{g_L}(V - E_L) + \overline{g_K}\, n^4 (V - E_K) + \overline{g_{Na}} m^3 h\, (V - E_{Na}) \\
& c\frac{dV}{dt} = \ -i + \frac{I_e}{A} \\
& \frac{dn}{dt} = \alpha_n(V)(1 - n) - \ \beta_n(V) n \\
& \frac{dm}{dt} = \alpha_m(V)(1 - m) - \ \beta_m(V) n \\
& \frac{dh}{dt} = \alpha_h(V)(1 - h) - \ \beta_h(V) h
\end{aligned}
\tag{2.6}
$$

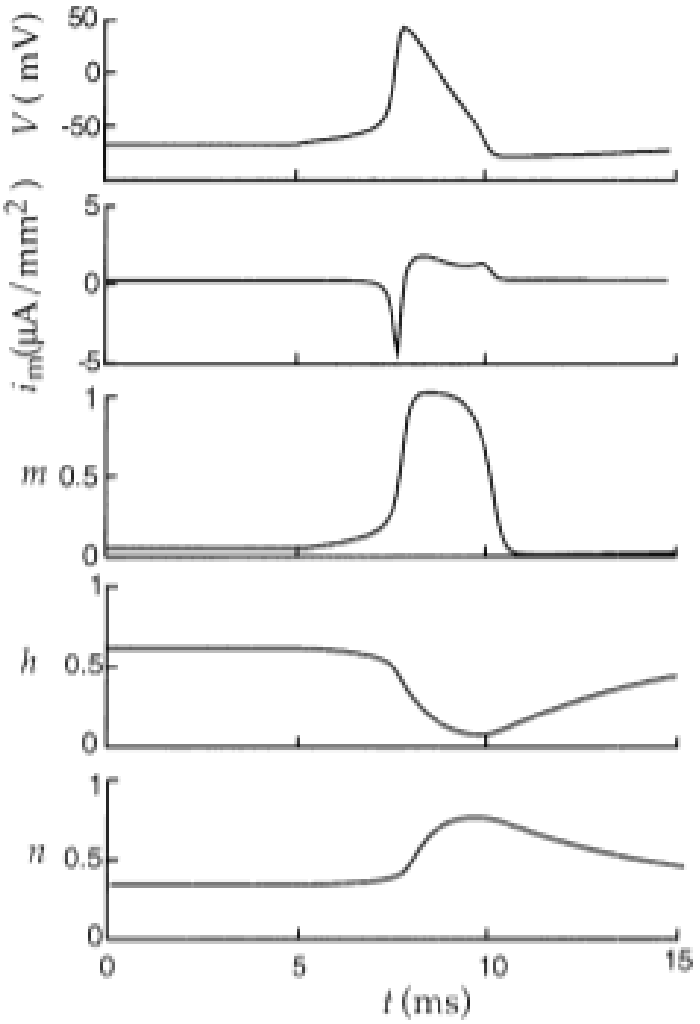

Fig 2.11 The membrane voltage, the membrane current and the gating variables during an action potential in the Hodgkin-Huxley model. [17]

Before a voltage spike, an increase in m, the sodium activation gating variable, with a moderate value for h, the sodium inactivation gating variable, causes the sodium channels to open, and a flow of sodium ions into the neuron. The flow is very rapid, in part from positive feedback, driving the membrane potential to around +50mV. As the depolarization continues, h goes towards zero, closing the sodium channels and stopping the influx of sodium. Simultaneously, the depolarization drives n towards 1, resulting in the opening of potassium channels. The outflow of potassium ions results in a hyperpolarized state, and subsequently the closing of the potassium and sodium channels, and a return to the initial state of the neuron. The Hodgkin-Huxley served as an early example of modeling the neuron, and the stochastic processes in an axon.

2.3 The Growth Cone

For the machinery of the nervous system to function, the neurons must find other neurons and form synapses. It is generally not believed that there is an intrinsic set of directions for neurons to find other neurons, but rather that the growing axons respond to sensory cues to form synapses. The growth cone, at the tip of the growing axons, responds to extracellular signals and directs the growth.

The growth cone can be divided into two major regions, based on the primary structural component. The axon itself is dominated by microtubules, which are also involved in the transport of the molecules to the growth cone. The microtubule dominated region, the C domain in the figure below, extends into the growth cone. At the leading edge of the growth cone, F-actin dominates; regions where actin is the primary structural component are called the P-domain. The P-domain is composed of two different regions. The filopodia and finger-like projections on the tip of the growth cone that explore the surface on which the axon is growing. The filopodia constantly move, including retraction into the lamellipodia and the extension of new filopodia. The C-domain and the P-domain do not have an abrupt change, but rather the area of gradual transition from actin dominance to microtubule dominance is termed the P-domain.

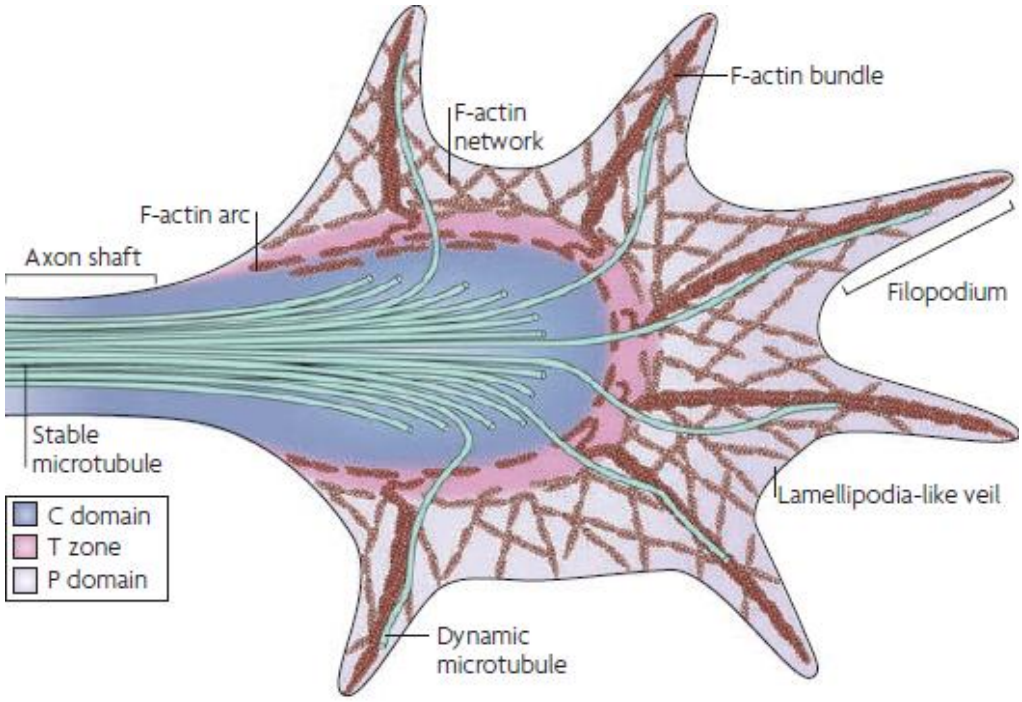

Fig 2.12 The structure of a growth cone [2]

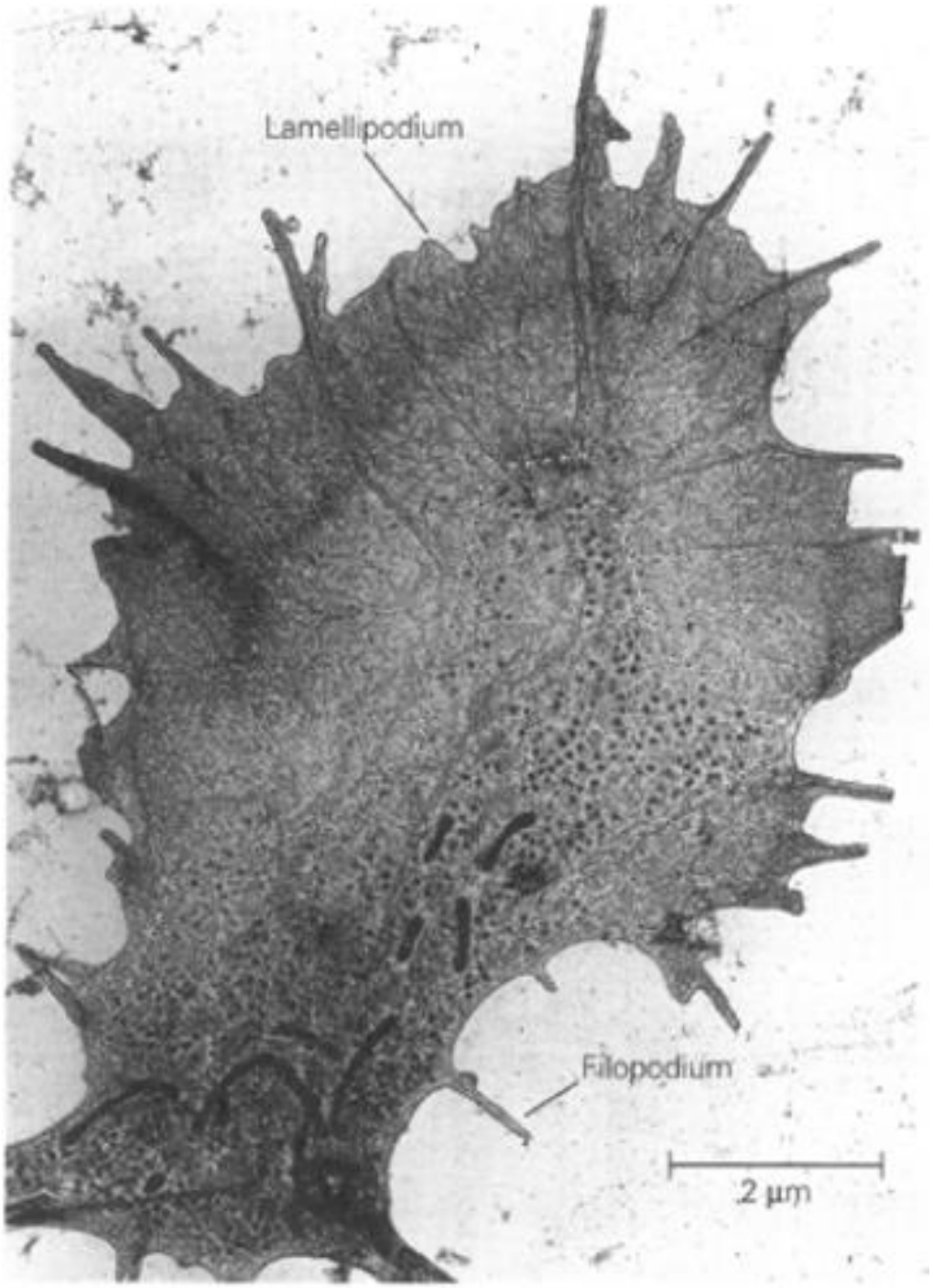

Fig 2.13 Electron Micrograph of a growth cone *in vitro*. [15]

The growth cone moves forward through a three stage process of protrusion, engorgement, and consolidation. In describing axonal growth, a motor is a useful analogy. Actin is the primary protein that drives growth, although growth is possible without actin. In a

resting state, actin in the filopodia is "treadmilling", where actin is polymerized at the tip of the growth cone, and flows back toward the axon (and soma), where it depolymerizes. Thus, the total length of the actin polymer is constant, even as the subunits are in constant motion, which is analogous to an idling engine. A current model for the growth cone protrusion is the clutch. Here, the membrane of the growth cone anchors to the substrate, which mechanically couples the receptors and the F-actin flow. As a result, retrograde flow is prevented, and the increase in actin causes protrusion of the growth cone.

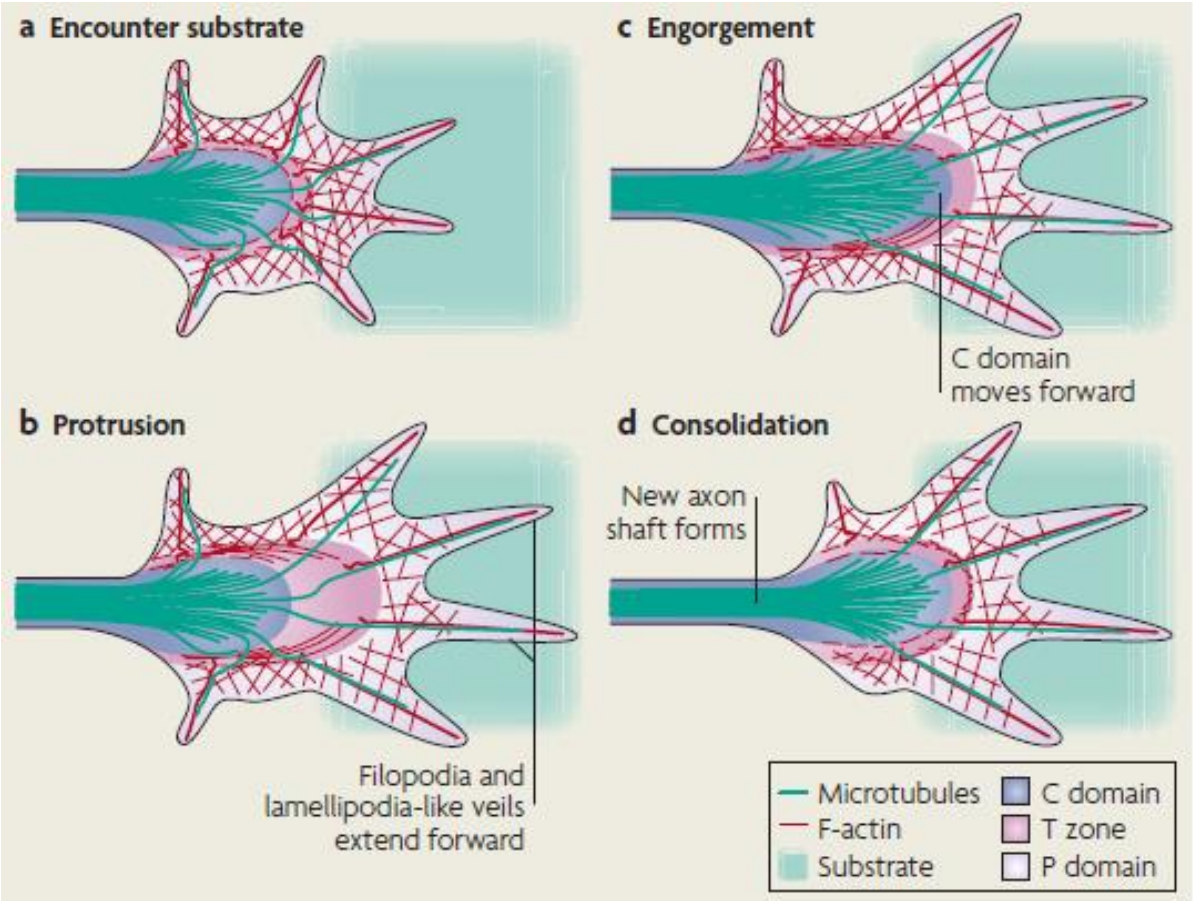

Fig 2.14 A growth cone extending after encountering a guidance cue [2]

Next, the F-actin bundles between the location of protrusion and C-domain disappear, with F-actin arcs forming a conduit between the two locations. Microtubules extend into the region, extending the C-domain, and moving the axon forward.

In addition to the forward growth of the axon, the growth cone must also steer the growing axon. Such guidance occurs through both positive cues, where protrusion on one side is increased, and negative cues which decrease protrusion. In this system, the growth cone must interpret and respond to a vast number of cues, and direct the growth as necessary. While the overall process of how the growth cone translates the guidance cues into growth is not well

understood, the effects of several molecules have been studied, including kinases, phosphates, calcium ions, and GTPases. The effects of Rho GTPases on the cytoskeleton have been extensively studied on other types of cells, which provide insight into the effects on neurons. In the growth cone, GTPases couple directional cues to the polymerization and depolymerization of actin. However, GTPase signaling is not a simple process. First, the GTPases must respond in a spatially localized manner so that the directionality of the signal can be transmitted. Furthermore, GTPases have several subclasses, such as RhoA, RAC1, and CDC42, which may respond differently to the same guidance cue. Similarly, controlling properties of microtubules, such as polymerization, stabilization and translocation along F-action, modifies the dynamics of the growth cone [2].

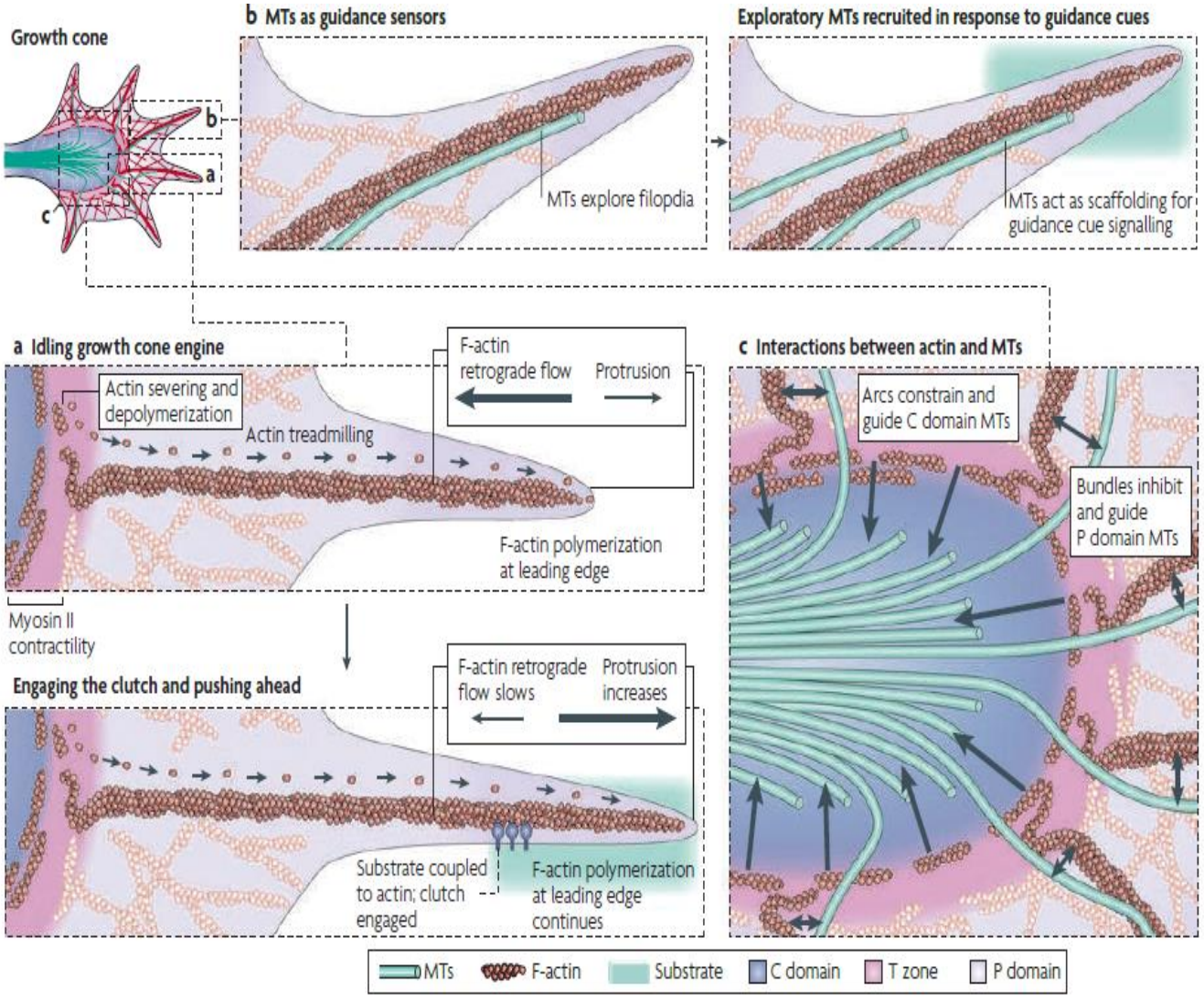

Fig 2.15 Diagram of the "motor" in a growth cone. Boxes are enlargements of specific areas on the growth cone. [2]

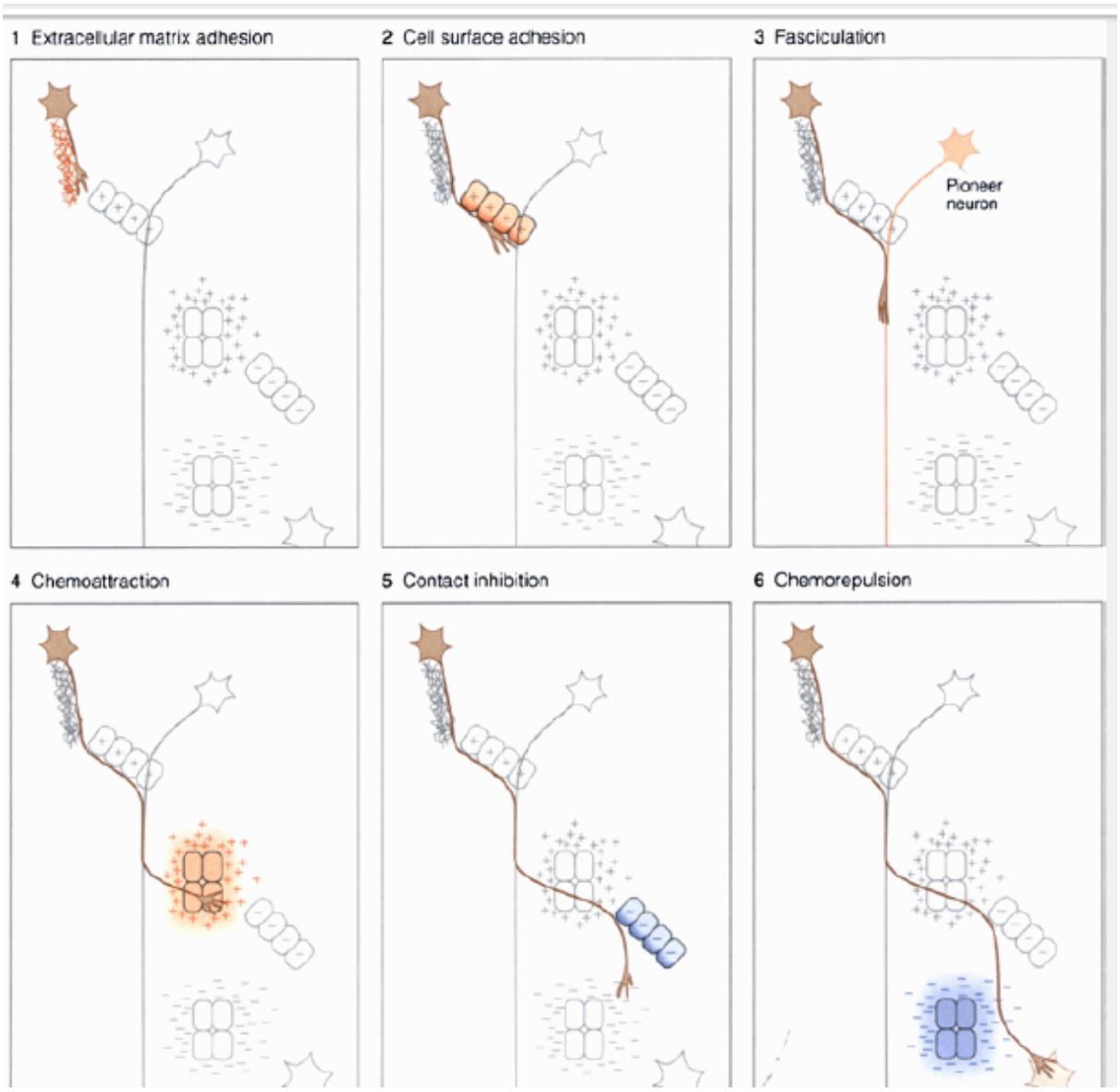

Fig 2.16 Examples of guidance cues interacting the growing axon. (1) Growth promoting molecules. (2) Adhesive molecules. (3) Fasciculation with another axon. (4) Soluble chemoattractant. (5) Intermediate repellant. (6) Soluble inhibitory molecule [15]

Extracellular proteins, such as laminin and fibronectin, interact with the cell membrane and control growth. Laminin consists of three subunits, A, B_1, and B_2, and is a significant part of non-neural tissues is in the peripheral nervous system. Both molecules play an important role in the growth of neurons *in vitro*. Such molecules affect growth by modifying the adhesion of the growth cone to the substrate or extracellular matrix. The extracellular matrix not only influences growth, but also the properties of the cell it is in contact with, for example, Schwann cells require contact with the matrix [14]. *In vivo* there is a layer, the basement membrane, between the neuron and the extracellular matrix.

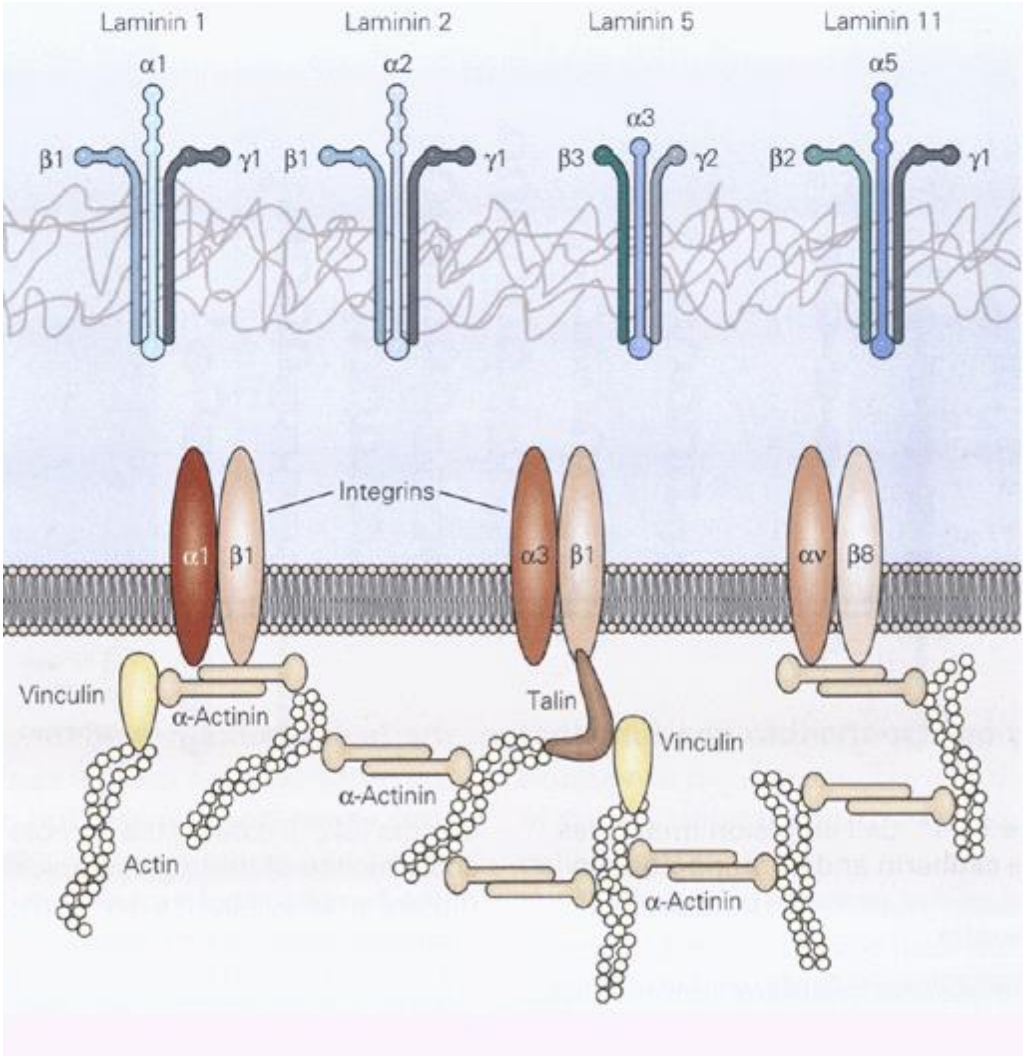

Fig 2.17 Laminins interact with integrins in the growth cone. There are several different types of laminin molecules, which consist of α, β, and γ subunits. Laminins facilitate the interaction between integrins and the extra-cellular matrix, and necessary step in growth cone extension.

Laminin and fibronectin, among others, are important molecules in the basement membrane, and can also be isolated and used in experiments. In conjunction with integrins, the substrate binds with the cytoskeleton, causing adhesion. In addition to mechanical adhesion, integrins, laminin and fibronectin activate intracellular signaling processes, including kinases, as described above.

The basic morphology of the neuron, with the soma, an axon, and dendrites creates the capability to transmit the action potential, which can be modeled with the Hodgkin-Huxley model. In the growth of the axon, the growth cone, a highly motile structure responds to guidance cues to direct the growth of the axon.

3. The Fokker-Planck Formalism and Modeling of Neuronal Growth

3.1 Classification of Models

While the Fokker-Planck equation provides a useful framework for modeling neuronal growth, it is not the only style of model used. Simpson et. al. classify models into three categories: phenomenological models, mechanistic models, and abstract models.

Phenomenological models use an empirical relation in some mathematical framework as the basis to describe neuronal growth, such as Boyle's law from the inverse relation between pressure and volume in a gas. Random walks are a common subclass of phenomenological models, and have been used in a variety of situations. In Katz et. al argued that a one dimensional random walk, with a number of parameters, describes axonal elongation [18]. In many phenomenological models, further properties of the system can be analyzed by applying various physical and mathematical principles to the concepts underlying the model. For example, in the random walk case, autocorrelation or crosscorrelation can provide additional insight into the behavior the growing axon, such in the example below from Simpson et. al. While phenomenological models do not specify a mechanism, they are still useful in providing a quantitative description of behavior and suggesting hypothesis of the underlying mechanisms.

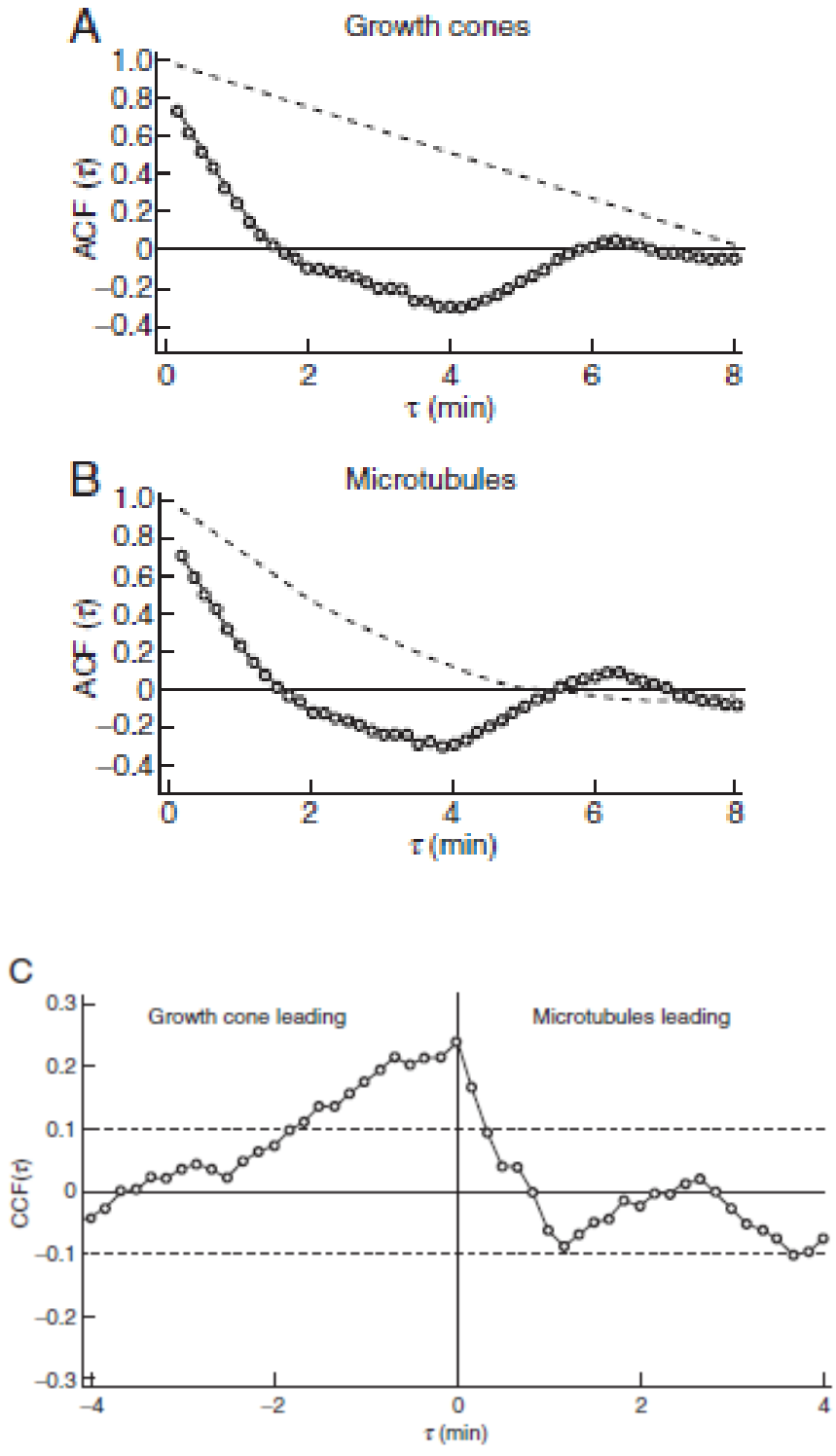

Fig 3.1 (a,b) Correlation between extension of the growth cone and microtubule polymerization (solid line) compared with expectation from random walk (dotted line). (C) The plot of cross-correlation indicates that the process interact. [19]

On the other hand, mechanistic models use specific biophysical processes to create a system for the model. However, in the context of growth cones and neuronal growth, the number of processes, the size of the parameter space, and the lack of specific knowledge about the biochemical processes themselves create challenges in creating useful mechanistic models. One example is modeling filopodial extension with "membrane elasticity, g-actin diffusion, lamellipodial extension rate, and the buckling of a-actin bundles under strain" [20, 21]. In particular, the model examines the effects of increasing the number bundled actin filaments on the length of the filopodia. Mortimer et. al. find that for too few actin bundles (<10), the membrane causes the actin to buckle, and that as the number of bundles increases, buckling becomes less likely but the filopodia requires more g-actin to extend. The balance of the constraints leads them to conclude that about 30 bundles is optimal. However, such analysis does not provide any insight into how such processes interact with the larger problem of the overall growth of the axon, for instance, how chemical gradients influence behavior.

The third classes of models, abstract models, describe behavior in general terms, without reference to how the neuron generates such behavior. One such model describes how a growth cone amplifies external signals through coupling the signal to an internal unstable, symmetric state from the signal is amplified [22]. A generally larger class of abstract models is simulations.

3.2 The Fokker-Planck Equation

The Fokker-Planck equation can be derived from a number of physical principles, but below, is one derivation which provides some insight into the Fokker-Planck equation.

Begin by considering a continuous random process, *x(t)*, which may be thought of as a particle undergoing random noise, which may be from Brownian Motion, collision etc. From this idea, the particle can be described by the Langevin equation:

$$\frac{dx}{dt} = \Gamma(t) + \mathrm{f}(t) \tag{3.1}$$

Here, Γ(t) incorporates the randomness or the noise, and f(t) is a force that the particle is experiencing. This force is typically considered to be the space derivative of some potential. Given that Γ is non-zero, the Langevin equation is non-deterministic, and so the behavior of the particle, *x*, must be described probabilistically. Therefore, one can introduce concepts such as autocorrelation, probability distributions, cumulative distributions for the resulting distribution of *p(x,t)*, the probability of finding the particle and at position *x* at time *t*. More precisely, *p(x,t)* is the probability of finding the particle between positions *x* and *x+dx* at time *t*.

The probability can be rewritten in a conditional form, using a known probability distribution from a previous time and some transition probability. Assuming the underlying process is uncorrelated, and that the initial probability distribution is some $p_0(x_0,t_0)$, the probability distribution at a later time, t, using the definition for a conditional probability, is given by,

$$p(x,t) = \int_{-\infty}^{\infty} p(x,t|x_0,t_0)\, p(x_0,t_0)dx_0. \tag{3.2}$$

One should note that the particles did not necessarily follow the same path from x_0 to x, and so therefore could have been at any x_1 at intermediate times between t_o and t. As a result, one can use the law of total probability and break the probability into two stages, getting from x_0 to x_1 and from x_1 to x. These probabilities need to be summed or integrated as in this case, which results in a Smoluchowski equation:

$$p(x,t_0|x_0,t_0) = \int_{-\infty}^{\infty} p(x,t|x_1,t_1)\, p(x_1,t_1|x_0,t_0)dx_1 \tag{3.3}$$

However, it is necessary to make one of two equivalent assumptions. One can assume that the process is Markovian, or precisely, that the correlation between $\Gamma(t)$ and $\Gamma(t_0)$ is zero unless $t=t_0$, where Γ is the noise function from the Langevin equation. Or alternatively, one can assume that the probability distribution functions between t_1 to t_0 and between t_1 to t are uncorrelated.

Now considering again the above situation, but only for the evolution of a small time scale over time Δt. Using the definition of a derivative, the time evolution can be written as

$$\frac{\partial p(x,t_0|x_0,t_0)}{\partial t} = \lim_{\Delta t\to 0} \frac{p(x,t+\Delta t|x_0,t_0) - p(x,t|x_1,t_1)}{\Delta t} \tag{3.4}$$

The transition probability over a small interval, Δt, can be approximated with a Taylor expansion of the delta function, because the delta function is the transition probability if $\Delta t = 0$. The delta function can be approximated in several different ways, such as using square waves, or Gaussian distributions. Using the first two terms of the expansion and the Smoluchowski equation, one finds:

$$\frac{\partial p(x,t|x_0,t_0)}{\partial t} = -\frac{\partial}{\partial x}[a_1(x)p(x,t|x_0,t_0)] + \frac{1}{2}\frac{\partial^2}{\partial x^2}[a_2(x)p(x,t|x_0,t_0)]. \tag{3.5}$$

Also from the Taylor expansion and the Langevin equation, one can find the moments of f around x_1 , over a small time of Δt. The noise terms, by assumption are uncorrelated, and terms of the order $(\Delta t)^2$ can be dropped. Thus the mean-square displacement is proportional to the change in time, and so from (3.5), the Fokker-Planck equation is derived.

$$\frac{\partial p(x,t)}{\partial t} = \frac{\partial}{\partial x}[V'(x)p(x,t)] + D\,\frac{\partial^2 p(x,t)}{\partial x^2} \tag{3.6}$$

Note that the preceding Fokker-Planck equation assumes the noise term, f(t) and the diffusion constant, D, do not depend on x [23].

The derivation above applies to the one-dimensional Fokker-Planck equation. The Fokker-Planck equation is generalizable into higher dimensions by replacing the derivatives with partial derivatives operator and deriving a multi-dimensional potential. The general form of the Fokker-Planck equation is:

$$\frac{dp(\boldsymbol{x},t)}{dt} = -\sum_{i=1}^{N}\frac{\partial}{\partial x_i}[V_i'(\boldsymbol{x})\,p(\boldsymbol{x},t)] + \sum_{i,j=1}^{N}\frac{\partial^2}{\partial x_i \partial y_j}D_{ij}p(\boldsymbol{x},t) \tag{3.7}$$

In this case, **x**, is a vector of length N, and so there are N different potentials. One application of the 2-dimensional case is modeling predator-prey interactions as a stochastic process [24]. The underlying Weiner processes are correlated, resulting in a model where the underlying intra-population dynamics have a random element introduced. They find that the both the strength of the noise and the correlations between sources of noise effect the behavior of the system at equilibrium, and that the median of the stochastic model corresponds to the results of a deterministic model. Unlike in the one-dimensional case, there are more parameters to consider in the multidimensional case, and the parameter space quickly increases in size with the number of variables in the system.

Another application of the Fokker-Planck equation in biology is to population genetics [25]. Tran et. al. extend the Wright-Fisher model to a global solution using the Fokker-Planck equation. The Wright-Fisher model assumes a diploid population with two alleles at a locus with discrete generations. Such assumptions naturally lead to a Markov chain. However, in a population with continuous generations, such a model fails, but using the Fokker-Planck equation allows for such an extension. As in other cases, they use an eigenfunction expansion to find time dependence and show the existence and uniqueness of solutions. However, in this case, the Fokker-Planck equation has neither drift term nor potential, but instead a space-dependent

diffusion coefficient. Using an initial condition where the proportion of one of the alleles is fixed, the Fokker-Planck equation is used to evolve the system in time. Evaluating the solution to the Fokker-Planck equation at a given time gives the probability distribution for allele frequencies. The Fokker-Planck equation also allows for calculation of other quantities relevant to population dynamics such as absorption time, fixation probabilities, moments, and homogeneity.

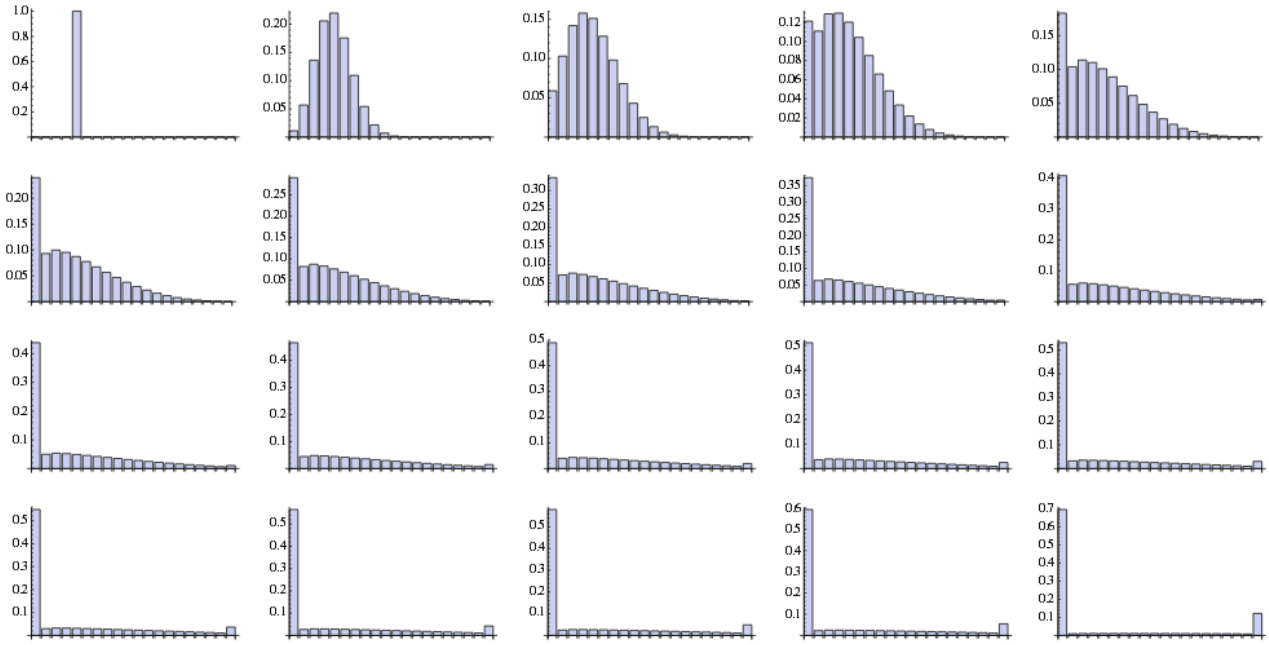

Fig 3.2 Initial frequency of the allele is .25. The plots show the time evolution to the state where one allele is the only found in the population. [25]

In mathematical biology, the integrate-and-fire model is a typical model of neuronal networks. In the basic integrate-and-fire model, the voltage increases until it reaches a threshold voltage, where the membrane potential is reset, indicating the action potential. Rosenbaum et. al. apply the Fokker-Planck equation to a system of two populations of integrate-and-fire neurons. They use a Fokker-Planck equation of the form:

$$\partial_t P(t,U) + div\left(F(U)P(t,U) - D\ M\ \nabla P(t,U)\right) = 0$$
$$M = \begin{pmatrix} 1 & c \\ c & 1 \end{pmatrix} \tag{3.8}$$

U is the pair of membrane voltages $U = (V, W)$, and f is the pair of drift velocities, and c is the correlation between the inputs to each of the integrate-and-fire neurons, V and W. The model is extended to include populations of neurons in the three refractory periods, one state for when only one neuron is in a refractory state, and a third for the condition when both are in a the

refractory period. Adding boundary conditions and transitions between states completes the model. This model is not solved analytically, but rather with numerical methods. Two methods were used: Monte Carlo simulations and the finite volume method. The results are not identical, but the structure of the model allows for the finite volume method to be used which is faster and allows for computations that could not be done in reasonable time with a Monte Carlo method [26].

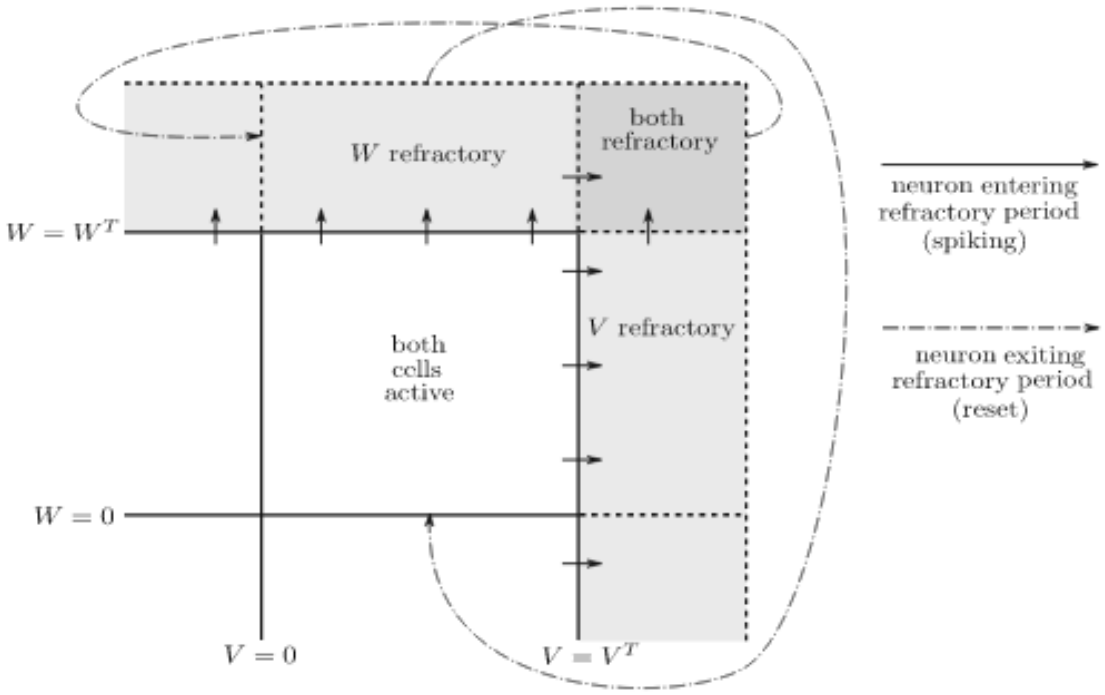

Fig 3.3 Schematic of the integrate-and-fire model for two neurons with refractory period where the neurons don't respond to input [26]

Calcium ion channels in *Xenopus* oocytes are another case where the Fokker-Planck equation has been used to model stochastic processes [27]. Cells release calcium through gated channels, with gates that respond to the concentration of ions, such as is the case for the action potential. The channels may be clustered together on the cell membrane, resulting in calcium release in the form of a "puff". The Fokker-Planck model results of the assumption of that the concentration is continuous, and the proportion of open channels is discrete, so the number of open channels jumps, and the transition probability between the number of open channels is approximated with the Kramers-Moyal expansion, so the Fokker-Planck equation is the result. The results of the Fokker-Planck formalism correspond well with discrete simulations, even for small numbers of channels (n=20).

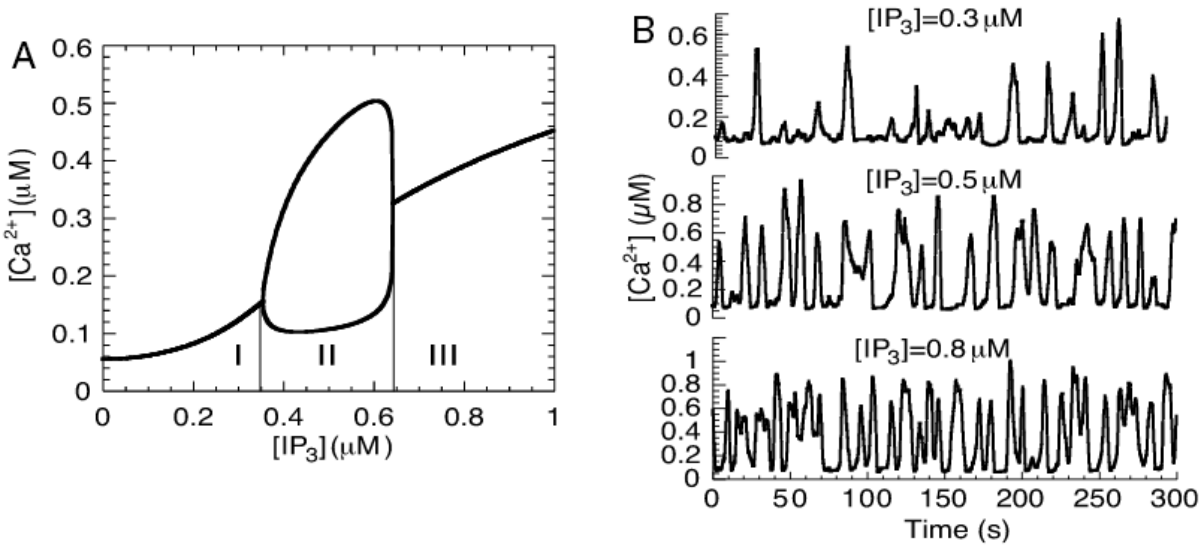

Fig 3.4 (A) The bifurcation from the deterministic Li-Rinzel model. (B) Simulation of stochastic processes with 20 channels, indicating "puffs" outside of cyclic regime (II), with qualitative similarities to the action potential. [27].

Betz applies the Fokker-Planck equation to modeling the growth cone and the effects of microtubules in directing the direction of growth. Specifically, the actin in the lamellipodium is tracked by fluorescently labeling it. The edge of the growth cone is clearly delineated by the actin, allowing for the edge of the cone to be traced over time, so the distance from the center of mass of the growth cone to the edge to be determined for all angles.

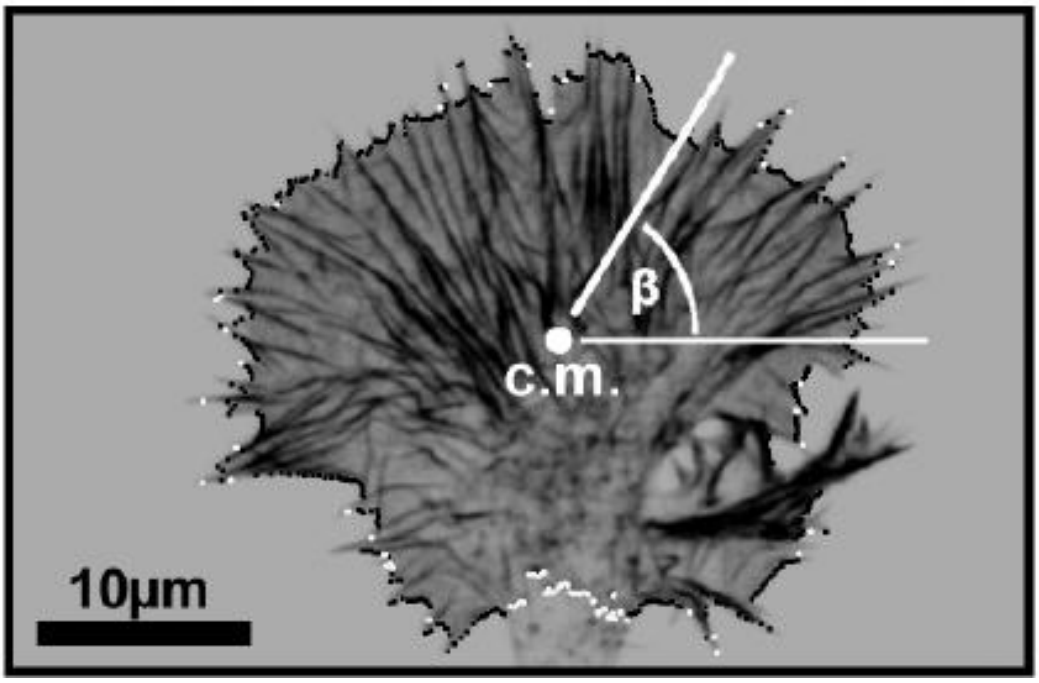

Fig 3.5 Confocal fluorescence of a growth cone, and the measurement of the distance to the edge at an angle β . [28]

The distribution of velocities is observed to be bimodal, leading to the conclusion that the velocity distribution is the combination of a retraction and extension phase, suggesting a two-state process. Based on measurements of 24 growth cones, retraction is measured at -1.60 ± .55 μ m/min and protrusion is measured at -1.56 ± .69 μ m/min. To measure the extent of stochastic behavior in the extension and protrusion, one considers the residence time distribution (RTD), which measures the length of time that the process is in a state (retraction or protrusion). On a logarithmic scale the plot is linear for each state, implying exponential decay, with parameters of $0.08 \pm 0.01\ s^{-1}$ and $0.11 \pm .01\ s^{-1}$ for retraction and extension, respectively.

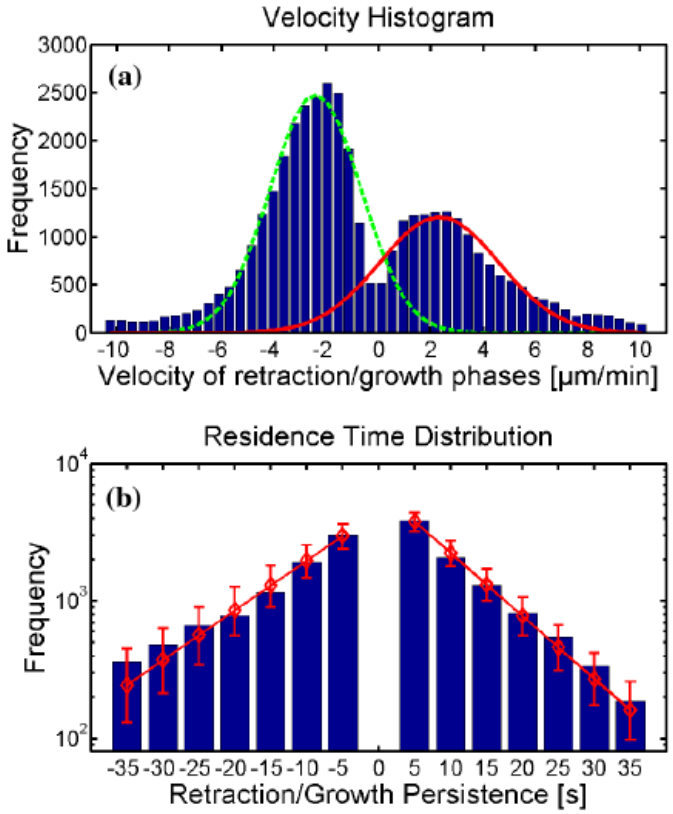

Fig 3.6 Statistical description of the behavior of the lamellipodium. (a) shows the measured velocity of the growth cone, and the two regimes of growth and protrusion. From the assumed random noise, the histogram is fit with a Gaussian distribution, with mean -2.36 ± .11 μ m /min (green) and 2.42 ± 0.18 μ m/min (red). (b) displays the persistence of each state on a logarithmic scale, with slope 0.08 ± 0.01 s^{-1} and 0.11 ± .01 s^{-1} for retraction and protrusion respectively. The errors and error bars are from a 95% confidence interval [28].

The residence time distribution combines the velocities over all angles for a global measurement. From the linear relation in (b) above, the residence time distribution follows an exponential decay distribution.

Exponential distributions are associated with independent random noise, from the lack of memory property of exponential distributions. In addition, it is important to note that the rates of decay are different between the two states of retraction and protrusion. A difference in rates suggests a bistable stochastic process. Therefore, one can use a Langevin equation:

$$\frac{dv}{dt} = -\frac{\partial V(v)}{\partial t} + \sqrt{2\eta}\, f(t) \tag{3.9}$$

where v(t) is the edge velocity at a given time t, V(v) is the potential, which depends on the velocity, η is a noise parameter and f(t) is the noise term. Because f(t) is assumed to be white

nose, $\langle f(t)\rangle = 0$ and $\langle f(t)f(t+\tau)\rangle = \delta(t-(t+\tau))$, i.e. the mean on the noise is zero, and the correlation of the noise at two different time point is zero (δ is the delta function). Because this Langevin equation is in velocity space, it is equivalent to a biased random walk where the walker controls the edge velocity. From the Langevin equation, one can derive a Fokker-Planck equation with *p(v,t)* being the probability distribution for the velocity at a given time t,

$$\frac{\partial p(v,t)}{\partial t} = \frac{\partial}{\partial v}[V'(v)p(v,t)] + \eta\frac{\partial^2}{\partial v^2}\,p(v,t) \tag{3.10}$$

It is assumed, for the cells used by Betz, that macroscopic properties change on the order of 10-30 minutes, such that 10 minute intervals are sufficient to capture the properties of growth. One can relate the potential and the probability distribution, with normalization constant C, by noting the left hand side must be zero in a stationary state, by definition, so the Fokker-Planck equation becomes a simple ordinary differential equation. The solution is of the form:

$$p(v) = C * \exp(-\frac{V(v)}{\eta}) \tag{3.11}$$

By taking the negative of the natural logarithm, one derives a formula for the potential from measurable data (except for a constant):

$$\frac{V(v)}{\eta} = -\ln\big(p(v)\big) - C \tag{3.12}$$

Following Kramer's approach, one can relate the velocity probability distribution and the residence time distribution by quantifying the decay of a bistable random process. The decay is related to a barrier in the potential to the curvature of the extrema of the potential.

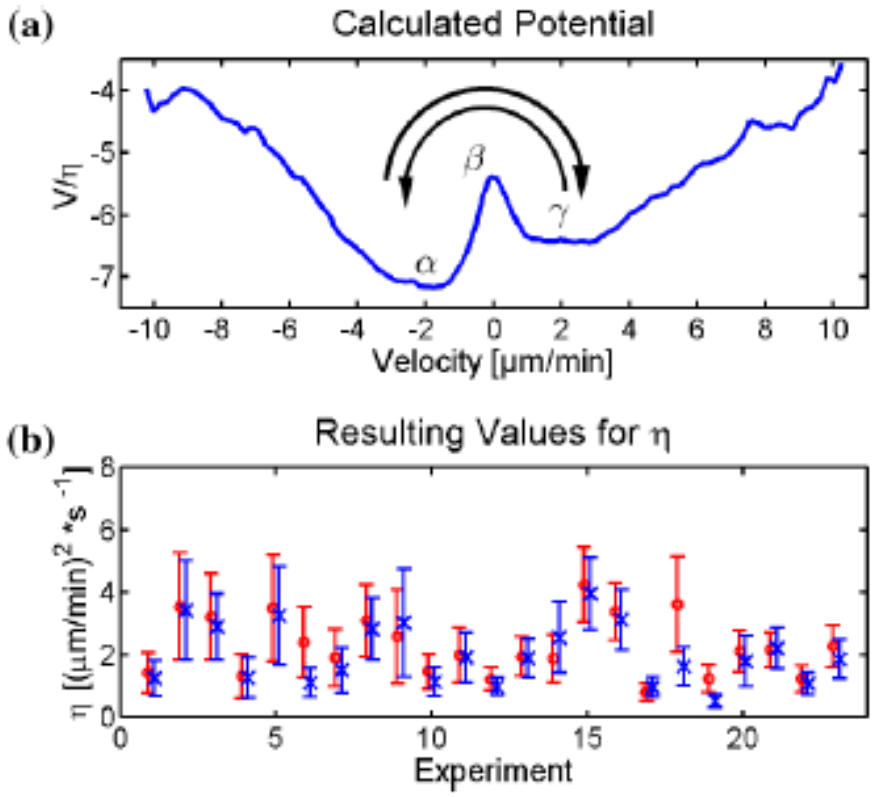

Fig 3.7

(a) The calculated potential, with the arrows showing the switching between protrusion and retraction. α and γ are the minima and the potential, and β is the maximum.

(b) The values for the noise parameter η, with retraction to protrusion in red, and protrusion on retraction in blue [28].

From this, Betz concludes that the protrusion and retraction of the growth cone are based on a bistable stochastic process. Actin, as the primary polymer in the lamellipodium, is the likeliest polymer which creates the bistable process modeled above. Actin polymerization depends on two processes, polymerization at the leading edge and retrograde flow (CITE). Retrograde flow is driven by myosin motors, leading to an inherently stochastic process, on a longer time scale than the polymerization on the leading edge, which changes on the order of seconds.

In context of neuronal development, it is expected that there is a long term trend of protrusion, so that the axons extend and form synapses. Therefore, the potential should favor positive values (extension) over negative values (retraction). As a result, Betz considers the potentials for motion in the direction of growth, and potentials for the direction perpendicular to growth.

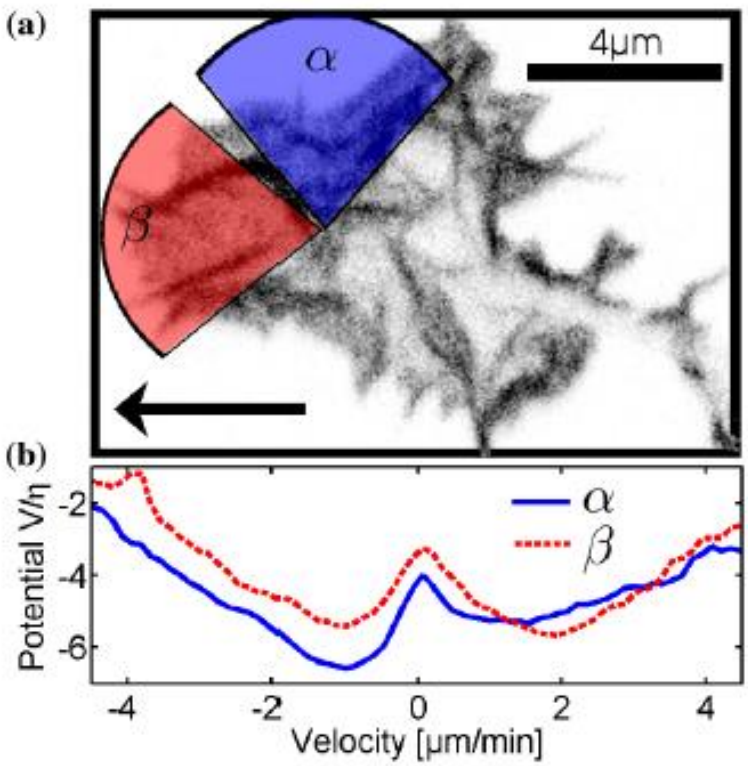

Fig 3.8

(a) Fluorescent image of actin in the growth cone, growing in the direction of the arrow. α and β are the two regions of perpendicular and parallel to the direction of growth

(b) The measured potentials for angles in the regions above. The blue solid line is for areas perpendicular to growth, and the red dashed line is for areas in the direction of growth. The tilted potential favors overall extension of the axon. [28]

In this setting of dividing the growth cone into two regions, Betz finds that retraction is favored in the perpendicular region (α), where the retraction states decay slower than the protrusion states, 5.5 ± 0.021 s^{-1} and 9.9 ± 0.014 s^{-1} respectively. In the direction of growth (β), the reverse is observed, where the retraction states decay faster than the protrusion states, 7.7 ± 0.008 s^{-1} and 7.1 ± 0.011 s^{-1} respectively. By considering separate regions, a bistable stochastic model describes the growth and the emergent properties of mechanisms in the growth cone.

3.3 The Fokker-Planck Equation in Two Dimensions

Schienbein and Gruler model the migration of granulocytes using the Fokker-Planck equation in velocity and angle space. The basis of their model is using an "automatic steerer", which controls the motion of the cell without responding to any feedback.

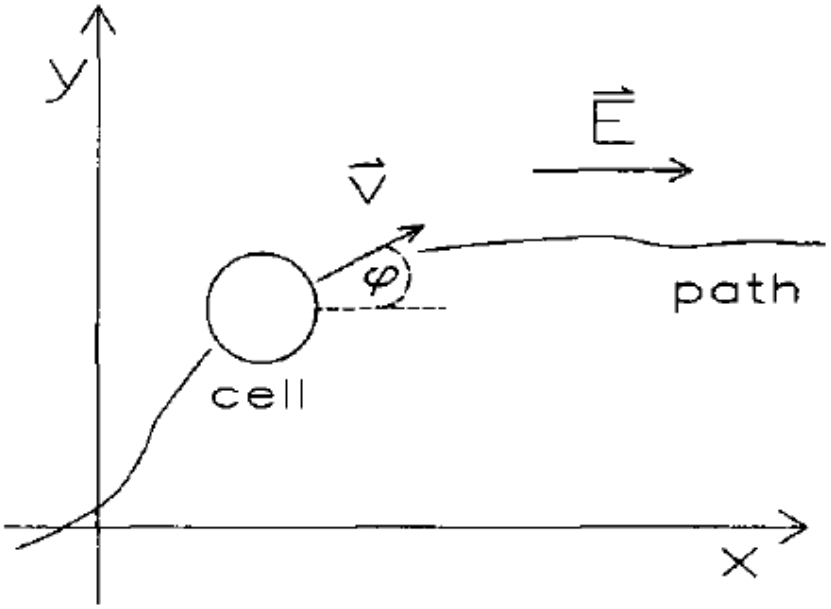

Fig 3.9 Figure of the cell, and the polar coordinate system in an electric field oriented along the x-axis. [7]

The cell movement is considered in two-dimensional space, and described by its velocity. It is convenient to write the velocity in polar coordinates:

$$\boldsymbol{v}(t) = \begin{pmatrix} v(t)\cos\phi(t) \\ v(t)\sin\phi(t) \end{pmatrix} \tag{3.13}$$

While not *a priori* the case, the two functions of time, v and ϕ are independent. Schienbein and Gruler reach this conclusion on the basis of two experimental results. First, v(t) and ϕ(t) are statistical independent. Second, the mean track velocity does not depend on the direction of migration, ϕ.

Because the motion is not deterministic, as observed in a variety of experiments, stochastic processes must be involved. From the independence of v and ϕ, one can consider the two functions separately. Thus, one begins by writing the Langevin equation for time. The Langevin equation used above by Betz:

$$\frac{dv}{dt} = -\frac{\partial V(v)}{\partial t} + \sqrt{2\eta}\, f(t). \tag{3.14}$$

Which can be rewritten as follows,

$$\frac{dv}{dt} + \gamma_v v = \gamma_v v_s + f(t) \tag{3.15}$$

Where *f(t)* again is a noise term, γ_v is a parameter governing the decay to equilibrium, and v_s is the mean speed. By taking the right hand side to be zero, the resulting differential equation has a solution of exponential decay:

$$\frac{dv}{dt} + \gamma_v v = 0 \tag{3.16}$$

In this solution, γ_v is the inverse of the characteristic time (τ). In the next case, only f(t)=0, so the solution of the differential equation is exponential decay towards some non-zero mean. The noise term, as before is white nose, with the following properties:

$$\langle f(t) \rangle = 0 \tag{3.17}$$

$$\langle f(t) f(t') \rangle = q_v \, \delta(t - t') \tag{3.18}$$

Where q_v quantifies the strength of the noise. In the general case where f(t) is not zero, the behavior of the cell cannot be predicted, and a Fokker-Planck equation is used to find a probability distribution for the velocity of a particle, as follows:

$$\frac{\partial p(v,t)}{\partial t} = \left(\gamma_v \frac{\partial}{\partial v}(v - v_s) + \frac{1}{2} \, q_v \frac{\partial^2}{\partial v^2} \right) p(v,t) \tag{3.19}$$

From the white noise assumption, the solution is a Gaussian distribution, with mean v_s and normalization constant p_0.

$$p_{st}(v) = p_0 \exp\left(-\frac{\gamma_v}{q_v}(v - v_s)^2 \right) \tag{3.20}$$

Solving for the normalization constant,

$$p_{st}(v) = \left(\frac{\gamma_v}{q_v \pi} \right)^{\frac{1}{2}} \exp\left(-\frac{\gamma_v}{q_v}(v - v_s)^2 \right) \tag{3.21}$$

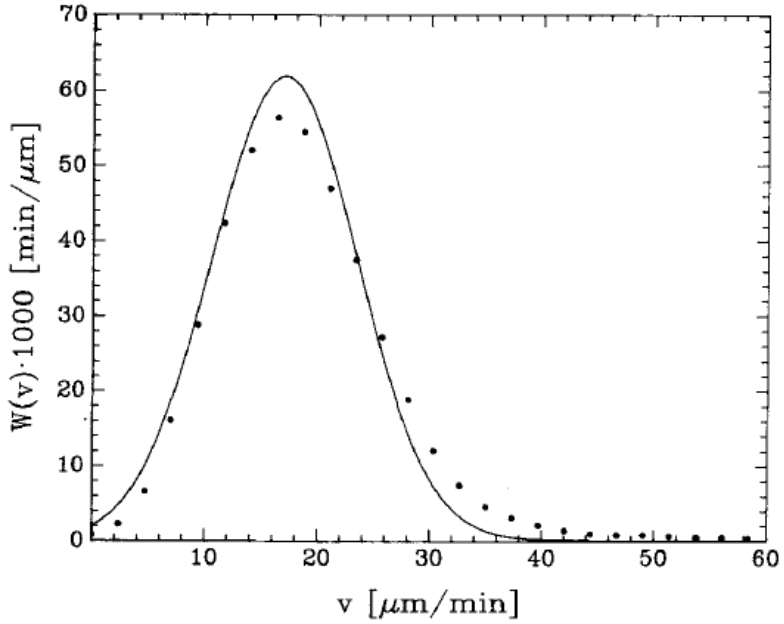

Fig 3.10 The stationary distribution, with the experimental data in the dots, and the least-squares best fit in the solid line, with mean 17μm/min [7]

Because v is not truly velocity, but rather the speed of the migration, negative values are physically meaningless, but a Gaussian distribution has non-zero negative properties. Therefore, the requirement that the probability of a negative velocity be much less than $\sqrt{\frac{\gamma}{q_v \pi}}$ is introduced. This requirement holds for the experimental data above. The ratio of the two parameters in the Gaussian probability distribution can be regarded as an experimental control parameter, viewed as a signal-to noise ration.

In this analysis, like in Betz, the position is not sampled continuously, but rather at discrete intervals, which introduces two sources of possible error. First, any error in position measurement is amplified when converted to velocities if Δt is small. Secondly, for larger positional steps, the measurements path is approximated with a polygonal path, which underestimates the total distance. This source of error, is mitigated if the measurement time is much less than the characteristic time of the Langevin equation i.e. $\Delta t \ll 1/\gamma_\phi$. Therefore, the standard deviation of the stationary distribution does not just depend on the properties of the cell, but also on the measurement process. It is also worth noting that the speed is homogeneous over time, such that the probability distribution can be viewed as the distribution for one cell over a long time, or as the distribution for a collection of cells [7].

The angular quantity, ϕ, has the same basic formalism as the speed. It is known that cells respond to electric field, and in particular, granulocytes move opposite to the electric field. Again, the system is not deterministic, and there is a noise term,

$$\frac{d\phi}{dt} = -k_p E \sin\phi(t) + f(t) \tag{3.22}$$

As in the schematic above, the electric field lines are parallel to the x-axis, so the effective force is maximal when the angle is perpendicular to the field, and minimal when parallel to the field. The strength of the effective force depends on the strength of the field, and a constant, k_p. Again, as before, the noise is assumed to be white noise, leading to the following properties, where q_ϕ is the strength of the noise:

$$\langle f(t) \rangle = 0 \tag{3.23}$$

$$\langle f(t) f(t') \rangle = q_\phi \, \delta(t - t') \tag{3.24}$$

Such a Langevin equation implies that that there is a torque, which is the effective force, rotating the cell toward the direction of the electric field, but there is a stochastic noise term introducing non-deterministic behavior. Therefore, the following Fokker-Planck equation for the velocity is used to find the angle:

$$\frac{\partial p(\phi, t)}{\partial t} = \frac{\partial}{\partial \phi}\left(-k_p E \sin\phi(t) + \frac{1}{2}\, q_\phi \frac{\partial^2}{\partial \phi^2}\right) p(v, t). \tag{3.25}$$

Setting $t_n = k_p t$ and $2\, k_p/q_\phi = K_G$, one can rewrite the Fokker-Planck equation as follows:

$$\frac{\partial p(\phi, t_n)}{\partial t} = \frac{\partial}{\partial \phi}\left(-E \sin\phi(t) + 1/K_G \frac{\partial^2}{\partial \phi^2}\right) p(v, t) \tag{3.26}$$

If there is no time dependence, the stationary solution can be analytically calculated as follows, where the denominator is the normalization constant:

$$p_{st}(\phi) = \frac{e^{(K_G E \cos\phi)}}{\int_0^{2\pi} e^{(K_G E \cos\phi)}\, d\phi} \tag{3.27}$$

The angular dependence, $e^{(K_G E \cos\phi)}$, follows experimental trends for various types of cells including granulocytes, fibroblasts and neural crest cells [7].

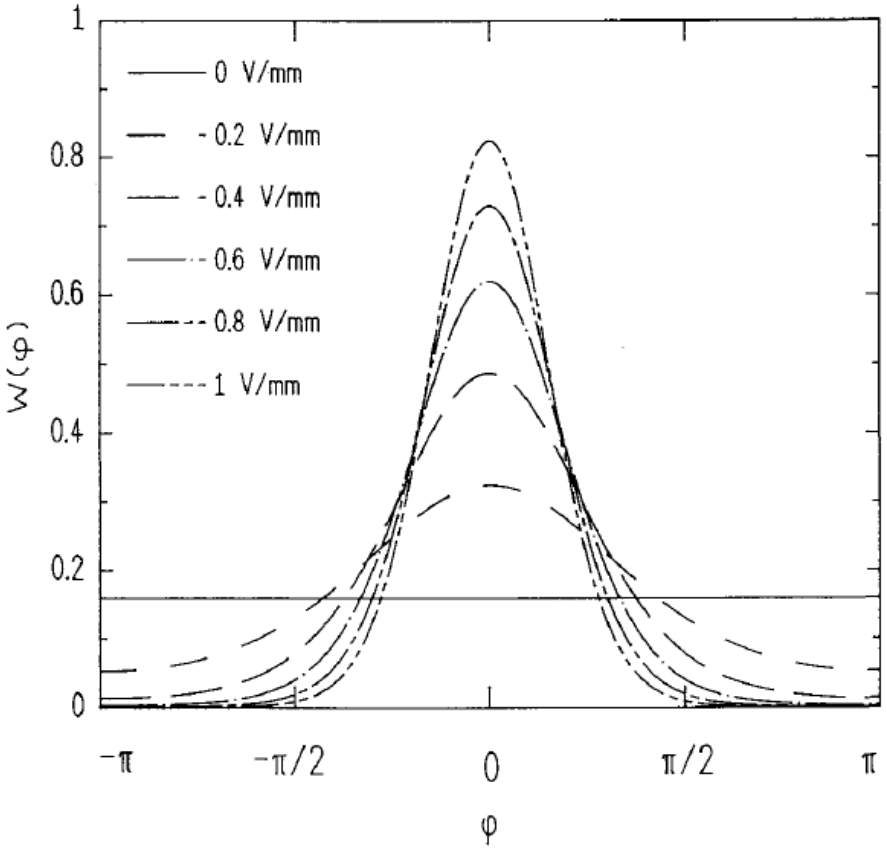

Fig 3.11 The stationary potential for different strengths of electric field,with K_G = 4.5 mm/V [7]

Such analysis for the angle of motion is not just limited to an electric field. Chemotactic gradients also result in an effective torque, which is proportional to -∇ ln c, where c is the concentration of the chemotactic molecule. From this, a similar Langevin equation results:

$$\frac{d\phi}{dt} = -\frac{k_{CT}^{0} K_R}{(c + K_R)^2}\frac{dc}{dx} \sin\phi(t) + f(t) \tag{3.28}$$

The Fokker-Planck equation allows for the calculation of time-dependent, instationary solutions. For example, the angular distribution is in a non-steady state, and one wants to see how the distribution evolves to its steady state, under a constant in time field. Therefore, the probability distribution can be separated and inserted into the Fokker-Planck equation, with operator L:

$$L\,\Theta(\phi) = -\lambda\Theta(\phi)$$

$$L = \frac{\partial}{\partial\phi}\left(-E\sin\phi(t) + 1/K_G\frac{\partial^2}{\partial\phi^2}\right) \tag{3.29}$$

Thus solving the Fokker-Planck is an eigenvalue problem, and one must find the eigenvalues and eigenfuntions of the Fokker-Planck operator. Note also, that a functionally similar operator is found for chemotaxis.

In the case where E=0, an analytic solution can be found. The eigenvalues are

$$\lambda_\mu = \frac{k_p\mu^2}{K_G} \tag{3.30}$$

The eigenvalues are degenerate, with a symmetric and antisymmetric solution for each eigenvalue.

$$\Theta_\mu^s = \frac{1}{\sqrt{\pi}}\cos\mu\phi \tag{3.31}$$

$$\Theta_\mu^a = \frac{1}{\sqrt{\pi}}\sin\ \mu\phi \tag{3.32}$$

The time dependent solution can be found by applying the initial condition to the eigenfunctions.

With the solutions for the speed and angle, the mean-squared displacement can be calculated. Noting that <x> =0 because the walk is isotropic, with no preferred direction, <x> is an uninteresting quantity. However, $\langle x^2\rangle$ is non-zero. Begin by noting the position of the particle is

$$\int_0^t v(t')\cos\phi(t')dt' \tag{3.33}$$

Therefore, the mean-squared displacement is

$$\langle x(t)^2\rangle = \langle[\int_0^t v(t')\cos\phi(t')dt']^{\,2}\rangle \tag{3.34}$$

Using the independence of v and ϕ, the mean-squared displacement is

$$\langle x(t)^2 \rangle = \left(\frac{A}{\Lambda} + \frac{B}{\lambda}\right) t - \frac{A}{\Lambda^2}(1 - e^{-\Lambda t}) - \frac{B}{\lambda^2}(1 - e^{-\Lambda t}) \tag{3.35}$$

With the constants defined as follows

$$\lambda = \lambda_1 = \frac{1}{\tau_\phi}$$

$$\Lambda = \gamma_v + \lambda$$

$$A = \frac{q_v}{2\gamma_v}$$

$$B = v_s^2$$

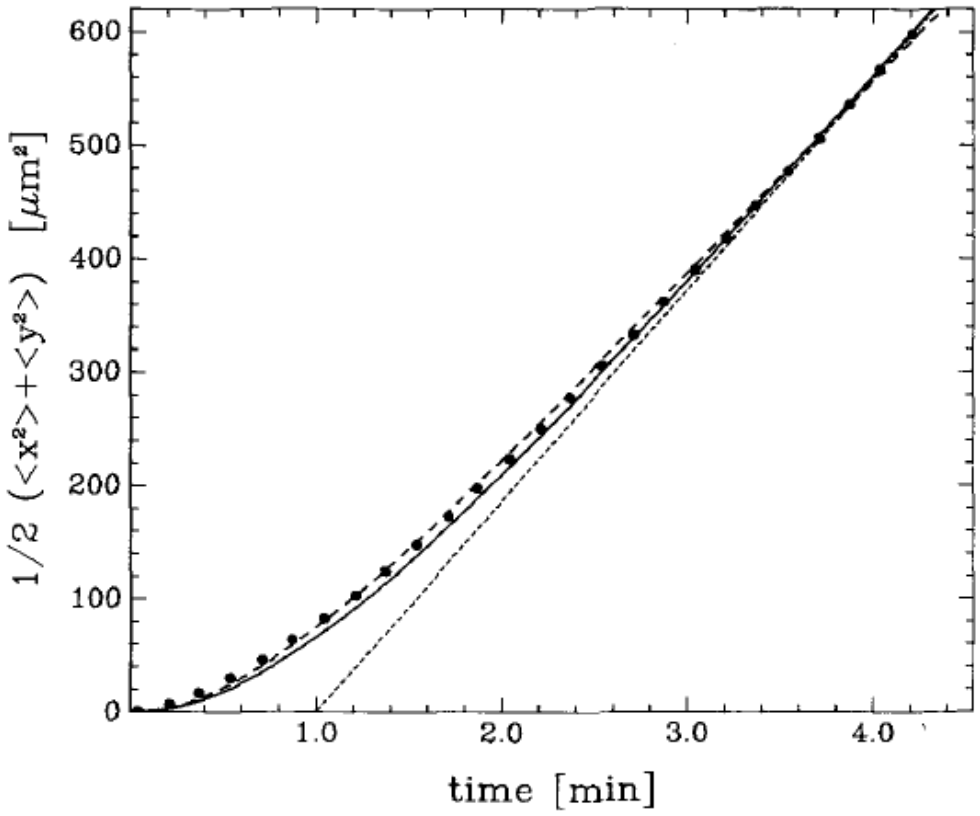

Fig 3.12 The mean squared displacement. The dots are the experimental data from granulocytes, with the best fit for large times as the dotted line. The approximation is the solid line. The dashed line is the an exponential fit to the data. [7]

The case when E is not zero means the L is not a Hermitian operator, and the case will be discussed later. However, for Betz, the eigenvalues of L behave quadratically with E, for small E.

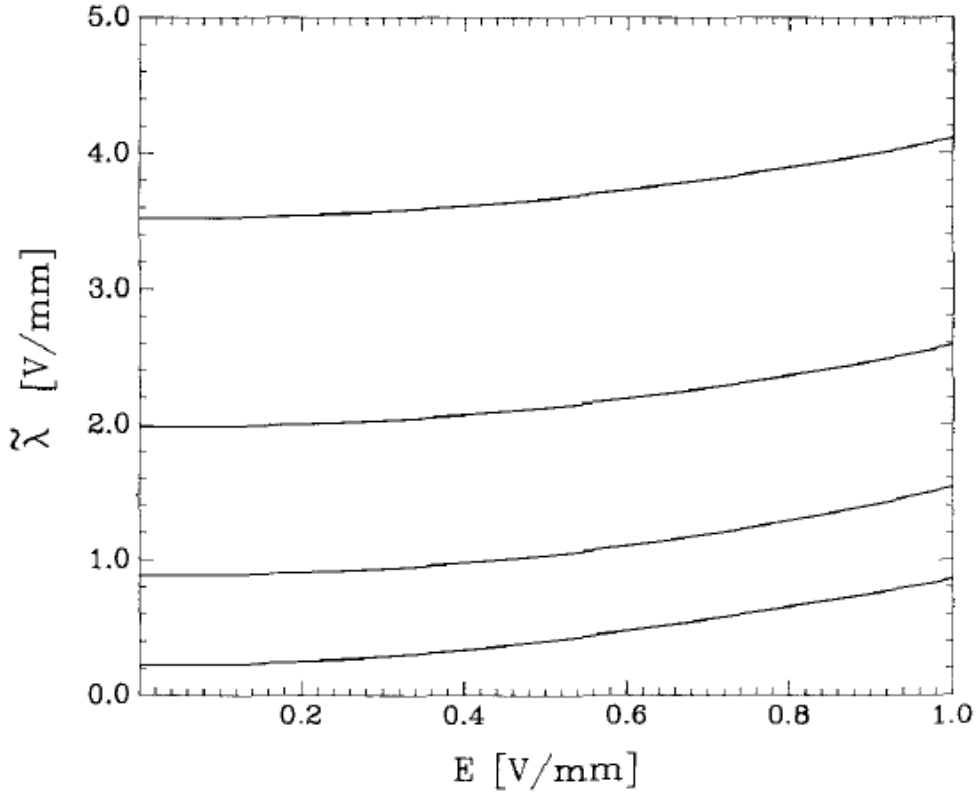

Fig 3.13 Plot of the eigenvalues of L as a function of E for K_G = 4.5 mm/V [7]

The Fokker-Planck analysis also allows for modeling of changing of experimental conditions. In the first case, an electric field of .8 V/mm is turned on at t=0 and turned off at t=150 seconds. In the second, the field again is turned on at t=0, but at t=200 seconds, the polarity is reversed.

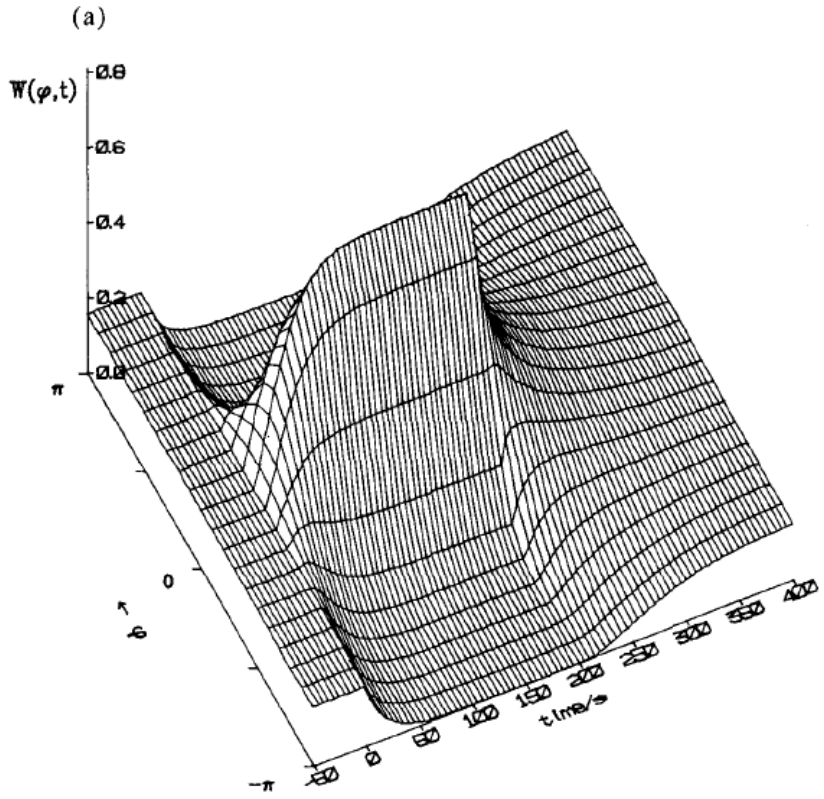

Fig 3.14 Angular distribution when the field is turned on at t=0 and off at t=150 [7]

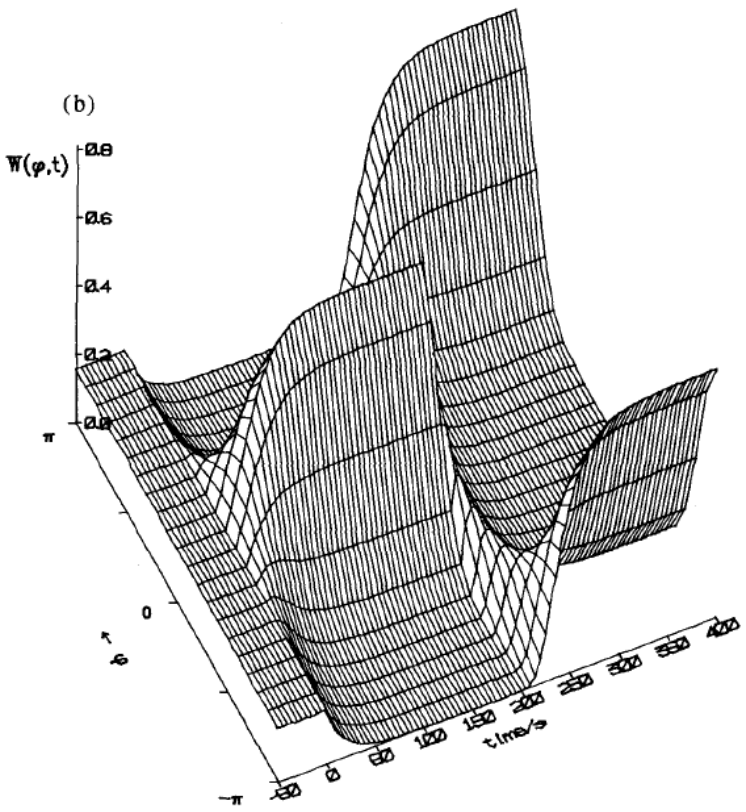

Fig 3.15 Angular distribution when the electric field is turned on at t=0 and the polarity reversed at t=200 [7]

Pearson et. al. take a different approach in describing the underlying stochastic processes by parameterizing with respect to the length of the axon, rather than time. By also considering errors in the measurement, they derive, via the Fokker-Planck equation, parameters that describe neuronal growth.

Rather than looking at p(**x**,t), which is the probability of finding the growth cone (particle) at the location **x** at time t, one can consider p(**x**, θ , s), which is the probability of finding the growth cone at a location **x**, within angle θ of the previous location of the growth cone at an arc length, s.

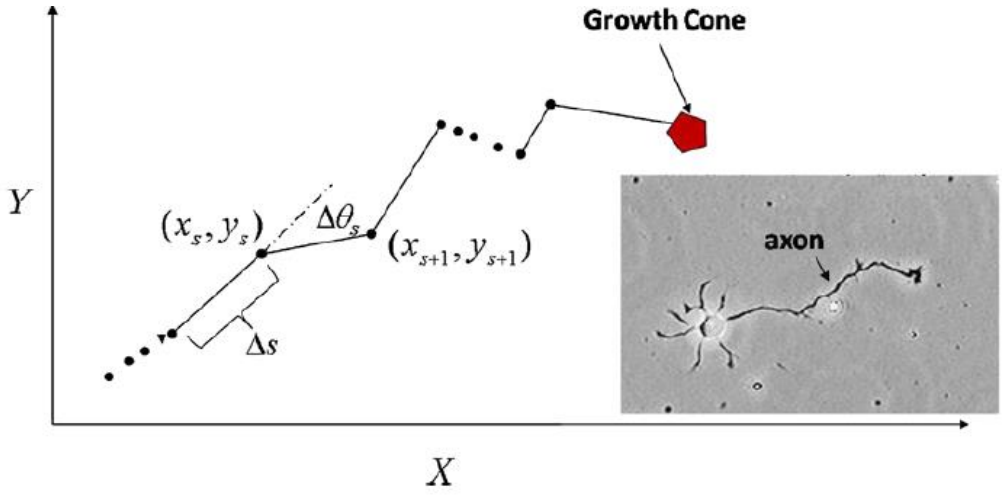

Fig 3.16 Schematic of the quantities defined in the probability [29]

From this, a system of stochastic differential equation naturally arises:

$$\begin{aligned} dx &= \cos\theta ds \\ dy &= \sin\theta ds \\ d\theta &= f(x,y,\theta,s)ds + D_\theta dW_\theta(s) \end{aligned} \tag{3.36}$$

In this case, f is the deterministic component of the stochastic differential equation, and W_θ is a Wiener process. In a case where there is no deterministic steering, such as an axon on glass, f is assumed to be zero everywhere. From this system of equations, a Fokker-Planck equation naturally arises:

$$\begin{aligned} &\frac{\partial P}{\partial s}(x,y,\theta,s) + \cos(x,y,\theta,s)\frac{\partial P}{\partial x}(x,y,\theta,s) \\ &\qquad + \sin\theta\,\frac{\partial P}{\partial y}(x,y,\theta,s) = D_\theta \frac{\partial^2 P}{\partial \theta^2}(x,y,\theta,s) - k_{end}p(x,y,\theta,s) \end{aligned} \tag{3.37}$$

The analytic solution of the Fokker-Planck equation allows for the computation of several properties of the distribution of states, including the mean-square displacement,

$$[\frac{2}{D_\theta^2}\left(e^{-sD_\theta^2-1}\right)]^2 \tag{3.38}$$

Simulations confirm the validity of the model, as shown below

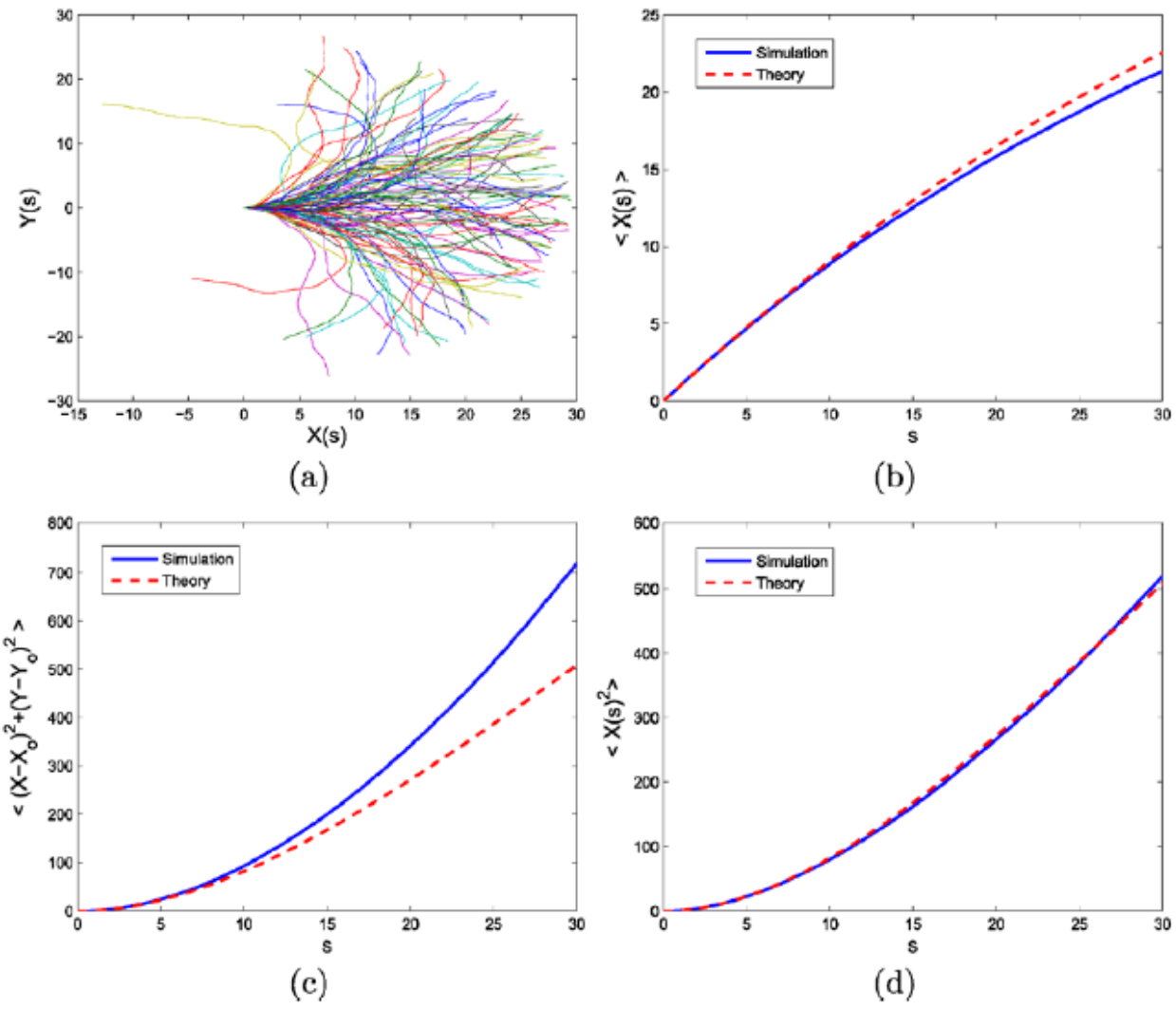

Fig 3.17 (a) 1000 simulated path with $D_\theta = 0.2$. (b-d) are the simulated and hypothesized moments and mean-squared displacement. [29]

However, when finding the parameters of the distributions of the variables of interest, the scale on which the measurements are taken have a significant impact on the calculated values. Specifically, as the length scale increases, the variability of the angular measurement, θ, increases. Like in the other examples discuses, the Fokker-Planck equation gives a framework for finding testable properties of the stochastic processes that underlie neuronal growth.

The Fokker-Planck equation has been used in a variety of modeling attempts to describe neuronal growth. The introduction of an effective potential and probability distributions allows for quantitative analysis of the model which produced the Fokker-Planck equation.

4. Neuronal Growth as Diffusion in an External Potential

4.1 Neuronal Growth in One Dimension

This section follows work published in *Neuronal growth as diffusion in an effective potential* by Daniel J. Rizzo, James D. White, Elise Spedden, Matthew R. Wiens, David L. Kaplan, Timothy J. Atherton, and Cristian Staii.

The Fokker-Planck formalism, which originally dealt with particles diffusing, is applicable to neuronal growth by treating the neuronal as a particle diffusing in an external potential. Such models are phenomenological models, considering the combined effect of different factors which promote or inhibit growth of a neuron. From time lapse videos of growing neurons, one can trace the growth of the neurite over time, and use the Fokker-Planck formalism to create a quantitative description of growth.

For the speed, as defined by the change in the arc length of the neurite, we found that a V-shaped potential describes the diffusion of the speed. It is important to note that the V-shaped potential indicates that the process is not simple diffusion. Using the Fokker-Planck equation, with a V-shaped potential, we found time-dependent probability distributions and a diffusion coefficient for the speed of axonal growth.

The neurons plated were from day 18 rat cortical neuron. The plated cells incubated for a further 8, 15, 19, 26, 33, or 46 hours. The samples were then loaded into the BioHeater Closed Fluid Cell, and imaged using the optical stage of the Atomic Force Microscope (AFM) from Asylum Researched, under a bright field. Each sample was measured every 5 minutes over a period of 15 minutes. Such an interval was chosen such that there was sufficient temporal resolution to approximate an instantaneous velocity while allowing for sufficient growth for detection over the interval, as the camera's resolution is approximately 0.1 μm. Each growing axon was then traced with the Nikon NIS-Elements Basic Research software, yielding the change in length over each interval.

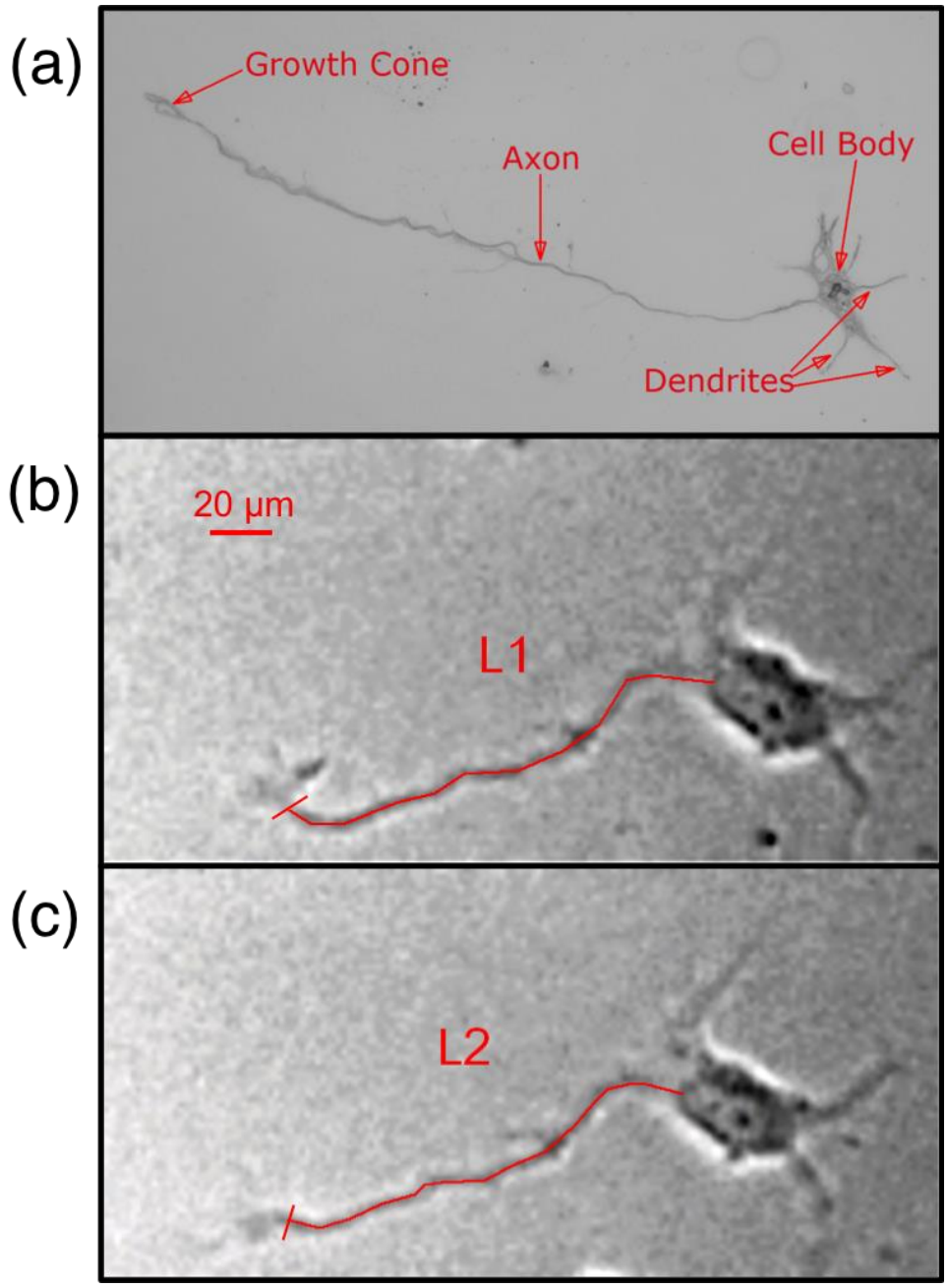

Fig 4.1: (a) image of a neuron from the time-lapse videos. (b), (c) depiction of the measurement of an axon over a 5-minute interval [30].

The speeds from each different measurement time (8, 15, 19, 26, 33, 46 hours) were combined to form a single time-independent distribution, with 986 individual measurements. Noting that in the Fokker-Planck equation,

$$\frac{\partial p}{\partial t} = \frac{\partial}{\partial v}[V'(v)p] + D\,\frac{\partial^2 p}{\partial v^2}. \tag{4.1}$$

When there is a stationary distribution, the left hand side is zero, resulting in the equality below. From the time-independent distribution, the stationary potential was calculated as:

$$\frac{V(v)}{D} = -\ln\big(P(v)\big) - \ln(N) \tag{4.2}$$

Where V(v) is the stationary potential, D is the diffusion coefficient, N is a normalization constant, and P(v) is the time-independent probability distribution for the speeds.

This is derived from the Fokker-Planck equation

$$\frac{\partial P}{\partial t} = \frac{\partial}{\partial v}[V'(v)P] + D\,\frac{\partial^2 P}{\partial v^2}. \tag{4.3}$$

by noting that if the distribution is stationary, dP/dt is zero. Integrating both sides with respect to the velocity, the result is the following ordinary differential equation:

$$D\,\frac{dP_{stat}}{dv} + V'(v)P_{stat} = const \tag{4.4}$$

The constant is the flux of probability at velocity v, which is zero because the distribution is stationary.

So the equation becomes:

$$d\,\frac{P_{stat}(v)}{P_{stat}(v)} = -\frac{1}{D}dV(v) \tag{4.5}$$

The solutions are

$$P_{stat}(v) = N\, e^{-\frac{V(v)}{D}} \tag{4.6}$$

Rewriting in terms of the stationary probability

$$\frac{V(v)}{D} = -\ln\left(P_{stat}(v)\right) - \ln(N) \tag{4.7}$$

The stationary potential (along with an initial condition) determines the time evolution of the probability distribution, which evolves until it reaches a stationary state.

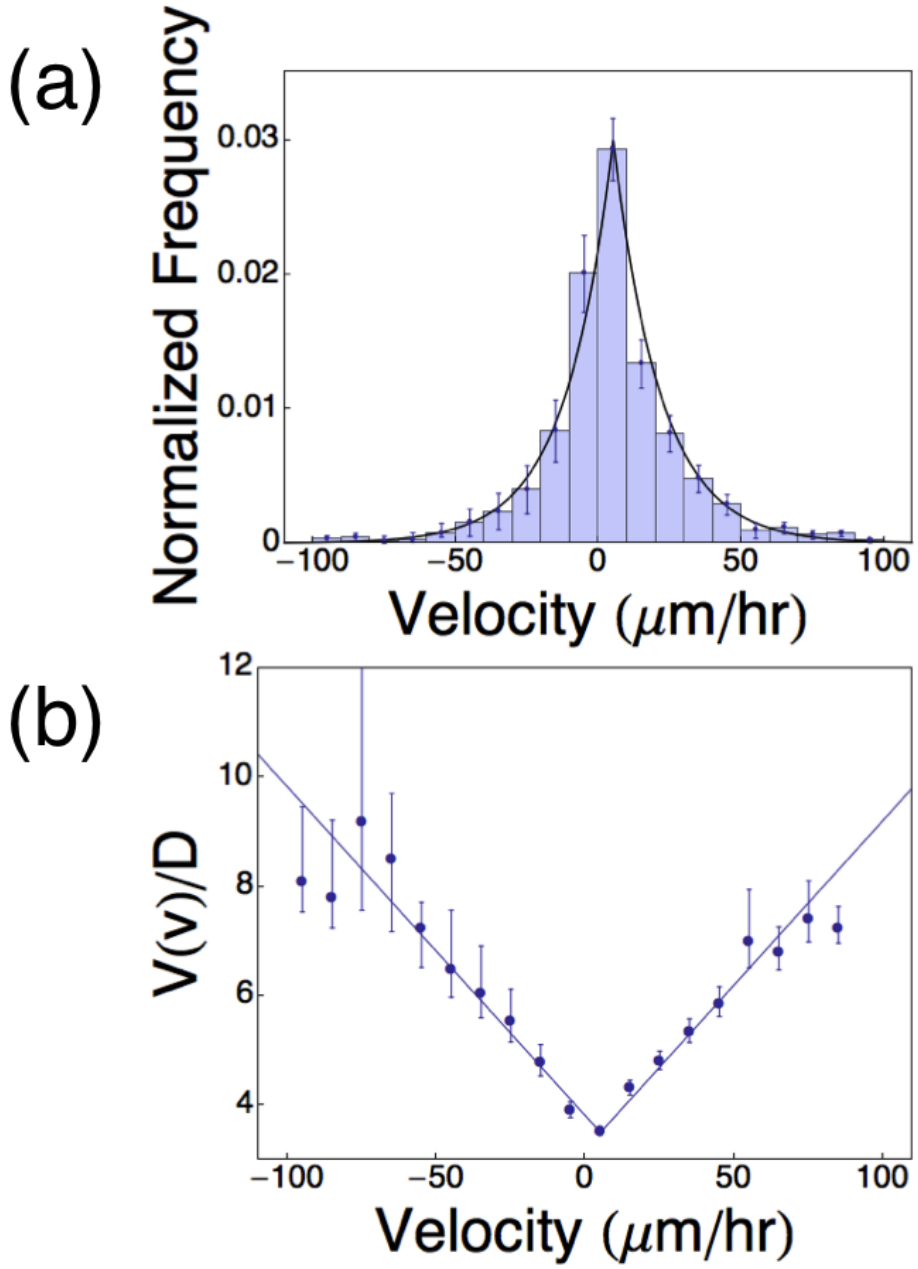

Fig 4.2: Time-independent velocity data. (a) A histogram of the velocities, with a best-fit Laplace distribution, with mean 5.1 μm/hr and scale parameter 16.7 μm/hr. (b) The corresponding stationary potential, which is V-shaped. In both the scale bars are from 95% confidence interval of a binomial distribution [30]

The Laplace distribution in fig 4.2a, has the form

$$p(v) = N\, Exp(-\kappa\, |v - v_c|\,) \tag{4.8}$$

With normalization constant N, scale parameter, κ, 16.7 μm / hr, and mean, v_c, 5.1 μm/hr. From these two equations, one finds the stationary potential:

$$V(v) = \kappa\, Abs(v - v_C) - \ln(N) \tag{4.9}$$

The constant term can be ignored, because the potential is differentiated in the Fokker-Planck equation, so the stationary potential can be simplified to

$$V(v) = \kappa\, Abs(v - v_C) \tag{4.10}$$

Therefore, the potential is V-shaped, and not constant or parabolic, which are two more common situations, corresponding to no potential and a simple harmonic oscillator. The effective force, which is the derivative of the potential, is constant is each region, driving the system back to equilibrium. Such behavior may correspond to the existence of bistable processes in the growth cone, which sense whether the growth is "too fast" or "too slow".

From a stationary potential and an initial condition, one can solve for the time-dependent solution. One well-known method transforms the Fokker-Planck equation into a Schrodinger-like equation, and uses methods well-known from Quantum Mechanics to obtain the solution [8]. For each term in the Fokker-Planck equation, there is a corresponding term in the Schrodinger equation: V_s for the Schrodinger potential and q(v,t) for the probability distribution. Each term transforms as follows:

$$\frac{\partial q(v,t)}{\partial t} = -V_s(v)q(v,t) + D\,\frac{\partial q(v,t)}{\partial v^2} \tag{4.11}$$

$$p(v,t) = \sqrt{p_{s(v)}}\,q(v,t) \tag{4.12}$$

$$V_s(v) = \frac{V'(v)}{4D} - \frac{V''(v)}{2} \tag{4.13}$$

For the experimentally derived V-shaped potential, the corresponding Schrodinger potential is

$$V_s(v) = D\frac{\kappa^2}{4} + D\kappa\,\delta(v - v_C) \tag{4.14}$$

Note that this Schrodinger potential is simply the infinite delta well centered at v_c , which is analytically solvable. The solution begins by separating the time and velocity variables. The velocity solution will be the linear combination of eigenfunctions of the time independent Schrodinger Equation. In particular, the solution has one bound eigenstate:

$$\psi_0 = \sqrt{\frac{\kappa}{2}}\,\exp(-\kappa\,|v - v_c|\,). \tag{4.15}$$

The unbound states have a continuous spectrum, with both symmetric and antisymmetric eigenstates.

$$\psi_k^{asym}(v) = \frac{1}{\sqrt{\pi}}\sin[\,\mathrm{k(v - v_c)}] \tag{4.16}$$

$$\psi_k^{sym}(v) = \frac{2k\cos[k(v - v_c)] - \kappa\sin[k|v - v_c|]}{\sqrt{\pi(4k^2 + \kappa^2)}} \tag{4.17}$$

The eigenvalue for the bound state is zero, and the eigenvalue for each choice of k is:

$$\lambda_k = D\frac{\kappa^2}{4} + Dk^2 \tag{4.18}$$

where k can take any real number. Each eigenstate has the typical time dependence when solving the Schrodinger equation:

$$\Psi_k(v,t) = \psi_k(v)\exp(-\lambda_k t) \tag{4.19}$$

Note that the bound state has no time dependence because the corresponding eigenvalue is zero. As in quantum mechanics, the time dependence is constructed from the initial conditions.

However, one notes that at all the experimentally observed times, the observed probability distribution is better modeled by the stationary distribution than any distribution at intermediate time steps. We assume a delta function centered at zero, δ(v), as an initial condition, which is physically reasonable given that no neurons are growing when the cells are plated. To determine if the stationary solution is the best fit of the observed distribution, we calculated the likelihood function in terms of Dt. If a non-stationary solution were the best fit, there would be a local maximum of the likelihood function. However, no such maxima is observed, thus any larger time is a better fit than a previous time, implying that the stationary distribution is the best fit. One example is shown in the figure below.

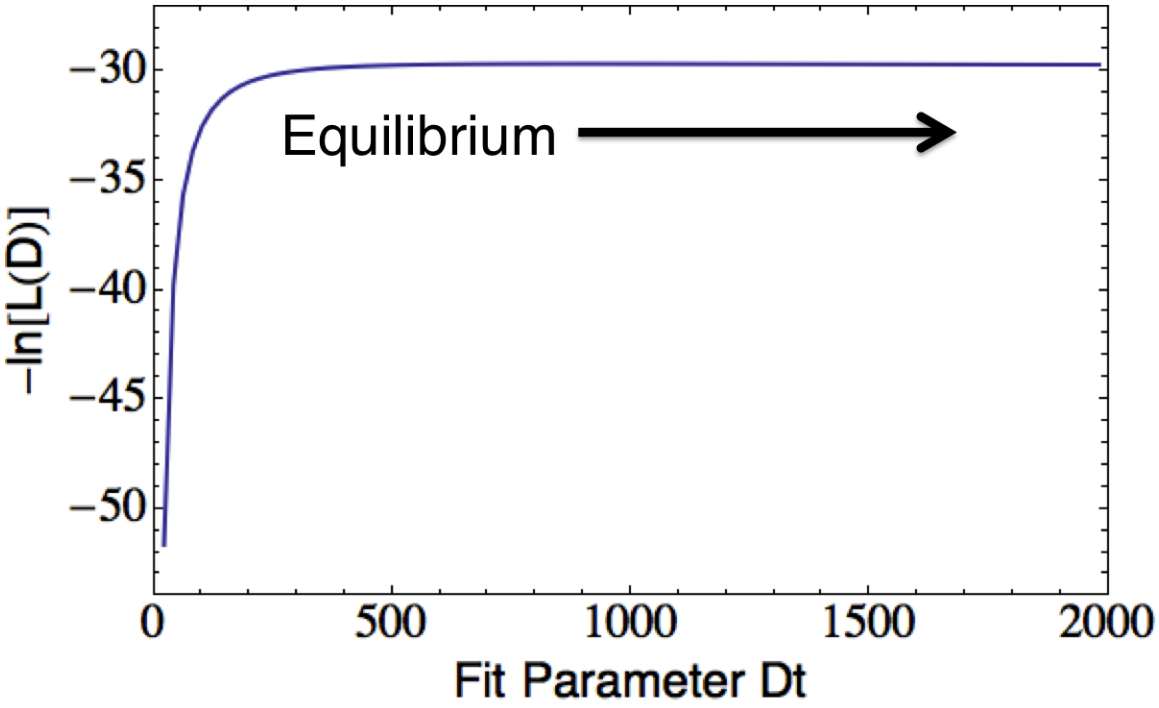

Fig 4.3: Likelihood function with no maximum value. [31]

By defining growth as the change in the length of the neurite, we develop a model for the growth of the neuron using the one dimensional Fokker-Planck equation. A time dependent solution is found using a transformation to the Schrodinger equation, and using an eigenfunction expansion. In this formalism, a V-shaped potential corresponding to a Laplace distribution best fits the experimentally derived data, and governs the time evolution of the growth.

4.2 Neuronal growth in Two Dimensions

However, neuronal growth is not linear, and just considering arc length does not fully capture the details for neuronal growth. The growth is a multidimensional process, and the one dimensional model simplifies the growth. Now, the growth can be written in polar coordinates, defined as:

$$\boldsymbol{v} = \begin{pmatrix} v_x \\ v_y \end{pmatrix} = \begin{pmatrix} v\cos\theta \\ v\sin\theta \end{pmatrix} \tag{4.20}$$

In this model, the growth is written in polar coordinates, with a Langevin equation for each component. It is possible to define θ in a number of different ways, but for this section, θ is defined as the change in angle of growth. Therefore, θ is not measured with respect to a fixed axis, but changes over time. If the angle were measured with respect to a fixed direction, the direction would be uniform on an isotropic surface, as there is no preferred direction.

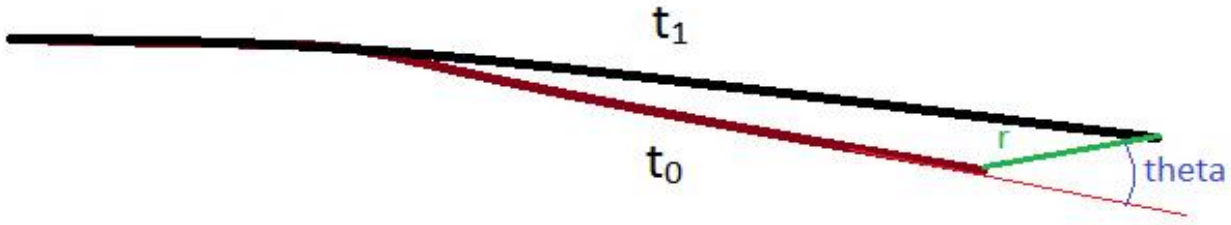

Fig 4.4: A neurite grows from t_0 to t_1, with parameters of growth r and θ. θ is measured with respect to the neurite at t_0, with that direction in red.

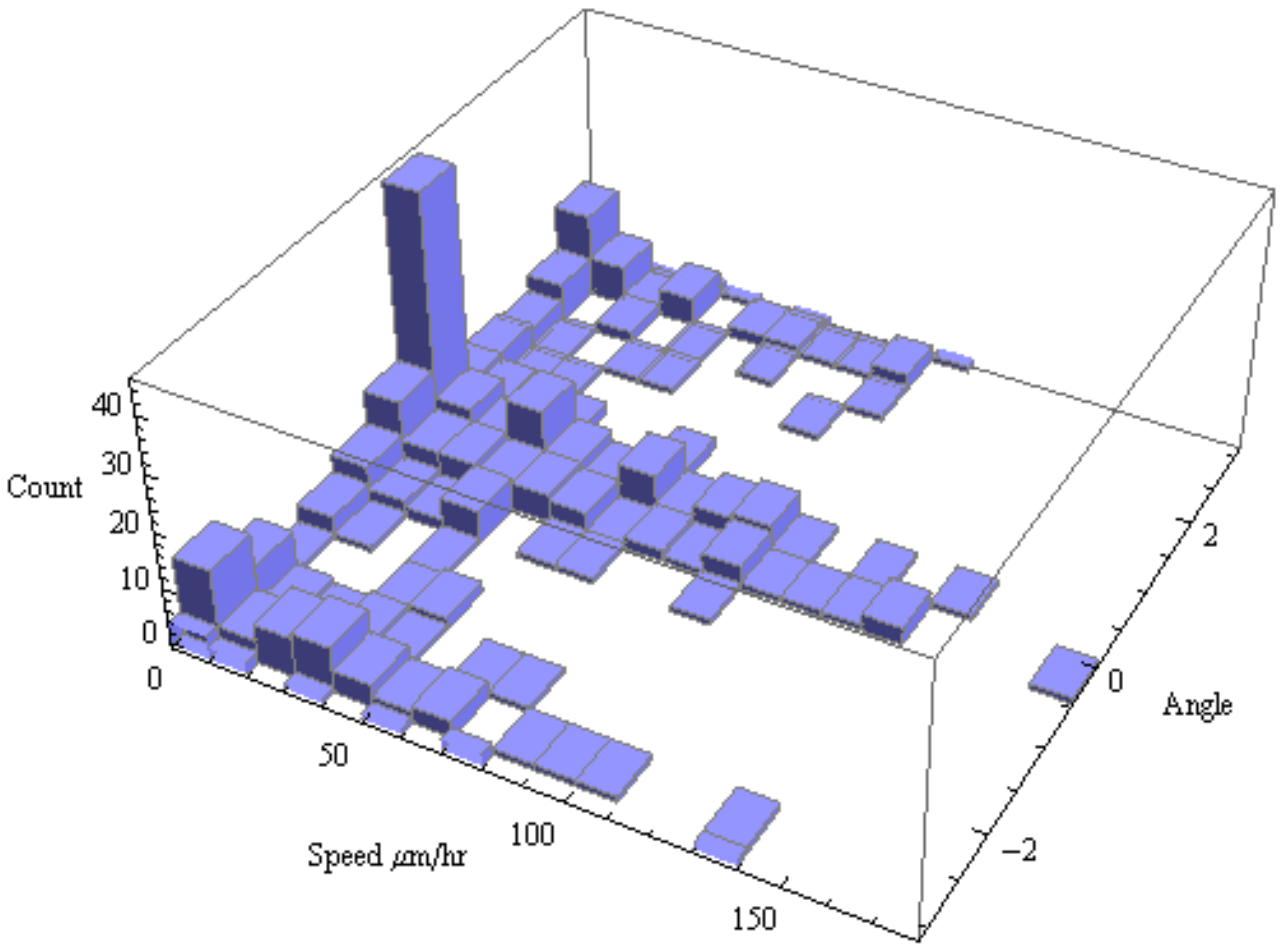

Fig 4.5. Histogram of neurite speeds and angle of growth (n = 357)

The Fokker-Planck equation in two variables is more complicated than the one dimensional case because of added cross terms:

$$\frac{dp(v,\theta;t)}{dt} = \left[-\left(\frac{\partial}{\partial v} D_v^{(1)}(v,\theta) + \frac{\partial}{\partial \theta} D_\theta^{(1)}(v,\theta) \right) + \left(\frac{\partial^2}{\partial v^2} D_{v,v}^{(2)}(v,\theta) + \frac{\partial^2}{\partial \theta \partial v} D_{\theta,v}^{(2)}(v,\theta) + \frac{\partial^2}{\partial v \partial \theta} D_{v,\theta}^{(2)}(v,\theta) + \frac{\partial^2}{\partial \theta^2} D_{\theta,\theta}^{(2)}(v,\theta) \right) \right] p(v,\theta;t) \quad (4.21)$$

Rewritten in this form, $D^{(1)}$ is the drift vector, and D_v and D_θ are the components of the vector. $D^{(2)}$ is the diffusion matrix, and again the subscripts indicate the entries in the diffusion matrix. When written in this form, it is easy to see how the Fokker-Planck equation can be generalized to higher dimensions, by adding more terms to the drift vector and the diffusion matrix. However, if the two terms are independent, the two-dimensional Fokker-Planck equation becomes two one-dimensional Fokker-Planck equations. Such a change reduces the number of constants in the equations and makes the potentials equations of one variable. In addition, such a change allows for easier solutions of the partial differential equation.

One way to qualitatively check for independence of the speed and angular velocity is to split the distribution by range of angle, and check that all follow the same qualitative distribution. From the arc length analysis, one expects that the speeds follow an exponential distribution, centered around a value close to zero.

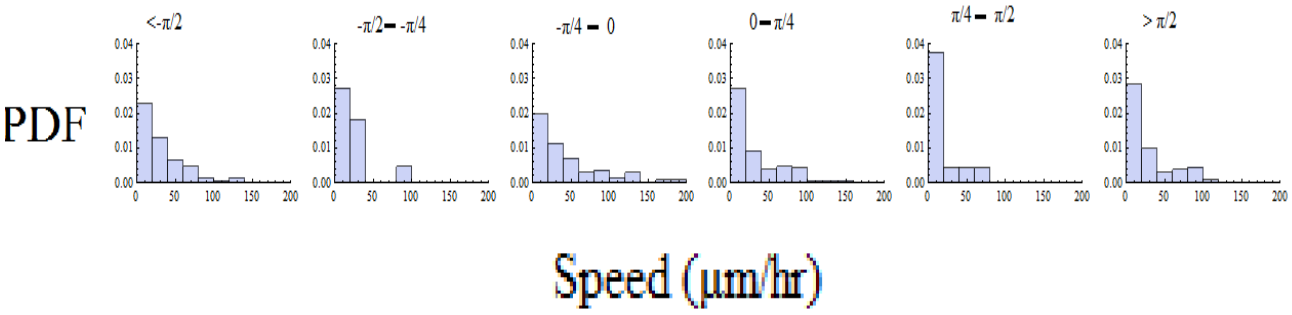

Fig 4.6: The speed distribution for different ranges of θ. Qualitatively, the distributions are the same, so the speed and angle are independent.

Quantitatively, the dependence between the speed and angle can be tested using a Kendall-Tau test, which has a test statistic of -.014 and a p-value .72, strongly indicating that the speed and angle are independent. In addition, the calculated correlation between the speed and angle is -.003. All these factors considered together lets one conclude independence and split the distribution into a speed and angle component.

To confirm the consistency of the two dimensional data with the one dimensional arc length data, the change in arc length in the two dimensional data can be approximated as follows:

$$v_{arc\ length} = v\cos(\theta) \tag{4.22}$$

This is a projection of the growth onto the previous path of growth. If the growth or retraction is continuing in the same direction, the change of arc length of the neuron is the same as the change is position. On the other hand, if the growth is perpendicular to the previous path, the neuron is not truly extending or retracting, but exploring the nearby area, assuming that the neuron does not make a sharp turn, on the order of microns.

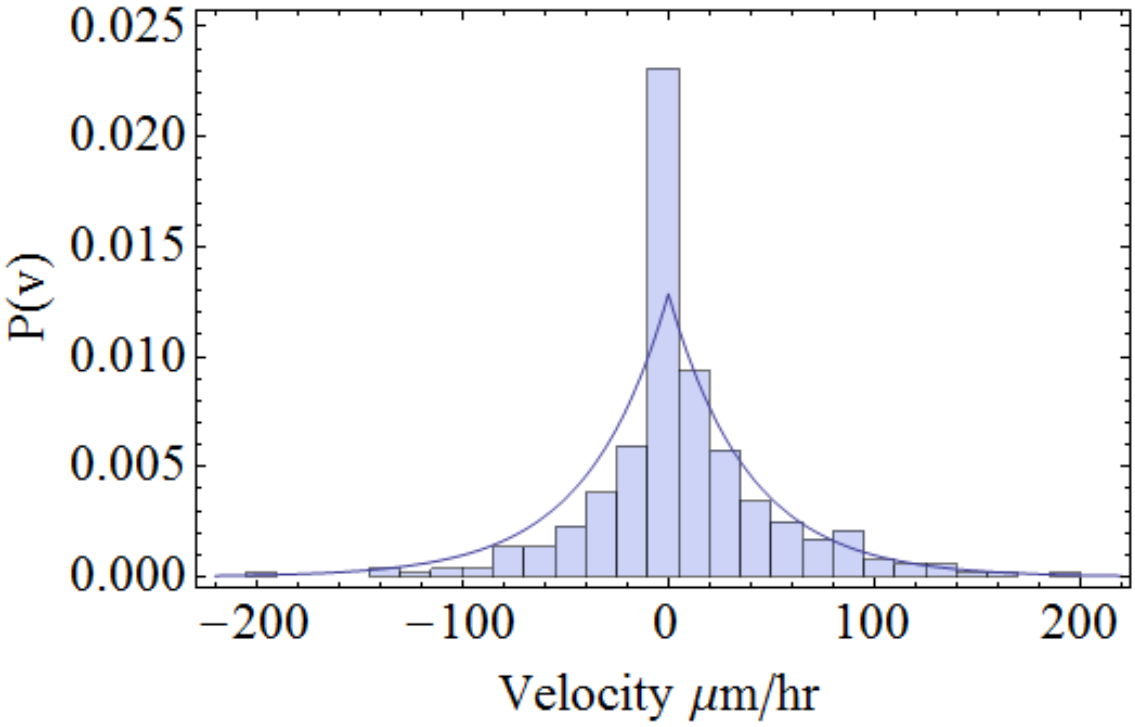

Fig 4.7: Histogram for the velocity, defined as a projection of the speed onto the path of the neurite, with the best-fit Laplace distribution, with mean 0 μm/hr, and scale parameter 38.8 μm/hr.

Unlike the arc-length case, now the Laplace distribution does not fit the data well around zero, because the distribution around zero has a much stronger peak than the arc-length case. However, the tails of the distribution are still reasonably exponential in shape. So I still use the analysis outlined above to model the velocities in the two dimensional case.

The same formalism will be applied to the angular variable, where a stationary potential is found, which governs the time evolution of the system. With a description for the angular and speed components, there will a complete model for the time evolution of the whole system.

Stepping back briefly from the angle defined above, one can also consider the angle of the neurite on the surface. On glass, there are no overall directional cues, and for all the neurons, the surface should be isotropic, so no surface direction should be favored. So given the lack of any directional cues, the x-axis is defined as on the orientation of the camera. Therefore, a uniform distribution is expected, which is confirmed by the data, as in the figure below:

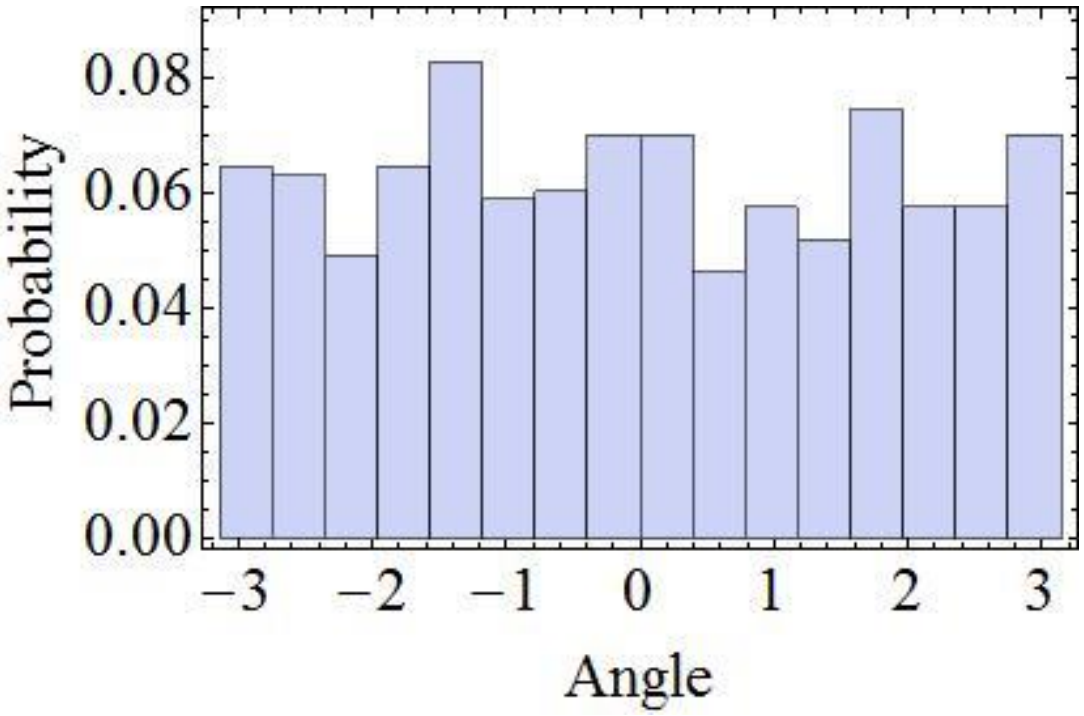

Fig 4.8: The surface angle of the neurite. As expected, the distribution is approximately uniform.

Now returning to the previous definition of angle, present again below:

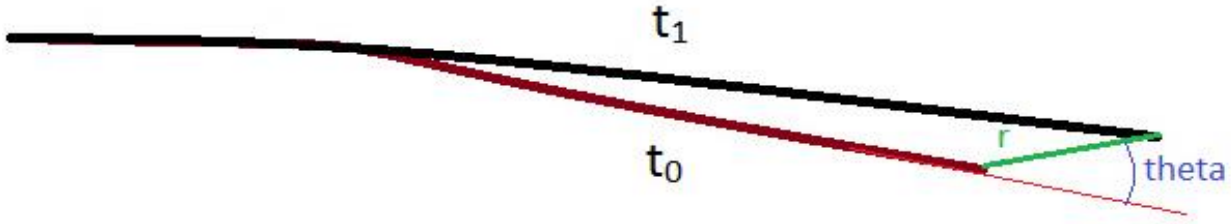

Fig 4.9: The definition of angle, relative to the direction of previous growth

Sharp turns are rarely observed in the samples, so the distribution of angles is expected to be bimodal, with the peaks at 0 and π, corresponding to extension and retraction respectively.

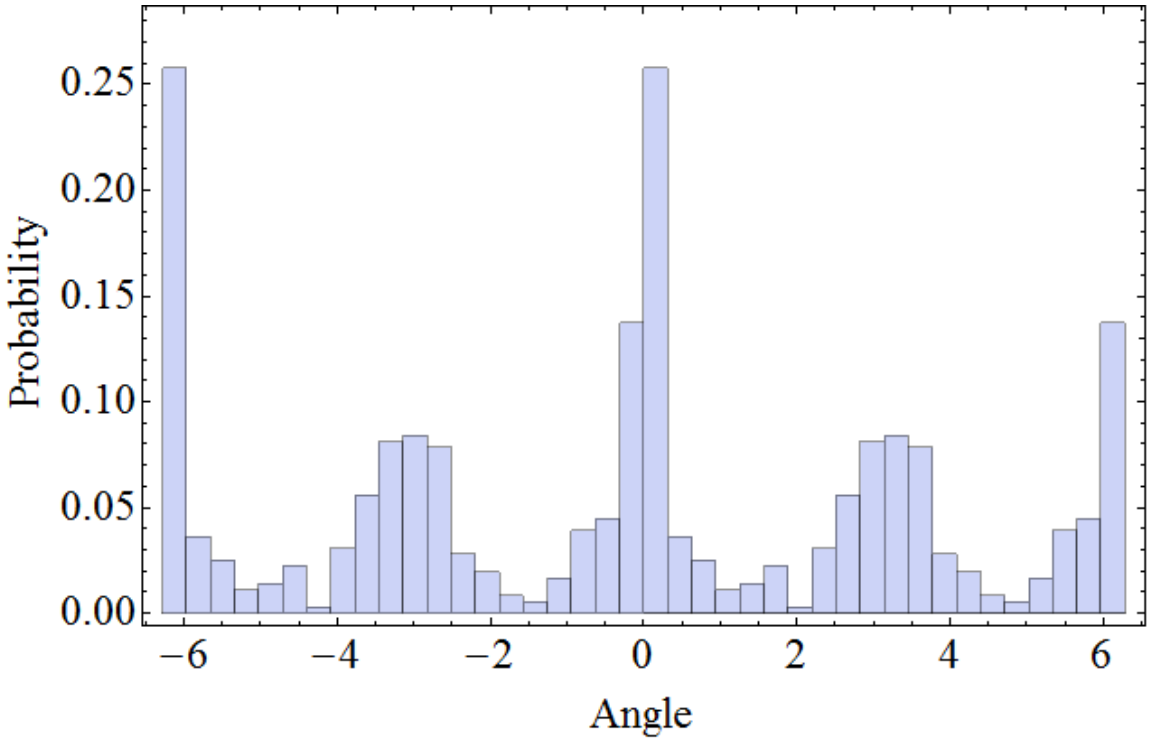

Fig 4.10: Two periods of the angular histogram, with peaks at nπ

As expected, there are two peaks at 0 and π, with the peak at zero much larger, corresponding to the overall growth of a neurite over time. Just as before, the stationary potential is the negative logarithm of the stationary probability distribution. In this case, the form of the stationary potential is assumed to be

$$V(\theta) = C + k\,Cos(2\theta) \tag{4.23}$$

Such a form captures the bimodal property of the distribution, with minima of the potential at 0 and π, corresponding to the peaks of the distribution. Conversely, the potential has maxima at π/2 and 3π /2. Such a potential also captures the behavior where the neurite can turn quickly, but tends to grow in an approximately straight direction.

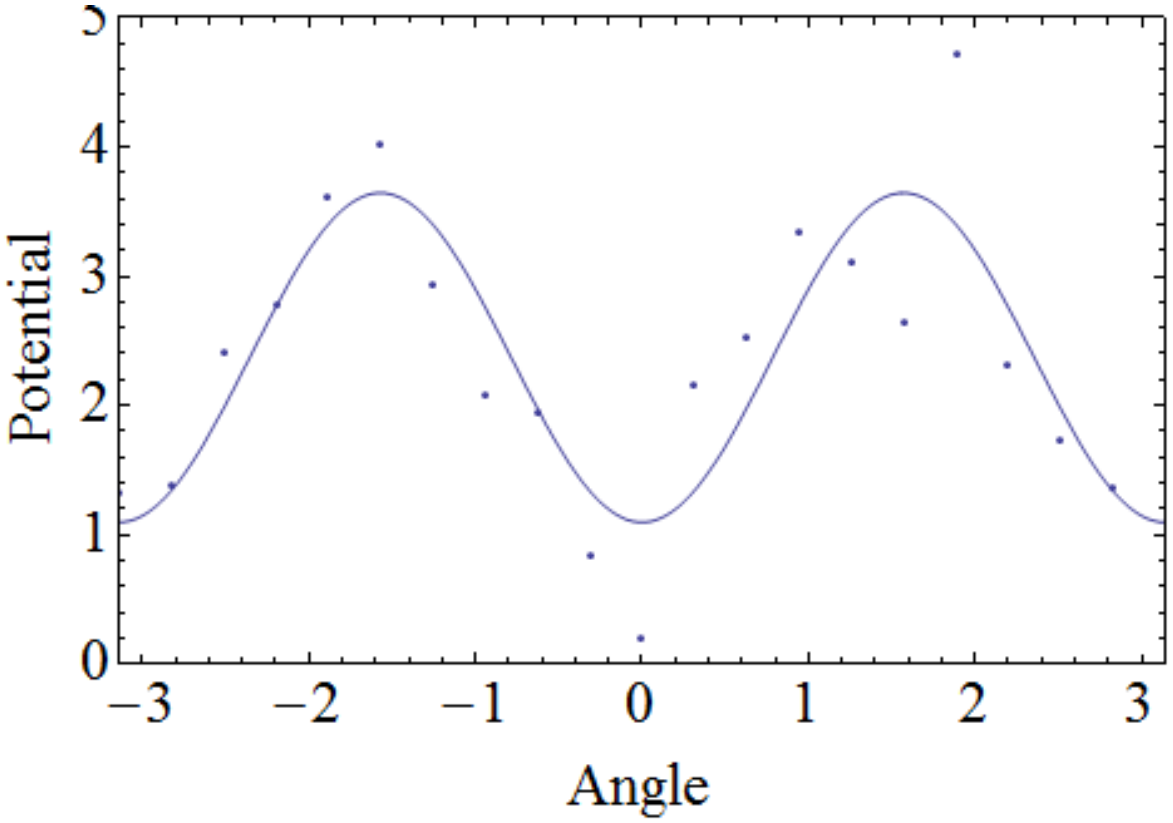

Fig 4.11: The line is the stationary potential, of the form -2.37 – 1.27 Cos(2 θ). The points correspond to the negative logarithm of the histogram.

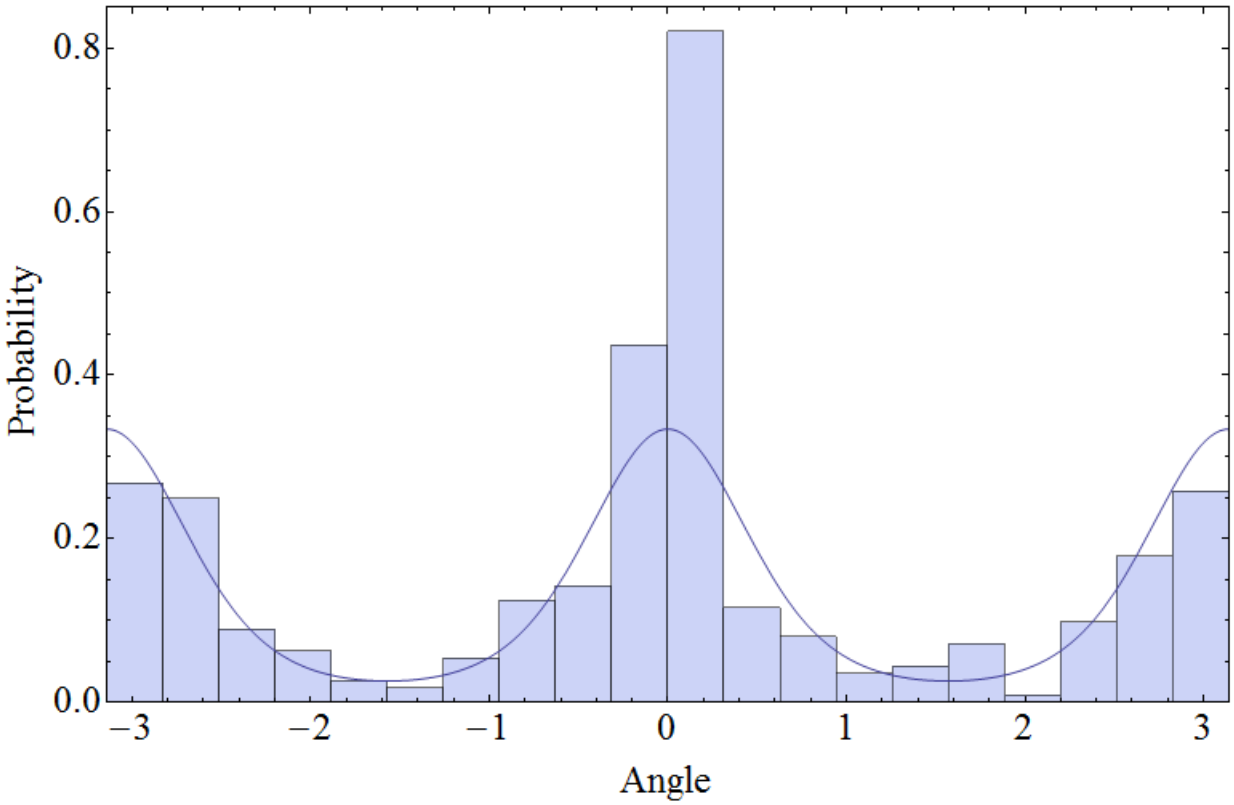

Fig 4.12: Angular histogram with the stationary probability distribution from the stationary potential overlaid.

As before, the time-dependent probability distributions can be calculated from the stationary potential given an initial condition. Unlike the case for the V-shaped potential, I will not use transformations to the Schrodinger equation, but rather use a different method to find the time dependent distribution, as described in [1,2].

First, assume a separation ansatz and for the ease of notation let $\phi = 2\theta$, so ϕ has one period over cosine:

$$P(\phi, t) = \Phi(\phi)e^{-\lambda t} \tag{4.24}$$

Rewriting the Fokker-Planck equation:

$$\frac{\partial P}{\partial t} = \left[\frac{\partial}{\partial \phi}[V'(\phi)] + D\ \frac{\partial^2}{\partial \phi^2}\right] P. \tag{4.25}$$

So define the Fokker-Planck operator, L:

$$L = \frac{\partial}{\partial \phi}[V'(\phi)] + D\ \frac{\partial^2}{\partial \phi^2} \tag{4.26}$$

With potential:

$$V(\phi) = -2.37 - 1.27\ Cos(\phi\ ). \tag{4.27}$$

More generally, where k is the constant from the potential divided by D, the diffusion coefficient, or i.e. set D to be 1.

$$V'(\phi) = k\ Sin(\phi). \tag{4.28}$$

Naturally, this leads to the following eigenvalue problem:

$$L\ \Phi(\phi) = -\lambda \Phi(\phi) \tag{4.29}$$

The potential has periodicity of 2 π, suggesting that a Fourier Expansion is a natural way to write the eigenstates:

$$\Phi(\phi) = \sum_{n=-\infty}^{\infty} c_n e^{i\,n\,\phi} \tag{4.30}$$

Inserting the Fourier expansion into the eigenvalue equation

$$\frac{n}{2}\, k\, c_{n-1} + \left(\lambda - \frac{n^2}{k}\right) c_n - \frac{n}{2} c_{n+1} = 0 \tag{4.31}$$

This is a system of infinite equations, and therefore, the coefficients are determined from an infinite matrix. However, the c_n corresponding to large eigenvalues decay rapidly, so the matrix can be terminated at some size, S, to approximate the solution. Therefore, one finds the eigenvalues and eigenvectors of the following matrix, centered around row n

$$\begin{pmatrix} \ddots & & & & \\ & \frac{n-2}{k} & \frac{n-2}{2} & 0 & 0 \\ & -\frac{n-1}{2} & \frac{n-1}{k} & \frac{n-1}{2} & 0 \\ & 0 & -\frac{n}{2} & n/k & n/2 \\ & 0 & 0 & -\frac{n+1}{2} & \frac{n+1}{k} \\ & & & & \ddots \end{pmatrix}$$

In this case, n ranged from -300 to +300, which is a matrix of 601 rows. The constants, c_n can be chosen to be real or imaginary. Real c_n correspond to symmetric eigenfunctions, and imaginary c_n correspond to antisymmetric eigenfunctions. Thus each eigenfunction can be denoted by Φ_μ^i, where λ_μ is the μth eigenvalue, and i denotes whether the eigenfunction is the symmetric (s) or antisymmetric (a) eigenfunction.

However, the operator L is not hermitian, so a related hermitian operator is introduced, L_H, defined as follows:

$$L_H = e^{\frac{\chi}{2}} L\, e^{-\frac{\chi}{2}} \tag{4.32}$$

With

$$\chi = k \cos\phi$$

Note that L_H has the same eigenvalues as L, so the eigenfunction of L_H are related to the eigenfunctions of L:

$$\eta_\mu^i(\phi) = e^{\frac{\chi}{2}}\Phi_\mu^i(\phi) \tag{4.33}$$

Unlike the eigenfunctions of L, the eigenfunctions of L_H can be normalized, leading to the normalization condition of the eigenfunctions of L_H:

$$\int_0^{2\pi} \eta_\mu^i \, \eta_\nu^j \, d\phi = \delta_{\mu\nu}\delta_{ij} \tag{4.34}$$

Transforming back to the operator L, the normalization condition for L is as follows:

$$\int_0^{2\pi} \Phi_\mu^i \, \Phi_\nu^j \, e^{\chi} d\phi = \delta_{\mu\nu}\delta_{ij} \tag{4.35}$$

Thus, all the Fourier coefficients, c_n^μ can be found for each eigenstate, and with the normalization the coefficients for the eigenfunction expansion, $d_\mu^{a,s}$ are computed from the initial condition:

$$P(\phi, 0) = \sum_{\mu=0}^{\infty} (d_\mu^s \, \Phi_\mu^s(\phi) + d_\mu^a \, \Phi_\mu^a(\phi)) \tag{4.36}$$

Adding in the time dependence, the time evolution is governed by:

$$P(\phi, t) = \sum_{\mu=0}^{\infty} e^{-\lambda_\mu t}(d_\mu^s \, \Phi_\mu^s(\phi) + d_\mu^a \, \Phi_\mu^a(\phi)) \tag{4.37}$$

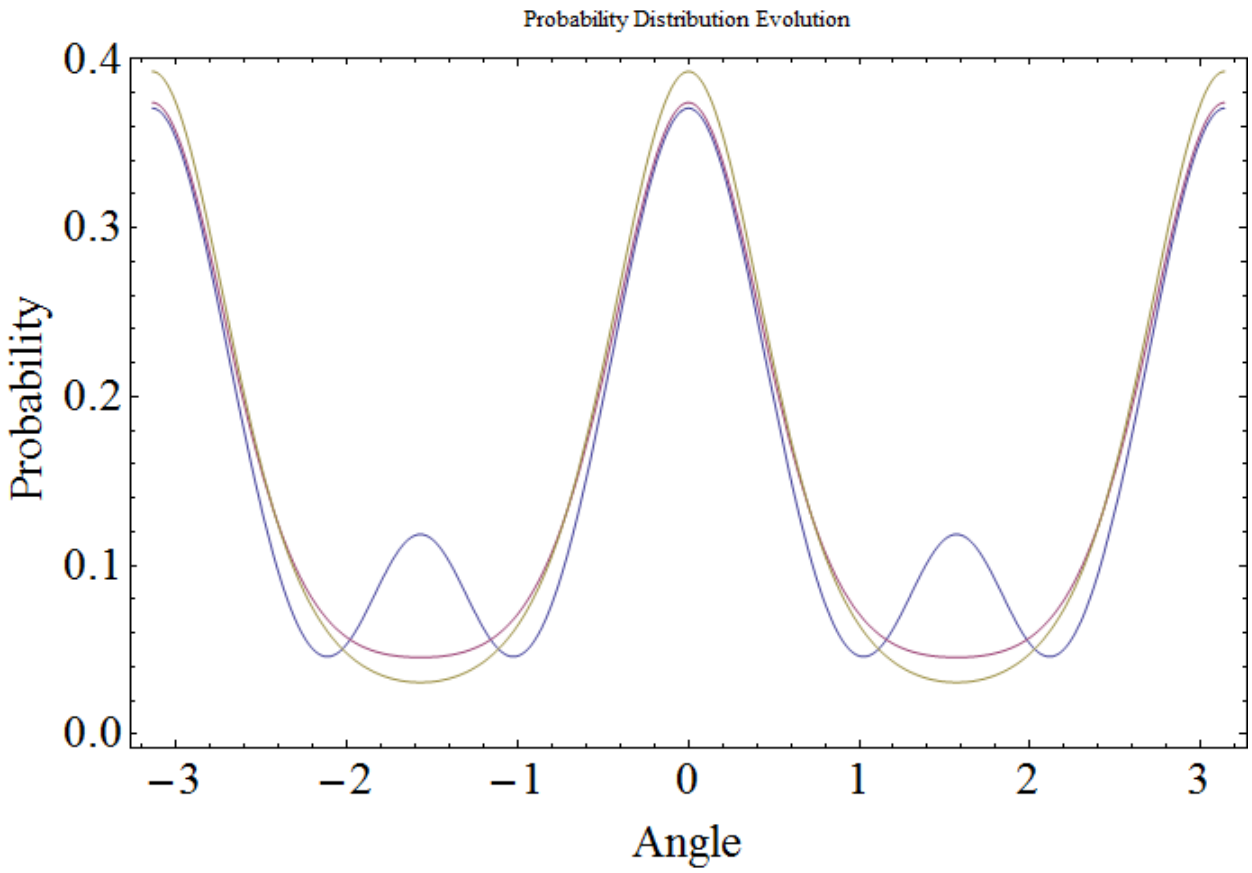

Fig 4.13: Time evolution of the angular distribution from a delta function initial condition. The blue curve is ¼ hours, the red curve is 2 hours, and the green is the stationary distribution.

With the potential for the angular distribution, the neuron growing on glass is described by two potentials of the form:

$$V_v(v) = \kappa\, v + C$$
$$V_\theta(\theta) = \sin(2\theta) + C \tag{4.38}$$

For each parameter, a delta function initial condition is used, which allows for the complete description of the time evolution of the system. The separation of variables is used because the growth rate and the angular velocity are independent on glass.

5. Neuronal Growth on Directional Surfaces

5.1 Ratchet Topography on Nano-PPX

This section follows work in *Effects of surface asymmetry on neuronal growth* by Elise Spedden, Matthew Wiens, Melik Demirel, and Cristian Staii submitted to Biophysical Journal.

Thus far, neurons have been restricted to growing on glass, a substrate without any further mechanical, electrical or chemical guidance cues. However, it is previously known that altering the substrate affects the outgrowth of axons. For example, cell differentiation depend on surface stiffness, where one study showed that embryonic rat cortexes grown on a substrate of 6 nN/μm favored glial cells over neurons, and on a surface of .75 nN/μm, the opposite was true.[32]. In addition, previous work has qualitatively described the impact of surface topography on neuronal growth. For surfaces with ridges on the order of micrometers wide and nanometers deep, neurons tend to grow in the valleys if the ridges are sufficiently wide and deep, and would grow over the ridges if the ridges were wide or shallow. [33]

Substrates with non-uniform surface topography can be manufactured uses a number of different materials. One such material is poly(chloro-p-xylylene), referred to as nano-PPX. The nano-PPX surface consists of a forest of rods, which can be bent to introduce non-uniform surface topography.

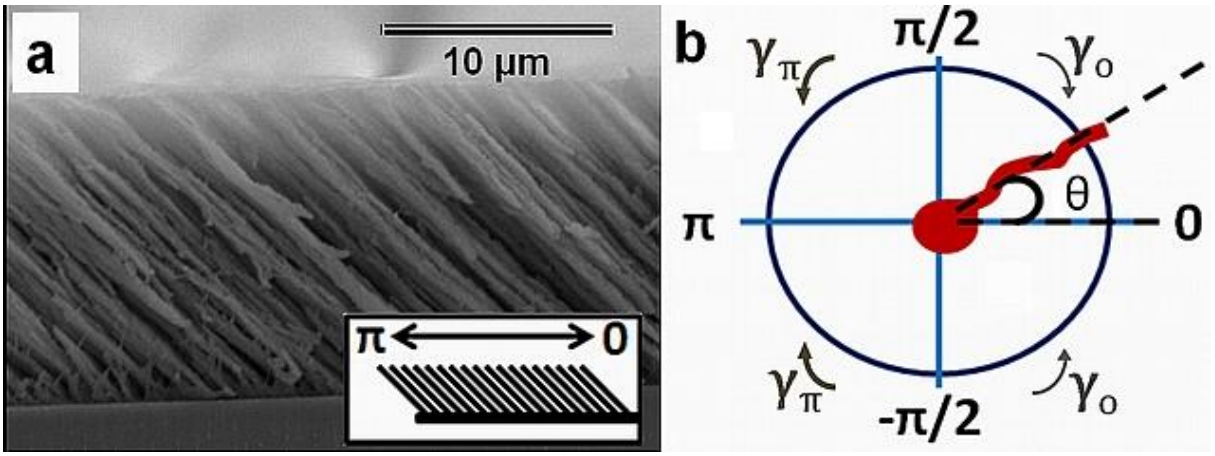

Fig 5.1: (a) SEM image of the tilted nano-PPX rods. (b) the definition of angles with respect to the surface.

The nano-PPX surface is coated with Poly-D-lysine to promote growth of neurons. On the surface, the angle of growth with respect to the surface now has a physical significance, because the substrate is anisotropic. The zero angle is defined to be against the direction of the tilt, with the π angle is defined to be in the direction of the tilt, as is fig 5.1.

The tilting of the nanorod structure introduces further emergent topographical properties, namely a ratchet structure. The details of the ratchet depend on the tilt of the rods, as the rods clump together to form pillars. Using atomic force microscope (AFM) scans, the ratchet can be quantified using two angles, α_π and α_0. α_π is the angle formed by the ratchet in the direction of the rod tilt, hence the π label, from the angle defined above. Similarly, α_0 is the angle in the direction opposite the rod tilt. The ratchet structure can be characterized by these two angles, but is more simply quantified using the ratio of the angles:

$$C_\alpha = \frac{\alpha_\pi}{\alpha_0} \tag{5.1}$$

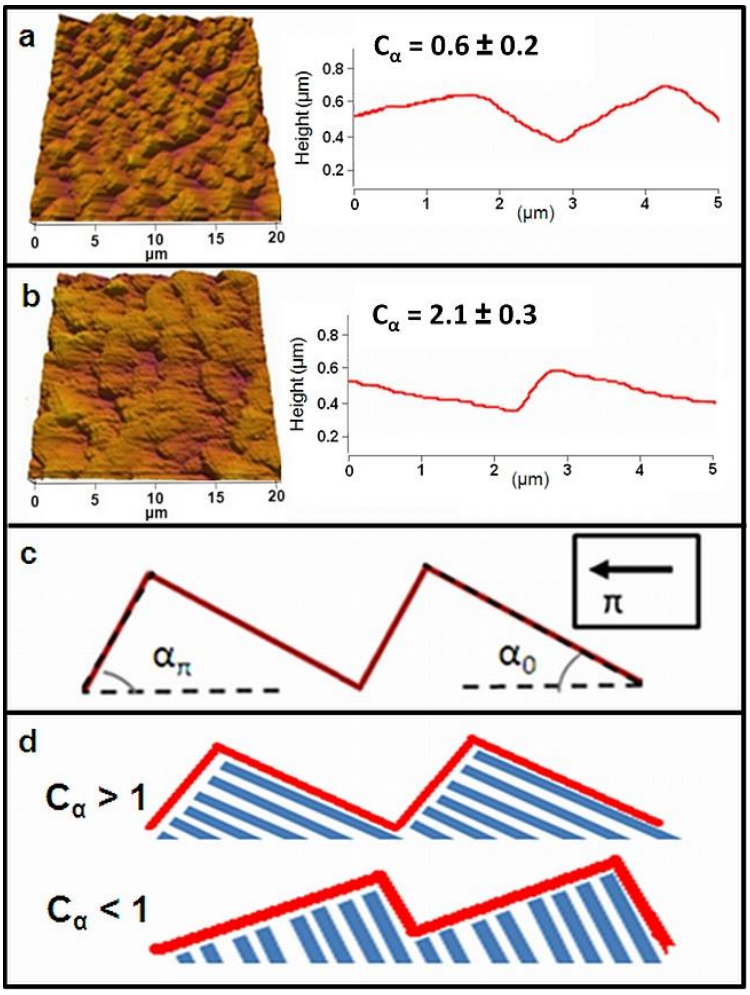

Fig 5.2 (a,b) AFM scans of the nano-PPX surface with ratchet structure. (c) Definition of α_π and α_0. (d) C_α in two different regimes: *<1*, and *>1*

The effect of the ratchet structure is further examined by creating ratchet structures will different surface topographies (fig 5.3).

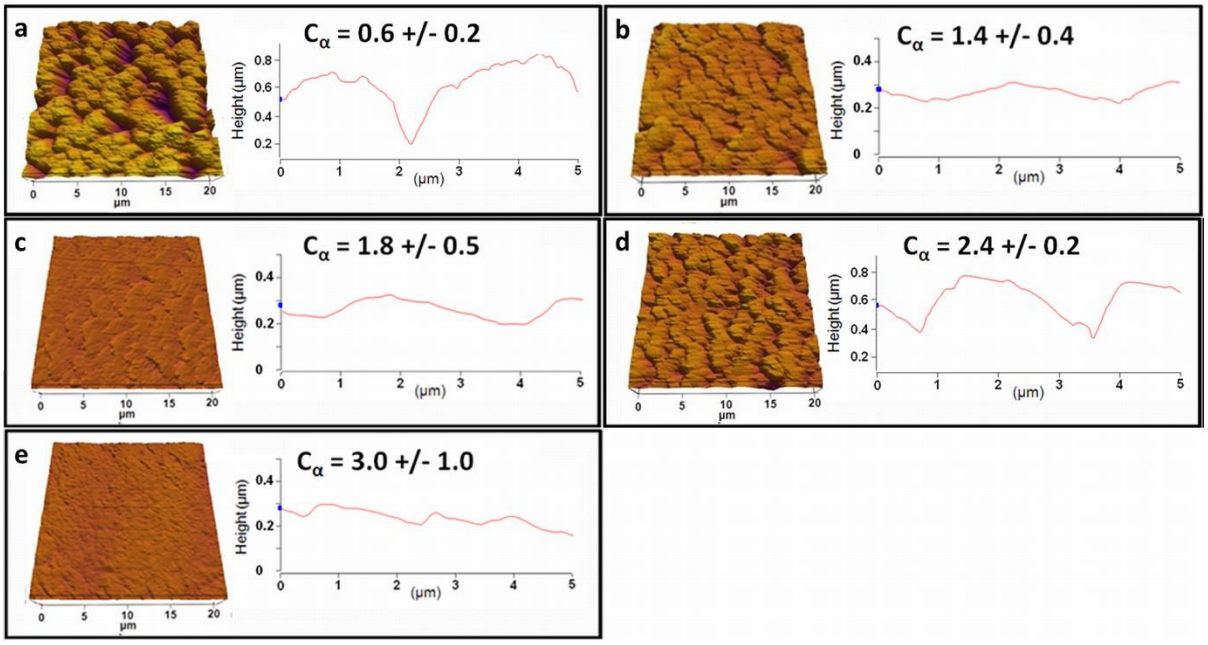

Fig 5.4 Additional nano-PPX surfaces with the ratchet topography, and AFM line scan across the surface.

The cortical neurons were cultured for five days on each of the nano-PPX surfaces. In all cases, growth is preferred along the direction of the ratchets, and opposite to the directions of the ratchet, the 0 and π directions. However, the bias for each direction is not equal. The growth is always preferential in the direction of the ratchet, but the difference in growth in the ratchet direction and opposite the ratchet direction depends on the underlying surface, i.e. C_α.

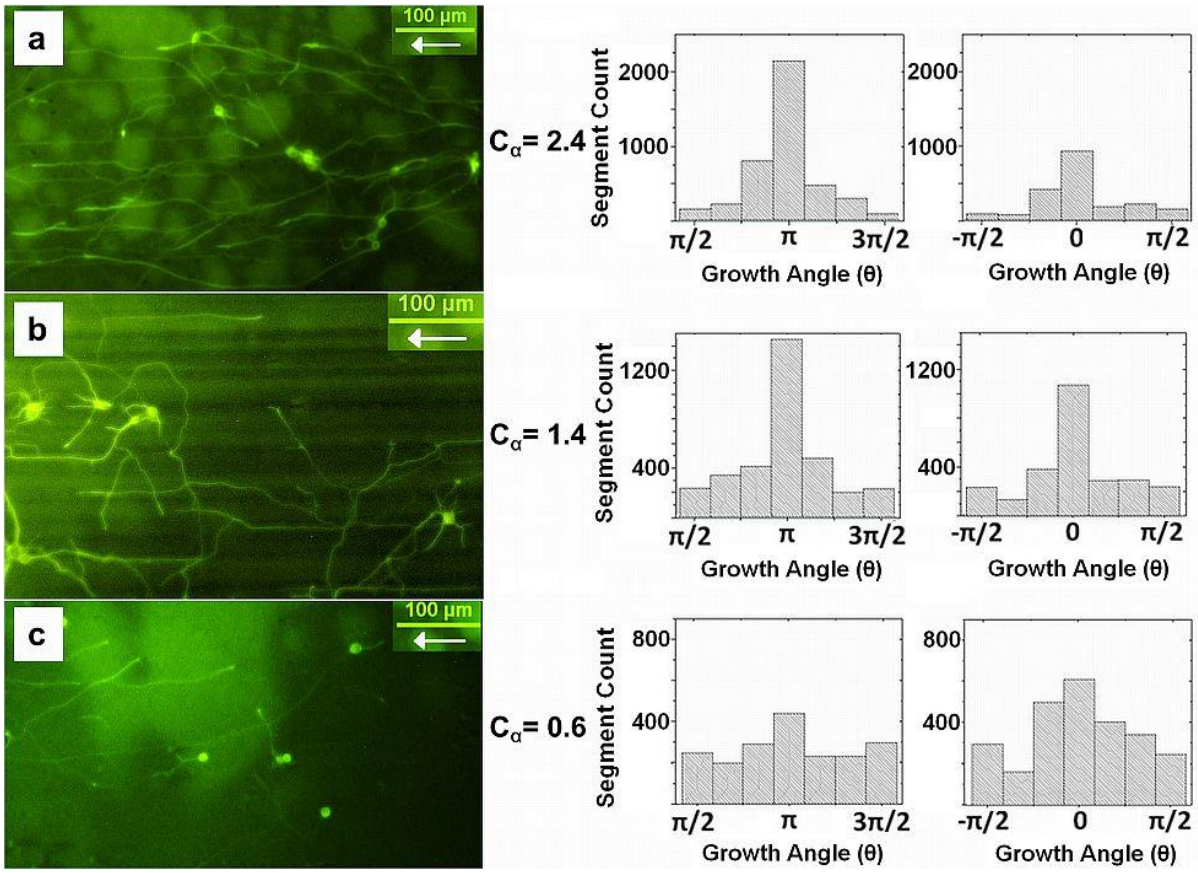

Fig 5.5 Fluorescent image of growth on nano-PPX surface for three different ratchet topographies: C_α = 2.4, 1.4 and 0.6.

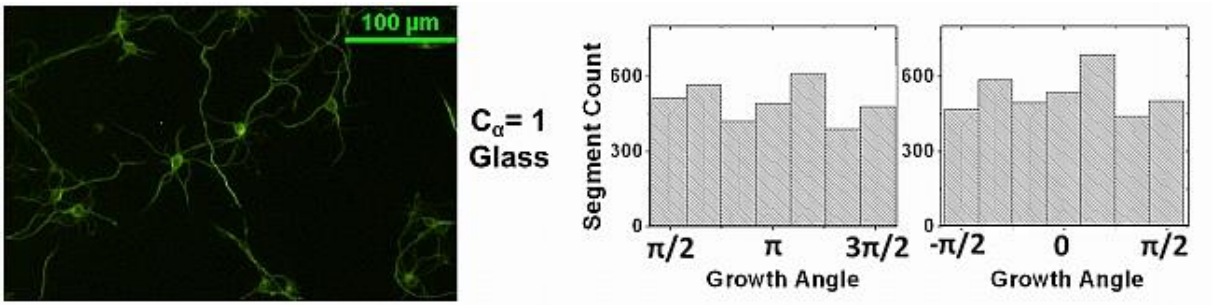

Fig 5.6 Fluorescent image of neurons grown on glass. No directional bias is observed.

The effect of topographical cues on the growth cone and guidance systems of the neuron can be further investigated through the use of drugs such as Taxol and Blebbistatin. Both drug modify the cytoskeleton; Taxol stabilizes microtubules, and Blebbistatin disruption myosin II, a key component of actin filament crosslinking. In the case of Taxol, a 10 nM dose was used on the surfaces with C_α = 1.8 and C_α =2.4. The neurons with Taxol show a decrease in directional growth, and no bias between the 0 and π angles. However, the growth cones still navigate on the

surface, indicating that chemotactic signaling was not inhibited. For Blebbistatin, a 10 nM dose was again used, but on the surfaces with $C_\alpha = 0.6$ and $C_\alpha = 2.4$. The effect for Blebbistatin was much the same as for Taxol: the directional bias in the 0 and π directions was reduced, but cell-cell connections were not inhibited, again suggesting that Blebbistatin does not affect chemotactic signaling.

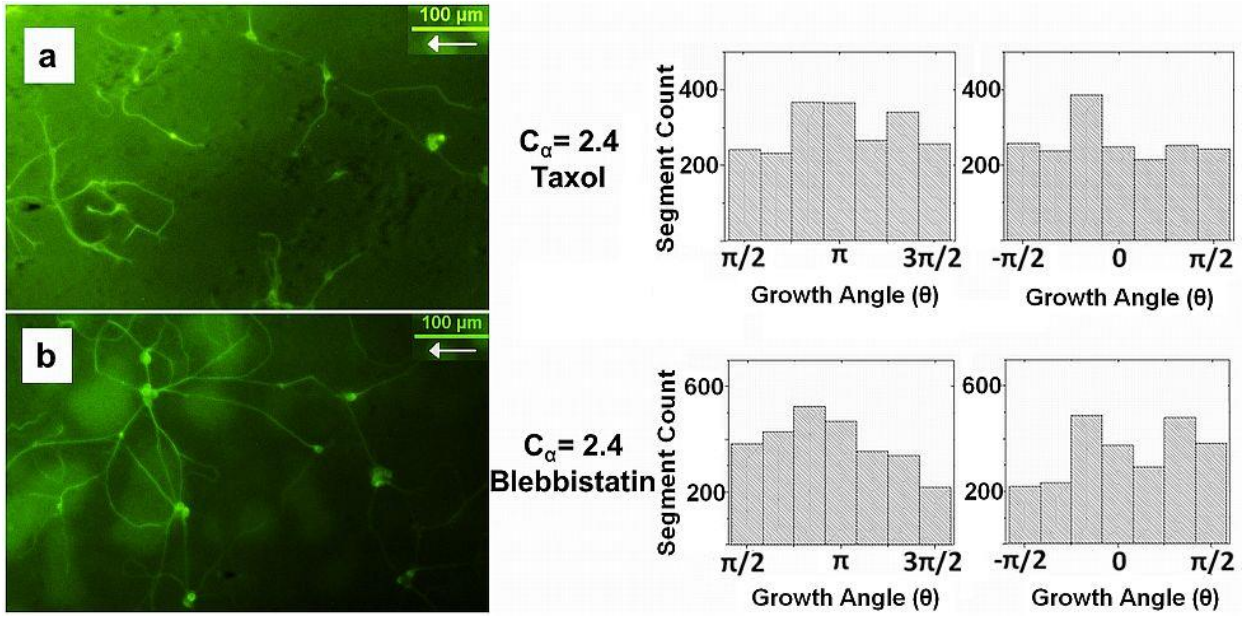

Fig 5.7 Neurons treated with (a) Taxol, and (b) Blebbistatin. There is a dramatic decrease in the directional bias in both cases.

The Fokker-Planck formalism previously developed is applicable to directional surfaces in much the same was as for glass. In the case of directional surfaces, consider the surface applying an effective torque to the growth of the neuron, directing the growth to π and 0, where the peaks in the angular distribution are observed. Such a situation is described by a Langevin equation:

$$\frac{dq(t)}{dt} = g \times \sin q(t) + G(t) \tag{5.2}$$

Such as model has been previously used in biology, for example the migration of human granulocytes in an electric field is modeled in the same way [7]. The first term on the right hand side serves as a deterministic torque, which is maximized when the neuron is growth along the ridges, and zero when the neuron is in a preferred state of growing over the ratchets. γ quantifies the strength of the torque, smaller values of γ lead to a noisier distribution, while larger values more quickly turn the axon to the preferred direction. *Γ(t)* is the random component of the growth, which can be considered as a stochastic torque. This captures the effect of growth

factors independent of the surface topography, such as chemotactic signaling. This function is assumed to be white noise:

$$\langle \Gamma(t) \rangle = 0$$
$$\langle \Gamma(t)\, \Gamma(t') \rangle = q\, \delta(t - t') \tag{5.3}$$

Where δ is the dirac delta, and q is the strength of the noise. Again as before, the Langevin equation has a corresponding Fokker-Planck equation:

$$\frac{\partial p(\theta, t)}{\partial t} = [\gamma \sin(\theta)\ p(\theta, t)] + D_\theta \frac{\partial^2 p(\theta, t)}{\partial t^2} \tag{5.4}$$

The Langevin and Fokker-Planck equations do not capture the asymmetry between the 0 angle and the π angle of growth. To introduce the difference between 0 and π, the strength of the torque, γ, is split into two constants, γ_0 and γ_π, each representing the semi-circle centered around 0 and π, respectively. Thus, using the same solution techniques as in the previous section, the stationary solution to equation 5.4 is

$$p(\theta) = A_{0,\pi}\, Exp\left[\frac{\gamma_{0,\pi}}{D_\theta} \cos(\theta)\right] \tag{5.5}$$

Where A is a normalization constant. To find the diffusion coefficient, D_θ, a best fit for all the angular distribution is performed, and D_θ is found using a maximum likelihood estimate. Using all the surfaces, an estimate of $D_q = 92 \pm^{5}_{7}$ rad^2/hr is found.

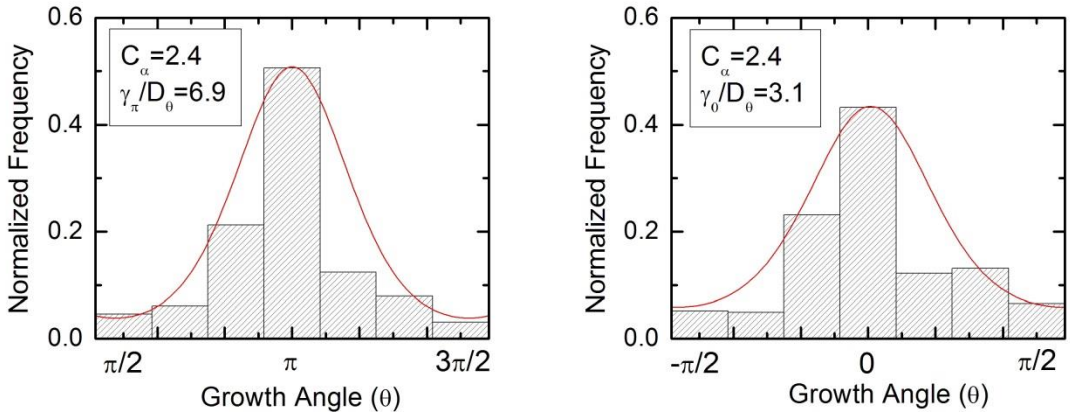

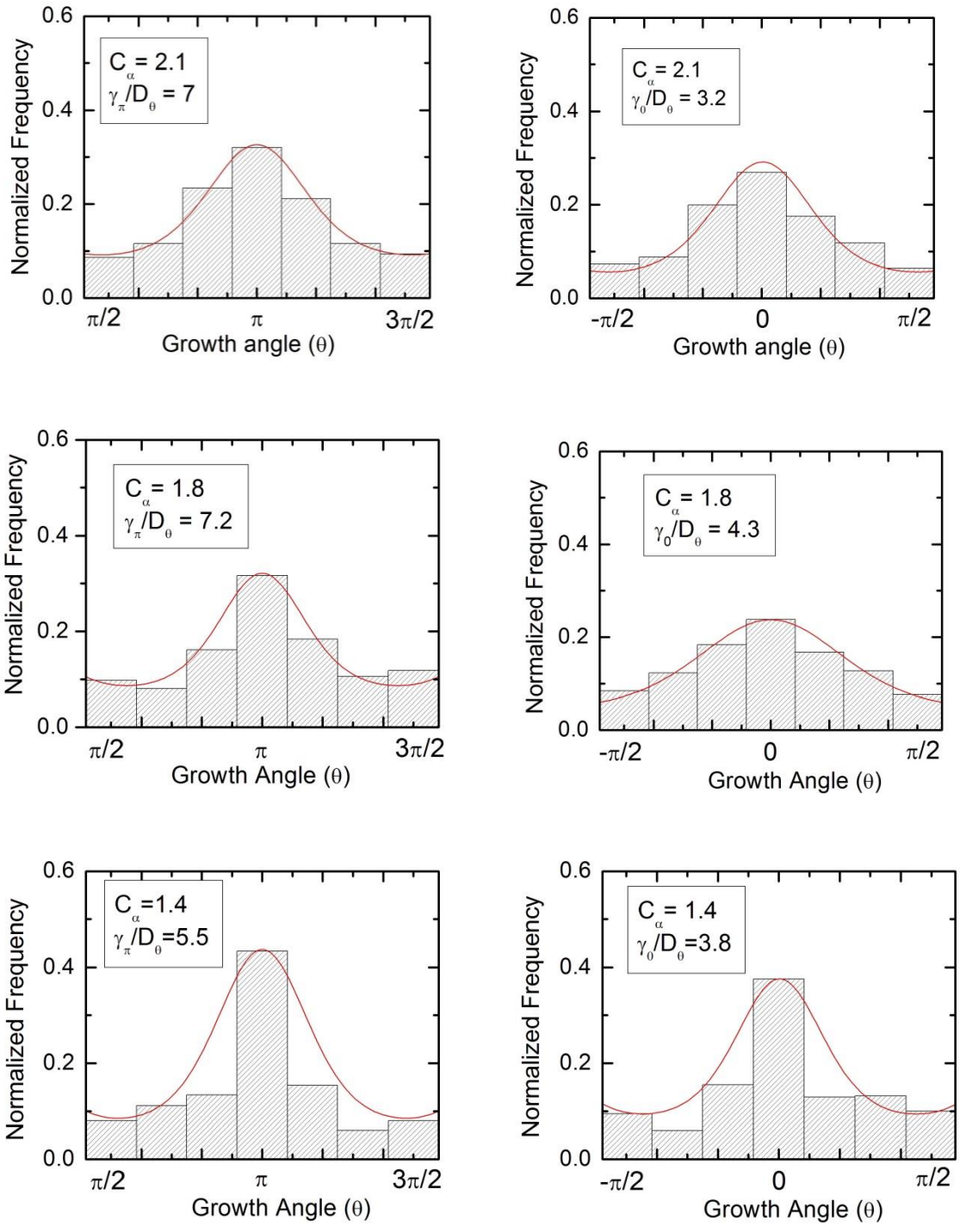

Fig 5.8 Frequency histogram with stationary distribution calculated through Fokker-Planck equation

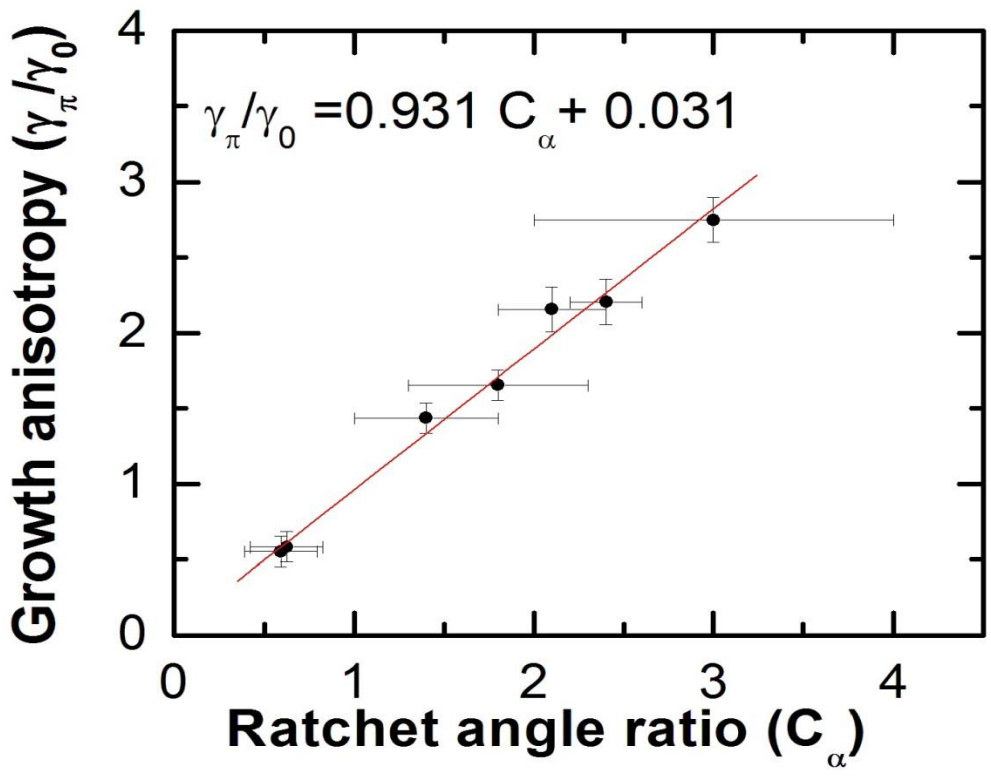

Fig 5.9 Linear dependence between ratchet angle and growth anisotropy

The dependence of the growth on the ratchet structure can be described by comparing the strength of the torque between growth in the 0 direction versus the π direction: γ_0/γ_π. This ratio is found to have linear relation with the ratchet angle ratio, C_α, indicating that the ratchet topography imparts directionality, and that the underlying rod tilt angle is not as important in axonal navigation.

5.2 The Effects of Cell Density on Directional Surfaces

The effects of a textured surface can be further investigated by varying the cell density of the plating. As cell density increases, more chemotactic cues and guidance molecules exist on the surface, strengthen the effects of those growth factors on neuronal guidance [9]. To investigate the effects, cells were plated on nano-PPX at densities of 2000, 6000, and 25000 cells/cm^2.

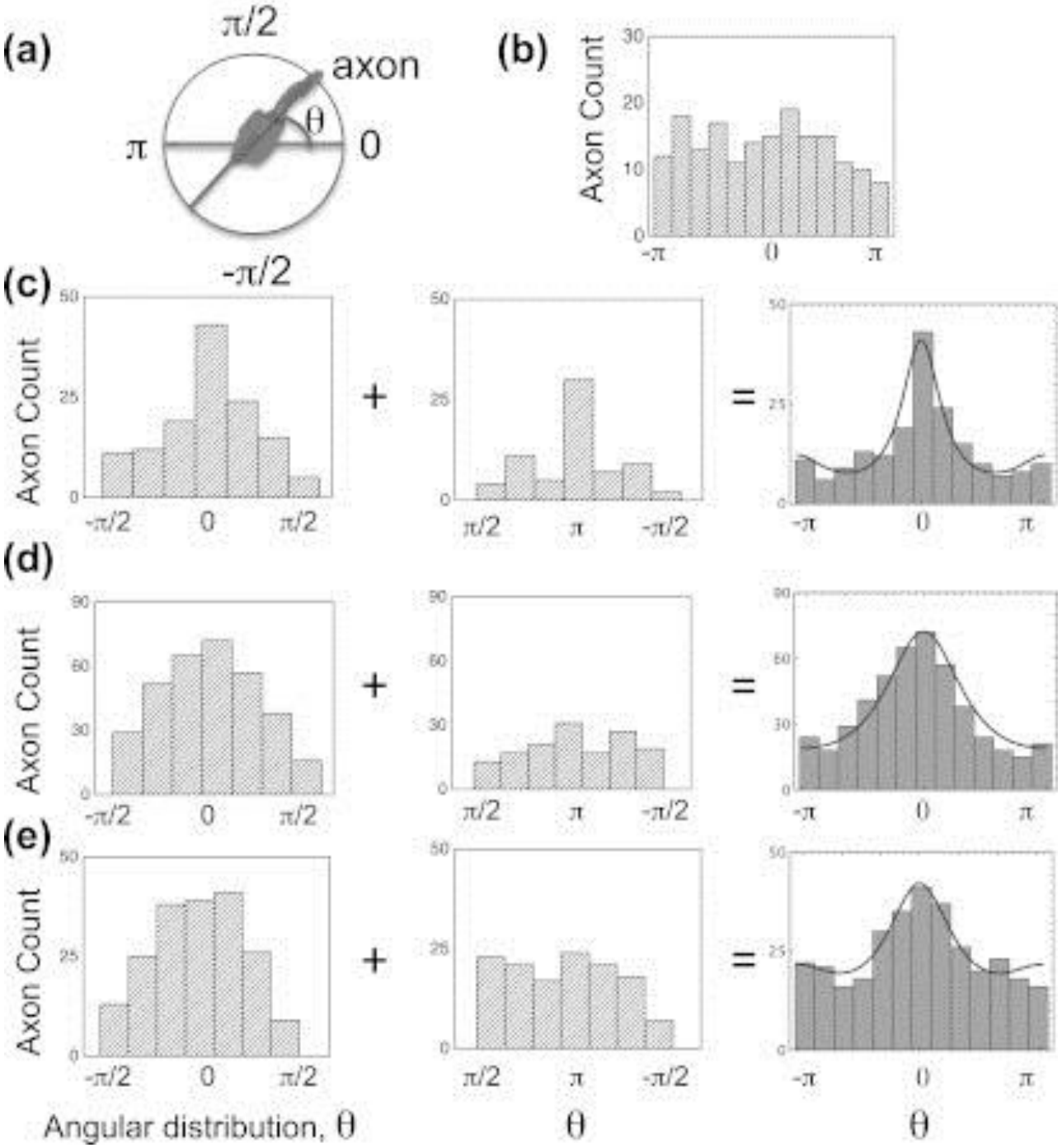

Fig 5.10 (a) Definition of angle with respect to the surface. (b) Glass surface at 2000 cells/cm^2, the control. (c) Nano-PPX at 2000 cells/cm^2. (d) Nano-PPX at 6000 cells/cm^2. (e) Nano-PPX at 25000 cells/cm^2. On Nano-PPX, peaks are seen at 0 and π, but with a weaker peak at π. The solid line is a theoretical fit of Brownian motion in a constant field [9].

At all cell densities there is a peak around 0, and at low cell densities, a peak around π. In all the cases, the peak is stronger in the 0 direction, indicating the stronger bias in growing opposite of the rod tilt. Furthermore, the distribution around the peak widens as the cell density increases, corresponding to the greater effect of cell-cell signaling.

As before, to quantify the effect of the field, a Langevin equation is introduced:

$$m\frac{d\boldsymbol{v}}{dt} = -\alpha\boldsymbol{v} + \boldsymbol{F} + \xi(\mathrm{t}) \tag{5.6}$$

Where m is the effective mass, α is the Stokes drag coefficient, F, is a constant force, and ξ is the random force of white noise $\langle\xi(t)\xi(t')\rangle = m^2\Gamma\mathrm{d}(\mathrm{t}-\mathrm{t}')$, where d is the dirac delta function [9]. The effect of the directional surface is introduced in two ways. First, there is assumed to be a constant force, and second the random force is not azimuthally symmetric, but axially symmetric. Three new parameters are introduced, which correspond to observables:

$$\begin{gathered}\gamma = \frac{\alpha}{m}\ (Reduced\ Drag) \\ v_0 = \mathbf{F}/\gamma \\ \kappa = v_o^2\,\gamma/\Gamma\end{gathered} \tag{5.7}$$

A Fokker-Planck equation corresponds to the Langevin equation, with the additional parameter δ, which is between -1 and 1 [9].

$$\frac{\partial p(v,t)}{\partial t} = \nabla[\gamma(v-vo)]p(v,t) + \left[(1+\delta)\frac{\partial^2}{\partial v_x^2} + (1-\delta)\frac{\partial^2}{\partial v_y^2}\right]p(v,t) \tag{5.8}$$

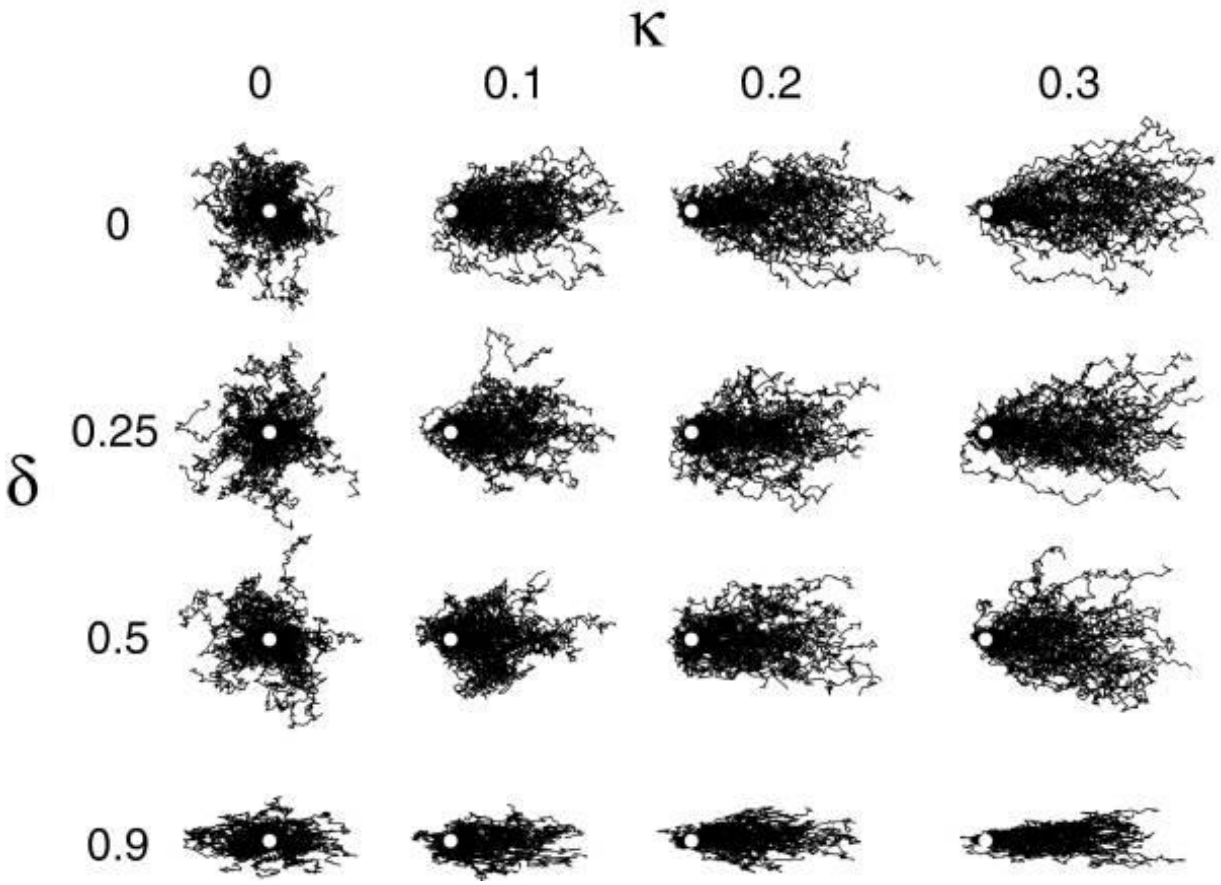

Fig 5.11 Images of 100 random walks with bias parameter κ, and azimuthal anisotropy parameter δ. The initial point of growth is indicated by a small white circle. [9].

From the experimental data, κ and δ can be estimated for each cell density. The values were estimated to be 0.17 ± 0.05 and 0.44 ± 0.08, 0.15 ± 0.03 and 0.06 ± 0.06, and 0.04 ± 0.01 and 0.17 ± 0.0 , for κ and δ respectively, and for 2000 cells/cm^2, 6000 cells/cm^2, and 25000 cells/cm^2. The value of κ decreases with cell density, which corresponds to the applied force on the growth cone balanced with the reduced drag force from chemotactic signaling. This model using the Langevin equation captures the directional effect of the surface, and the greater effect of an anisotropic surface at lower seeding densities [9].

5.3 Neuronal Growth on PDMS Surfaces with Ratchet Topography

From the last two major results presented, one concludes that the ratchet structure imparts directionality on the growing axon, not the rods or the nano-PPX surface itself, as long as the seeding density is not too high. To further investigate the effects of directional surfaces, a simpler surface, with more consistent ratchets is made from Polydimethylsiloxane (PDMS).

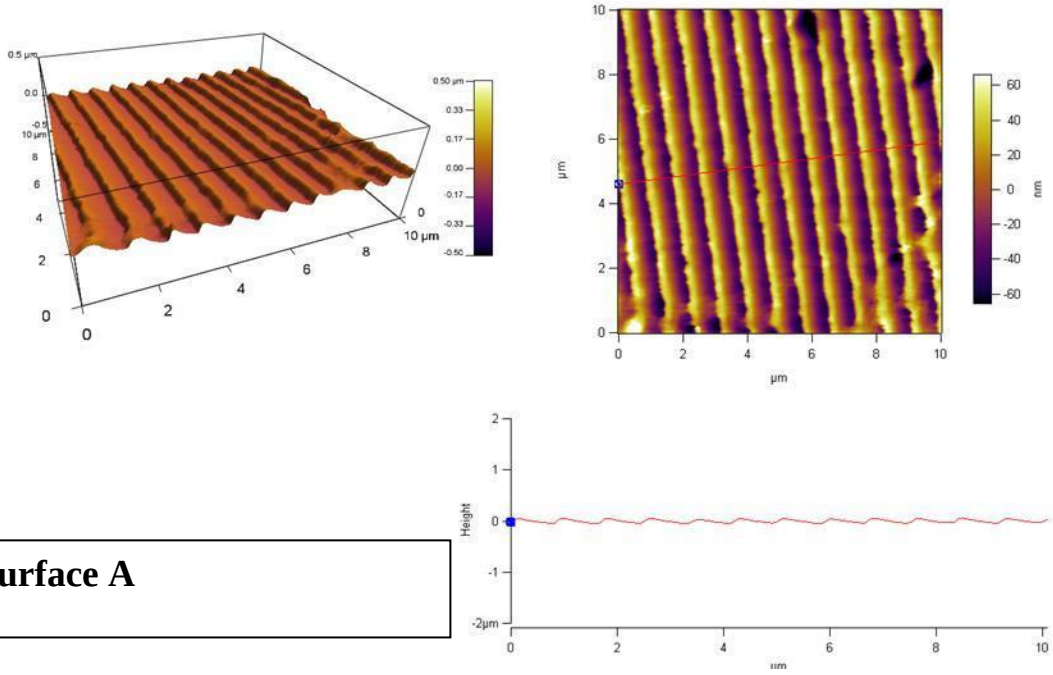

Surface A

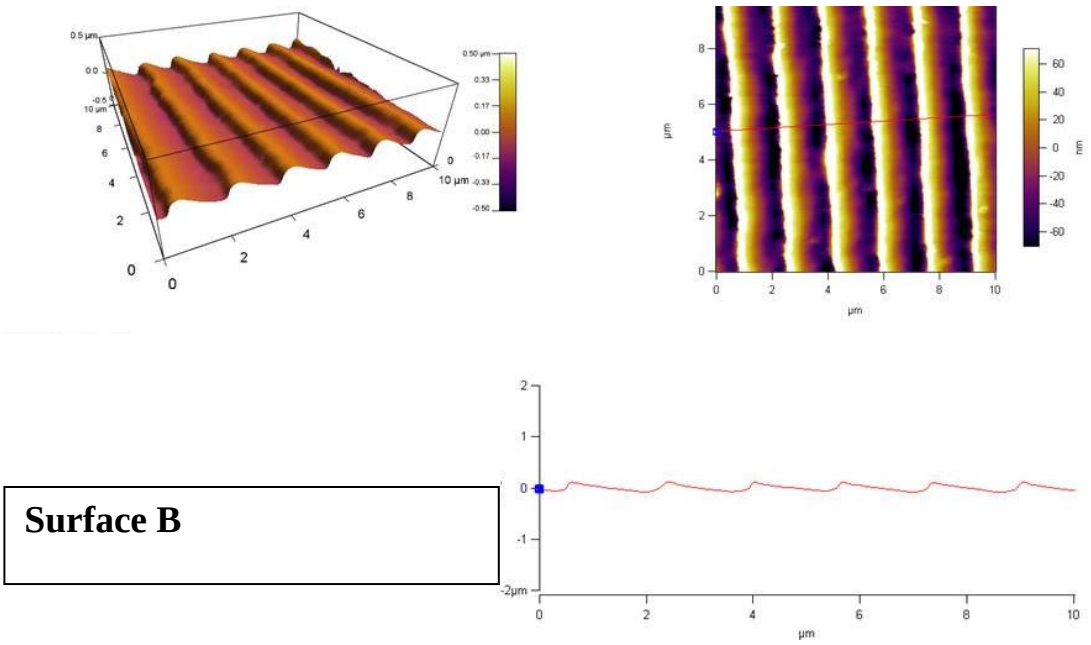

Fig 5.12 The PDMS surfaces, with AFM height scans. The two have a slightly different ratchet structure. Surface A has narrower and shallower ridges than surface B.

On surface 3, the neurons were imaged at 18 hours after plating. On sample 5, images were taken at 18 hours and 70 hours after plating. As before, the neurons are imaged every five minutes over 30 minutes, for a total of seven frames for each time lapse video.

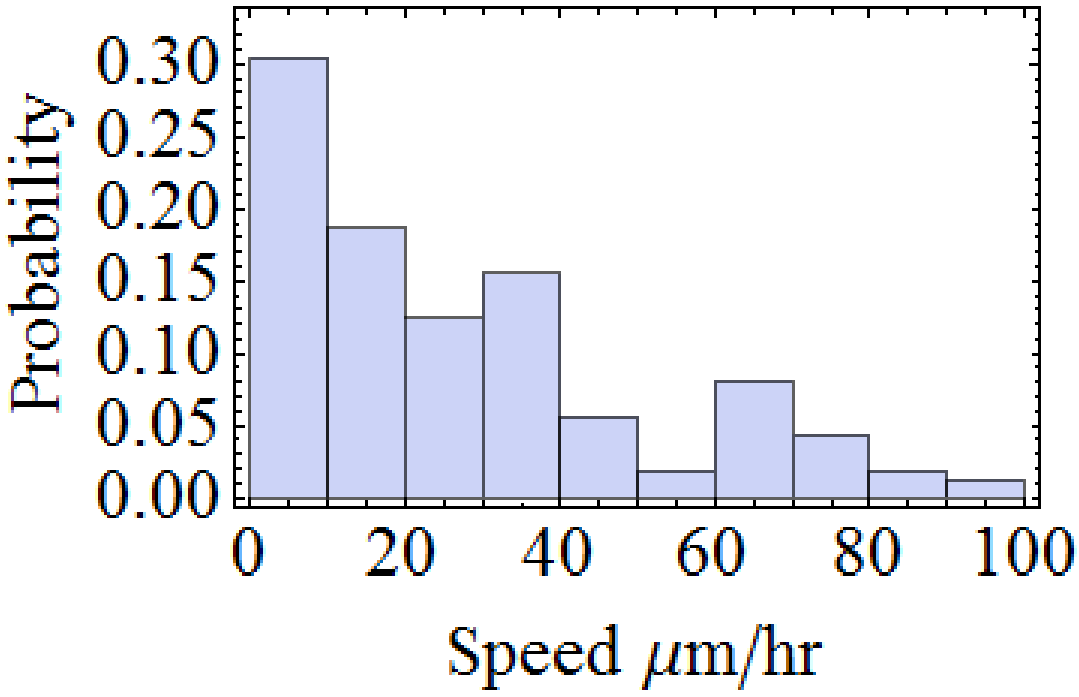

Fig 5.13 Distribution of the speed of the growth cone, on surface A, 18 hours after plating. The general exponential trend of the speed is preserved from the case of growth on glass.

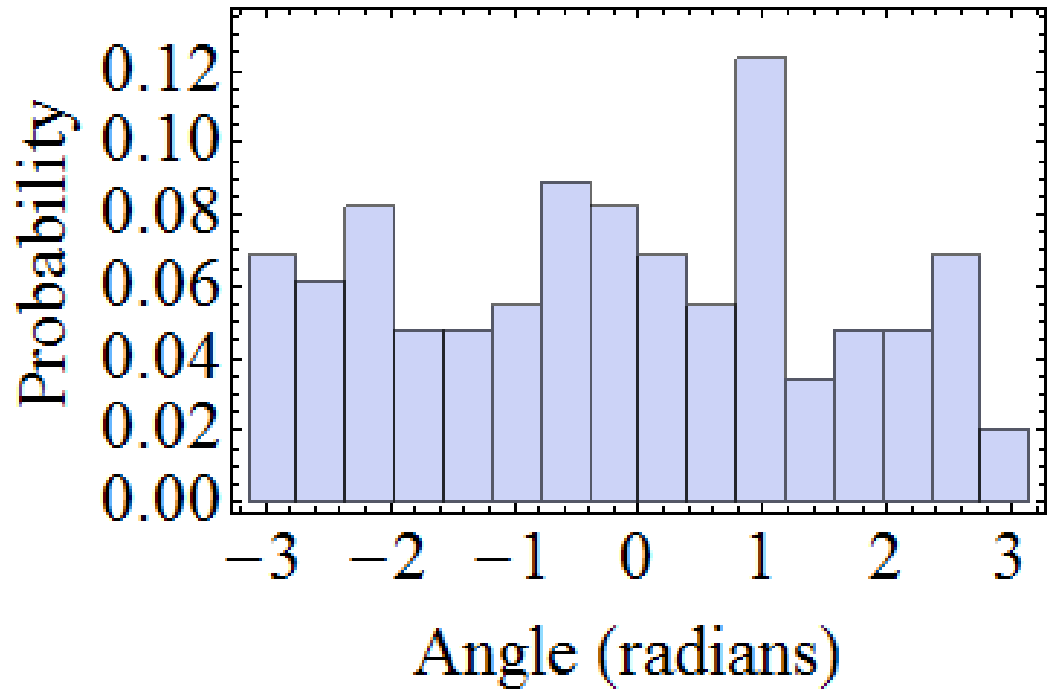

Fig 5.14 Angular distribution for surface A, with 18 hours of growth. The ratchet is oriented to the right (0 radians)

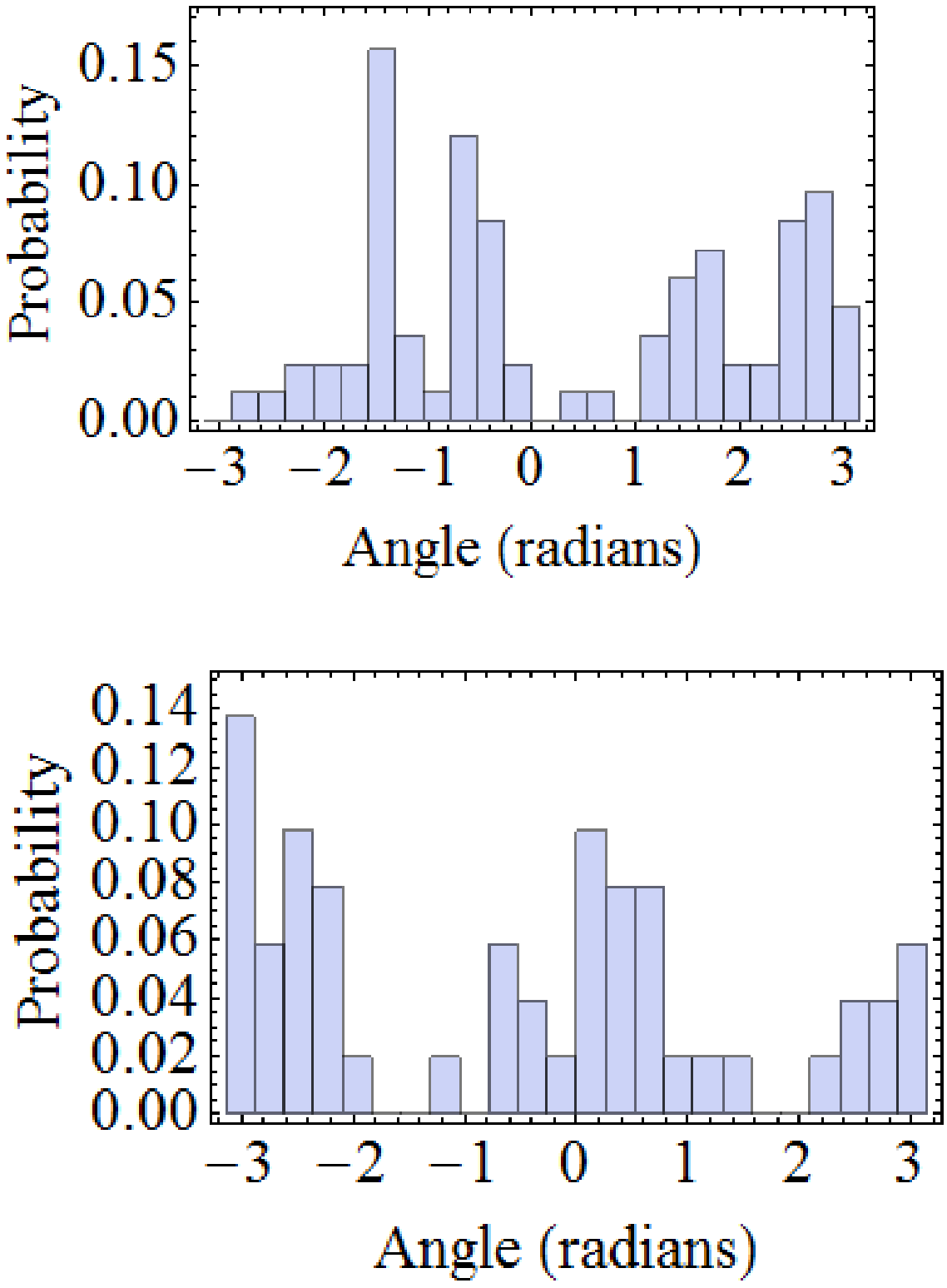

Fig 5.15 Angular distribution for surface B, 18 and 70 hours after plating. The ratchet is oriented to the right (0 radians).

The neurons respond differently to the ratchet structure at 18 hours compared to 70 hours after plating. At 70 hours, growth is consistent with the results from tracing one frame, as outlined in the previous section, where there is strong anisotropy, with the preferred directions at 0 and π . However, at 18 hours the axons do not preferentially extend in the 0 and π directions, corresponding to growth over the ratchet, but rather there is some bias in the growth along the ridges. As before, this situation can be modeled as a Fokker-Planck equation with a deterministic torque:

$$\frac{\partial p(\theta,t)}{\partial t} = [\gamma \sin(\theta)\ p(\theta,t)] + D_\theta \frac{\partial^2 p(\theta,t)}{\partial t^2} \tag{5.9}$$

Here, the effect of the directional surface is quantified by a parameter γ. Because growth in the 0 and π directions exhibit different degrees of asymmetry, the Fokker-Planck equation is split into two regimes: one around 0 and one around π. For each area, there is a corresponding parameter γ, which determines the strength of the torque, and therefore the effect of the directional surface. After a long enough time, the distribution of neurons will favor growth in the π and 0 radian directions. However, as discussed in the previous chapter, based on an initial condition, growth at non-stationary times has not yet reached the stationary distribution, and so the observed directional bias is not as strong.

Directional surfaces with topographical features of a size on the order of the size of a growth cone impart a clear bias in neuronal growth. One such feature, a ratchet structure can be described by a ratchet angle ratio, the ratio between the pair of angles which form the ratchet. This angle is correlated to the degree of bias in the growth in the direction of the ratchet. Also, when seeding density is increased, the resulting increase in signaling molecules dampens the effect of the directional surface. Furthermore, when measuring growth of directional neurons, the time since plating is an important parameter in the response of the growth cone to the substrate. Directional surfaces, made of both PDMS and nano-PPX, give a way to direct neuronal growth.

6. Conclusions and Future Directions:

Neuronal growth responds to a wide variety of guidance cues in the process of forming synapses with other neurons. The use of phenomenological models based on the Langevin equation and the Fokker-Planck equation capture the effects of the variety of parameters, and

allow for testing of experimental conditions. In particular, the Fokker-Planck formalism has been used to describe the effects of cell density and directional surfaces. On glass, the speed follows a V shaped potential indicating that the process is not simple diffusion through velocity space. In combination with the sine wave potential for the angular distribution, the time evolution of neuronal growth is completely described.

Neurons were also grown on surfaces other than glass. Both nano-PPX and PDMS surfaces with a ratchet topography impart a directional bias on the growth. The growing axons are biased to grow over the ratchets, regardless of the underlying rods, with a linear relation between growth anisotropy and the degree of ratchet asymmetry. Such a situation is described by a Fokker-Planck equation with a deterministic torque from the surface, and a stochastic torque from other guidance factors not dependent on the surface.

To further quantify the effect of directional surfaces, traction forces between the growth cone and the surface will be further investigated using beads in the surface to measure the forces exerted by the growth cone. The spacing of the beads is of roughly the same size as a filopodia. Therefore, the forces exerted by the growth cone can be linked to the torque parameter, γ, in the Fokker-Planck equation. The forces exerted can then be linked to cytoskeletal changes or other dynamics within the growth cone to further the understanding of how the growth cone interacts with substrates. Also, there is some evidence to suggest that the time after plating effects how the growth cone responds to directional surfaces, an effect not observed on glass, and will be further investigated. Previous observations indicate differences in behavior during initiation of growth compared to growth at later times.

Furthermore, directional surfaces can be extended to more complicated surfaces or 3-D scaffolds. For example, there is evidence that neurons grow well on silk substrates, which allows for flexibility in the condition of the substrate. Creating 3-D scaffolds for neuronal growth in one such application of the silk substrate, and combining them with directional surfaces may more closely mimic the brain during development. Silk is also biocompatible, so directional surfaces made from silk can be implanted in the body to guide nerve repair in the peripheral nervous system.

Appendix 1:

Mathematica code to import neruonJ tracings, and to calculate the stationary potential on glass for the change in angle of growth.

```
(* Finds the joint probability distribution between the change in angle
 and speed  by importing the files *)
(*Load the 3 functions at the top first *)
movieImport[folderName_] :=
 Module[{ file, points, neurites, numFrames, i, j, k, temp },

  (*This the the folder where set of folders containing the tracings is stored *)
  file = "FILENAME";

  (* How many frames are in each time lapse videos
   CHANGE this as necessary*)
  numFrames = 4;
  points = {};
  temp = {};
  (* Import the points *)
  (* Need one csv file per frame per neuron *)
  (* Each folder should be labeled as "foldername"Frame1,
  "foldername"Frame2 etc."
Folder Name is a variable set in the main function *)

  (* Imports the set of points for each neuron *)
  For[i = 1, i ≤ numFrames, i++,
   temp = frameImport[file <> folderName <> "Frame" <> ToString[i] <> "\\"];
   AppendTo[points, temp];
  ];


  ends = {};
  beginnings = Map[First, points[[1]], 1];
  points = Flatten[points, 1];
```

```
ends = Map[Last, points[[1]], 1];
braces = Function[ x , {x}];
(* These nested loops link the tracings from each frame *)
neurites = Map[braces, points[[1]]];
For[i = 2, i ≤ numFrames, i++,
 (* Find neurons in other frames and add to list *)
 For[j = 1 , j ≤ Length[points[[i]]], j++,
   For [k = 1, k ≤ Length[neurites], k++,
     If[ Norm[points[[i]][[j]][[1]] - neurites[[k]][[-1]][[1]] ] ≤ 8,
      AppendTo[neurites[[k]], points[[i]][[j]];
     ]

    ];
  ];
];

(* If a neurite does not appear in all the frames, remove it from the list *)
For[i = Length[neurites], i ≥ 1, i--,
 If[Length[neurites[[i]] ] < numFrames , neurites = Delete[neurites, i]];
];

(* Set a neurites in all frames to start at (0,0)   NOT necessary at this time
 Uncomment if necessary, for example to reduce drift*)
(*For[ i =1, i≤ Length[neurites], i++,
  For[j=1, j≤ Length[neurites[[i]] ] , j++,
    For[ k=Length[neurites[[i,j]]] , k ≥  1, k--,
      neurites[[i,j,k]] -= neurites[[i,j,1]];
     ];
   ];
 ];
*)

 Return[neurites];

]
```

```
frameImport[loc_] := Module[{i, files, data},
  location = loc;
  SetDirectory[location];
  files = FileNames[];

  data = {}; (* List of lists of points each neuron at a given time *)
  For[i = 1, i ≤ Length[files], i++,
   (*The files containg the tracing have 2 "." in the filename,
   so import those file *)
   If[StringCount[files[[i]], "."] == 2,
     AppendTo[data, Import[files[[i]], "csv"]];
    ];
  ];
  Return[{data}]

 ]
```

```
(* Find the velocity and angle for each video
 Angle is defined as the change in angle of growth,
NOT with respect to the orientation on the surface*)
calculate[ neurite_ ] :=
 Module[ {i, j, k, step , pairs , neurites, velocities, growth, angleDiff} ,
  neurites = neurite;
  step = 8; (* Step used to calculate angle *)
  pairs = {};
  (* Find the change in position *)
  velocities = Map[ Function[  Differences[ Last /@ # ]   ], neurites, 1];

  For [ i = 1, i ≤ Length[neurites], i++,
   For [j = 2,  j ≤ Length[ neurites[[i]]], j++,

     growth = Floor[ Norm[ velocities[[i, j - 1]] , 1]];
     If[ (velocities[[i, j - 1]] == {0, 0}) , angleDiff = 0 ,
      angleDiff =  (ArcTan[velocities[[i, j - 1, 1]], velocities[[i, j - 1, 2]] ]) -
         (ArcTan[

           (* Pick the appropraite points to use to calculate angle *)
          neurites[[i , j , -1 , 1]] - neurites[[i , j ,
            Max[-step, -Length[neurites[[i, j]]]] , 1]] ,
          neurites[[i , j , -1, 2]] - neurites[[i , j ,
            Max[-step, -Length[neurites[[i, j]]]] , 2]]
         ] );];
     (* The factors convert pixes to μm, and the time unit to hours *)
     AppendTo[pairs, {.64 * 12 Norm[ velocities[[i, j - 1, 1]]] ,
       Mod[angleDiff, 2 Pi, -Pi]}];
    ];
  ];
  Return[pairs];
 ]
```

```
Needs["ErrorBarPlots`"]
neurites = {};
(* The names of the folders which contain the tracing.  For each there
 should be 4 folders,with Frame1, Frame2 etc. appended to the name *)
files = { "7hr35min" , "8hrs", "8hrs30min", "14 5 hrs" , "15hr15min",
   "15hr30min", "18hrs", "19hrs", "26hrs", "26hrs25min", "26hrs50min",
   "32 5 hrs",  "32hrs45min", "33hr05min", "33hr25min", "45 30 hr min ",
   "45hr50min" };
For[ i = 1, i ≤ Length[files] , i++,
  AppendTo[ neurites, movieImport[files[[i]]]];
 ];

pair = {};
For [ i = 1, i ≤ Length[neurites], i++,
  AppendTo[pair, calculate[neurites[[i]]]];
 ];

data = Flatten[pair, 1];
```

```
(* Used to generate best fit for sine wave*)
(* The best fit for the sine wave is used in the calculation of the time-
 dependent growth. *)
histTable = Union[N[ Range[-Pi, Pi, Pi / 10] ], N[ Range[-Pi, -3 Pi / 4, Pi / 20]],
   N[Range[3 Pi / 4, Pi, Pi / 20]], N[Range[ -Pi / 4, Pi / 4, Pi / 20]]];
(* For complicated binning *)
hlist = HistogramList[Last /@ data, {-Pi, Pi, Pi / 10}, "PDF"];
hlistCount = HistogramList[Last /@ data, {-Pi, Pi, Pi / 10}];
n = Length[data];
errorList  = ErrorBar [
     center =  # / n / (Pi / 10 );
     range = 1.96 Sqrt[1 / n # / n (1 - # / n) + 1 / (4 n^2) ×1.96^2];
     posEnd = -Log[center + range] + Log[center];
     negEnd = -Log[ center - range] + Log[center];
     {posEnd, negEnd}

    ] & /@ hlistCount[[2]];
(* Find the potentials from the histogram *)
potList = Transpose[{ Most[hlist[[1]]], -Log[hlist[[2]]] }];
Clear[k, a];
nlm = NonlinearModelFit[potList,
  a + (*b Sin[ x] + c Cos[ x]*)(* + d Sin[ 2x]  *)+ e Cos[ 2 x ] , {a, e },
  x, MaxIterations → 100 000]
Show[
 Plot[ Normal[ nlm], {x, 0 - Pi, Pi}, Axes → None, Frame → True,
  FrameLabel → {"Angle", "Potential"} , FrameStyle → Large,
  PlotLabel → "Potential from Histogram and Fourier Expansion Best Fit " <>
    "  \n " <> ToString[NumberForm[Normal[nlm], 3]],
  PlotRange → {{-Pi, Pi}, {0, 5}}] ,
 ListPlot[Transpose[{ Most[hlist[[1]]], -Log[hlist[[2]]] }] ] ]

(* Plot the histogram with the probability distribution found from the
 potential *)
Show[ Histogram[ Mod[(Last /@ data) , 2 Pi, -Pi], {-Pi, Pi, Pi / 10}, "PDF",
  Axes → None, Frame → True, FrameLabel → {"Angle", "Probability"} ,
  FrameStyle → Large, PlotRange → {{-Pi, Pi}, {0, .85}}],
 Plot[ Exp[- Normal[nlm]], {x, -Pi, Pi} ]]
```

```
(* This section looks at correlation between angle and speed.  It makes
 several graphs of speed vs. angle,
and a table of independence tests using several different tests *)
N[Correlation[Transpose[data][[1]], Transpose[data][[2]]]]
(* Do statistical text for all applicable tests *)
IndependenceTest[Transpose[data][[1]], Transpose[data][[2]], {"TestDataTable", All}]
(* Plot all data as pairs *)
ListPlot[data, AxesLabel → {"Speed μm/hr", "Angle"}]
(* Plot all data with abs of angle *)
ListPlot[ Abs[Last[#]] & /@ data,
 AxesLabel → {"Speed μm/hr", "Abs value of Angle"}]
```

```
(* Look at sections of ranges of velocities
 and plots a histogram for each one *)
sliced = {};
AppendTo[sliced, Select[data, (#[[1]] < 25 ) &]];
AppendTo[sliced, Select[data, ( #[[1]] < 50 && #[[1]] ≥ 25 ) &]];
AppendTo[sliced, Select[data, (#[[1]] < 75 && #[[1]] ≥ 50)  &]];
AppendTo[sliced, Select[data, (#[[1]] ≥ 75 &)]];
Histogram[ Transpose[#][[2]], {-Pi, Pi, Pi / 8}, "PDF",  Frame → True,
   FrameLabel → {"Angle", "Probability" }, Axes → None, FrameStyle → Medium]  & /@
 sliced

(* Look at velocities for slices of angles.
  and plots the histograms. *)
sliced = {};
AppendTo[sliced, Select[data, (#[[2]] < -Pi / 2 ) &]];
AppendTo[sliced, Select[data, ( #[[2]] < -Pi / 4 && #[[2]] ≥ -Pi / 2) &]];
AppendTo[sliced, Select[data, ( #[[2]] < 0 && #[[2]] ≥ -Pi / 4) &]];
AppendTo[sliced, Select[data, ( #[[2]] < Pi / 4 && #[[2]] ≥ 0 ) &]];
AppendTo[sliced, Select[data, (#[[2]] < Pi / 2 && #[[2]] ≥ Pi / 4)  &]];
AppendTo[sliced, Select[data, (#[[2]] ≥ Pi / 2 &)]];
Histogram[ Transpose[#][[1]], {0, 200, 20}, "PDF",
   PlotRange → {{0, 200}, {0, .04}}]  & /@ sliced
```

```
(* Finding the fit of the 1-D velocity using the 2D data computed above *)
(* Velocities are the projection of the change in position onto the
 direction of the neurite at its end.  I.e. project r onto s *)
velocities  =  Sign[Cos[#[[2]] ] # [[1]] & /@ data;
DistributionFitTest[ velocities,
 LaplaceDistribution[ mu , b] /.
  FindDistributionParameters[velocities, LaplaceDistribution[mu, b]]]

Show[Histogram[velocities, {-220, 220, 15}, "PDF",
  FrameLabel → {"Velocity μm/hr" , "P(v)"}, FrameStyle → Large, Frame → True,
  Axes → None],
 Plot[
  PDF[ LaplaceDistribution[ mu , b] /.
    FindDistributionParameters[velocities, LaplaceDistribution[mu, b]] , x ] ,
  {x, -220 , 220} ] ]
FindDistributionParameters[velocities, LaplaceDistribution[mu, b]]

(* Velocities are the norm of r, thus always positive values  *)
velocities  = Norm[ #[[1]] & /@ data;
DistributionFitTest[ velocities,
 ExponentialDistribution[ mu] /.
  FindDistributionParameters[velocities, ExponentialDistribution[ mu]]]

Show[Histogram[velocities, {0, 200, 10}, "PDF",
  FrameLabel → {"Speed μm/hr" , "P(v)"}, FrameStyle → Large, Frame → True,
  Axes → None],
 Plot[
  PDF[ ExponentialDistribution[ mu] /.
    FindDistributionParameters[velocities, ExponentialDistribution[ mu]] , x ] ,
  {x, 0, 200} ] ]

(* A 3-D histogram of the data *)
Histogram3D[data, {45, 10}, AxesLabel → {"Speed μm/hr", "Angle", "Count"},
 AxesStyle → Medium, PlotRange → {{0, 180}, {-Pi, Pi}, All}]

(* Find potentials for speed and fit to a linear model *)
Clear[a, b]
vels = First /@ data;
Histogram[vels, {0, 140, 14}, "Probability",  Axes → None, Frame → True,
 FrameLabel → {"Velocity", "Probability"} , FrameStyle → Large ]
hlist  = HistogramList[vels, {0, 140, 14}, "PDF"];
potlist = Transpose[{ Most[hlist[[1]]], -Log[hlist[[2]] ] }];
```

```
lm = LinearModelFit[potlist, x, x];
lm["RSquared"]
Show[ Plot[ Normal[ lm], {x, 0 , 140}, Axes → None, Frame → True,
  FrameLabel → {"Velocity", "Velocity Potential"} , FrameStyle → Large,
  PlotLabel → "Potential from Histogram and Linear Best Fit"] ,
 ListPlot[Transpose[{ Most[hlist[[1]]], -Log[hlist[[2]]] }] ]]
```

```
(* Plot 2 periods of the angular histogram to better see how data fits
 around both peaks*)
Show[Histogram[ Mod[(Last /@ data) , 2 Pi], {-2 Pi, 2 Pi, Pi / 10},
  "Probability", Axes → None, Frame → True, FrameLabel → {"Angle", "Probability"} ,
  FrameStyle → Large, PlotLabel → "2 Periods of Angular histogram" ],
 Histogram[ Mod[(Last /@ data) , 2 Pi, -2 Pi], {-2 Pi, 2 Pi, Pi / 10}, "Probability"] ]
```

```
(* Likeihood calculations *)
angles = Last /@ data;
sinWaveEst = Exp[ -Sum[ nlm[ angles[[i]] ] , {i , 1, Length[angles]}] ]
```

```
(* Plot one period of the angular distribution *)
Histogram[Last /@ data , {-Pi, Pi, Pi / 15}, "Probability", Axes → False,
 Frame → True, FrameStyle → Large, FrameLabel → {"Angle (radians) ", "Probability" }]
```

Appendix 2:

Mathematica code to find the time evolution of the angular probability distribution, as outlined in (4.24)-(4.37).

```
(*Create the matrix for the system of linear equations*)
k = 1.27404; (*From the stationary potential fit *)
mat = Table[ Piecewise[ {{-i/2, i = j-1}, {i^2/k, i = j }, {i/2, i = j+1}}],
   {i, -300, 300}, {j, -300, 300}] ;
eigvals = Reverse[Eigensystem[mat][[1]]][[1 ;; 60 ;; 2]];
consts = Reverse[ Eigensystem[mat][[2]]];
(*Tke the first 50 constants that form the basis for the eigenfunction.
  This improves computation time *)
consts = #[[ 275 ;; 325]] & /@ consts;



(* μ represents the eigenfunction for the μth non-zero eigenvalue *)
(* θ and ρ correspond to the functions defined in equations 4.32, 4.33*)

θs[ϕ_, μ_] :=
 Sum[ consts[[μ +1]][[n+1]] * Re[Exp[ (n - Floor[ .5 Length[consts[[μ+1]]] ) ϕ I]] ,
   {n , 0, Length[consts[[μ +1]] - 1}] /
  Sqrt[
   Integrate[
    Sum[consts[[μ +1]][[n+1]] *
        Re[Exp[    (n - Floor[ .5 Length[consts[[μ+1]]])      ϕϕ I] ],
       {n , 0, Length[consts[[μ +1]] - 1}]^2 Exp[ - k Cos[ϕϕ] ] , {ϕϕ , -Pi, Pi}]]


θa[ϕ_, μ_] := Module[ {func},
   func =
    Sum[ consts[[μ +1]][[n+1]] * Im[Exp[ ( n - Floor[ .5 Length[consts[[μ+1]]] ) ϕ I]] ,
      {n , 0, Length[consts[[μ +1]] - 1}] /
     Sqrt[
      Integrate[
       Sum[ consts[[μ +1]][[n+1]] *
           Im[Exp[  (n - Floor[ .5 Length[consts[[μ+1]]] )     ϕϕ I] ],
          { n , 0, Length[consts[[μ +1]] - 1}]^2 Exp[ - 1.27 Cos[ϕϕ] ] ,
       {ϕϕ , -Pi, Pi}]]
  ];
```

```
ρs[ϕ_, μ_] :=
 Exp[ - k /2 Cos[ϕ]]
  Sum[ consts[[μ +1]][[n+1]] * Re[Exp[ (n - Floor[ .5 Length[consts[[μ+1]]] ) ϕ I]] ,
    {n , 0, Length[consts[[μ +1]]] - 1}] /
   Sqrt[
    NIntegrate[
     Sum[consts[[μ +1]][[n+1]] *
         Re[Exp[     (n - Floor[ .5 Length[consts[[μ+1]]])      ϕϕ I] ],
        {n , 0, Length[consts[[μ +1]]] - 1}]^2 Exp[ - k Cos[ϕϕ] ] , {ϕϕ , -Pi, Pi}]]
```

```
(*Add the stationry probability to the eigenfunctions defined above,
with the initial condition of a Dirac delta function *)
p[ϕ_, t_] := Exp[-(2.3704334683485966 - 1.274043585076636 Cos[ ϕ]) ] +
  Sum[  Exp[ -( eigvals[[nn+1]] t) /k] Exp[ k /2 Cos[ϕ] ] Exp[ k /2]
    ( ρs[ 0, nn] *ρs[ ϕ , nn] )  , {nn , 1, 15(*Length[eigvals] -1*)}]
```

```
(*Plot the time evolution of the angular distribution at 3 different times *)

margProb[time_] := NIntegrate[Re[p[aaaa, time]], {aaaa, -Pi, Pi}, MaxRecursion → 13];
Plot[{ p[2 a, 1/4] / margProb[1/4], p[2 a, 2] / margProb[2] , p[2 a, 15] / margProb[15]},
 {a, -Pi, Pi},   Axes → False, Frame → True,
 FrameLabel → {{"Probability" }, {"Angle"}}, FrameStyle → Large,
 PlotLabel → "Probability Distribution Evolution" , LabelStyle → Large]
```


```
(*Plot the time evolution of the angular distribution at 3 different times *)

margProb[time_] := NIntegrate[Re[p[aaaa, time]], {aaaa, -Pi, Pi}, MaxRecursion → 13];
Plot[{ p[2 a, 1/4] / margProb[1/4], p[2 a, 2] / margProb[2] , p[2 a, 15] / margProb[15]},
 {a, -Pi, Pi},   Axes → False, Frame → True,
 FrameLabel → {{"Probability" }, {"Angle"}}, FrameStyle → Large,
 PlotLabel → "Probability Distribution Evolution" , LabelStyle → Large]
```


```
(*Show the eigenfunctions *)
For[ kk = 0 , kk < 6, kk++,
 Print[Plot[ρs[ x, kk], {x , -Pi, Pi}, Axes → False, Frame → True,
    PlotLabel → "Symmetric Eigenfunction #" <> ToString[kk]]];
]
```

Appendix 3:

Revised "calculate" function from Appendix A.1 to change the definition of angle to be the angle from the x-axis (ratchet direction).

```
(* Find the velocity and angle for each video *)
calculate[ neurite_ ] :=
 Module[ {i, j, k, step , pairs , neurites, velocities, growth, angleDiff, angle} ,
  neurites = neurite;
  step = 8; (* Step used to calculate angle *)
  pairs = {};
  velocities = Map[ Function[  Differences[ Last /@ # ]   ], neurites, 1];

  For [ i = 1, i ≤ Length[neurites], i ++,
   For [j = 2,  j ≤ Length[ neurites[[i]]], j ++,
     growth = Floor[ Norm[ velocities[[i, j - 1]] , 1]];

     (* Angle is the angle of growth relative to the x-axis *)
     If[ (velocities[[i, j - 1]] = {0, 0}) , angle = 0 ,
      angle = ArcTan[velocities[[i, j - 1, 1]], velocities[[i, j - 1, 2]] ];];
     AppendTo[pairs, {.64 * 12 Norm[ velocities[[i, j - 1, 1]]] ,
       Mod[angle, 2 Pi, -Pi]}];
    ];

  ];

  Return[pairs];
 ]
```

References

[1] K. Franze and J. Guck, "The biophysics of neuronal growth," *Reports on Progress in Physics,* vol. 73, pp. 094601, 2010.

[2] L. A. Lowery and D. V. Vactor, "The trip of the tip: understanding the growth cone machinery," *Nat. Rev. Mol. Cell Biol.,* vol. 10, pp. 332-343, print, 2009.

[3] S. Maskery and T. Shinbrot, "Deterministic and stochastic elements of axonal guidance," *Annu. Rev. Biomed. Eng.,* vol. 7, pp. 187-221, 2005.

[4] T. Mitchison and M. Kirschner, "Cytoskeletal dynamics and nerve growth," *Neuron,* vol. 1, pp. 761-772, 1988.

[5] P. C. Letourneau, "Differences in the organization of actin in the growth cones compared with the neurites of cultured neurons from chick embryos." *J. Cell Biol.,* vol. 97, pp. 963-973, 1983.

[6] E. A. Codling, M. J. Plank and S. Benhamou, "Random walk models in biology," *Journal of the Royal Society Interface,* vol. 5, pp. 813-834, 2008.

[7] M. Schienbein and H. Gruler, "Langevin equation, Fokker-Planck equation and cell migration," *Bull. Math. Biol.,* vol. 55, pp. 585-608, 1993.

[8] H. Risken, *Fokker-Planck Equation.* Springer, 1984.

[9] R. Beighley, E. Spedden, K. Sekeroglu, T. Atherton, M. C. Demirel and C. Staii, "Neuronal alignment on asymmetric textured surfaces," *Appl. Phys. Lett.,* vol. 101, pp. 143701, 2012.

[10] M. J. Katz, E. B. George and L. J. Gilbert, "Axonal elongation as a stochastic walk," *Cell Motil.,* vol. 4, pp. 351-370, 1984.

[11] D. J. Odde, E. M. Tanaka, S. S. Hawkins and H. M. Buettner, "Stochastic dynamics of the nerve growth cone and its microtubules during neurite outgrowth," *Biotechnol. Bioeng.,* vol. 50, pp. 452-461, 1996.

[12] H. Meinhardt, "Orientation of chemotactic cells and growth cones: models and mechanisms," *J. Cell. Sci.,* vol. 112, pp. 2867-2874, 1999.

[13] E. Kandel, J. Schwartz, T. Jessell, S. Siegelbaum and A. J. Hudspeth, *Principles of Neural Science, Fifth Edition.* McGraw-Hill Education, 2013.

[14] I. B. Levitan and L. K. Kaczmarek, *The Neuron :Cell and Molecular Biology.* New York: Oxford University Press, 1991.

[15] E. R. Kandel, J. H. Schwartz and T. M. Jessell, *Principles of Neural Science.* Norwalk, Conn.: Appleton & Lange, 1991.

[16] I. B. Levitan and L. K. Kaczmarek, *The Neuron: Cell and Molecular Biology.* Oxford University Press, 2002.

[17] P. Dayan, L. F. Abbott and L. Abbott, "Theoretical neuroscience: Computational and mathematical modeling of neural systems," 2001.

[18] M. J. Katz, E. B. George and L. J. Gilbert, "Axonal elongation as a stochastic walk," *Cell Motil.,* vol. 4, pp. 351-370, 1984.

[19] D. Mortimer, T. Fothergill, Z. Pujic, L. J. Richards and G. J. Goodhill, "Growth cone chemotaxis," *Trends Neurosci.,* vol. 31, pp. 90-98, 2008.

[20] H. D. Simpson, D. Mortimer and G. J. Goodhill, "Theoretical models of neural circuit development," *Curr. Top. Dev. Biol.,* vol. 87, pp. 1-51, 2009.

[21] D. Mortimer, T. Fothergill, Z. Pujic, L. J. Richards and G. J. Goodhill, "Growth cone chemotaxis," *Trends Neurosci.,* vol. 31, pp. 90-98, 2008.

[22] H. Meinhardt, "Orientation of chemotactic cells and growth cones: models and mechanisms," *J. Cell. Sci.,* vol. 112, pp. 2867-2874, 1999.

[23] A. Siegman, "Simplified derivation of the Fokker-Planck equation," *American Journal of Physics,* vol. 47, pp. 545, 1979.

[24] A. Buonocore, L. Caputo, E. Pirozzi and A. G. Nobile, "A Non-Autonomous Stochastic Predator-Prey Model," *Math. Biosci. Eng.,* vol. 11, pp. 167-188, APR, 2014.

[25] Tat Dat Tran, J. Hofrichter and J. Jost, "An introduction to the mathematical structure of the Wright-Fisher model of population genetics," *Theory Biosci.,* vol. 132, pp. 73-82, JUN, 2013.

[26] R. Rosenbaum, F. Marpeau, J. Ma, A. Barua and K. Josic, "Finite volume and asymptotic methods for stochastic neuron models with correlated inputs," *J. Math. Biol.,* vol. 65, pp. 1-34, JUL, 2012.

[27] S. Rüdiger, "Stochastic models of intracellular calcium signals," *Physics Reports,* vol. 534, pp. 39-87, 1/10, 2014.

[28] T. Betz, D. Lim and J. A. Käs, "Neuronal growth: a bistable stochastic process," *Phys. Rev. Lett.,* vol. 96, pp. 098103, 2006.

[29] Y. E. Pearson, E. Castronovo, T. A. Lindsley and D. A. Drew, "Mathematical Modeling of Axonal Formation Part I: Geometry," *Bull Math Biol,* vol. 73, pp. 2837, 2011.

[30] D. J. Rizzo, J. D. White, E. Spedden, M. R. Wiens, D. L. Kaplan, T. J. Atherton and C. Staii, "Neuronal growth as diffusion in an effective potential," *Physical Review E,* vol. 88, pp. 042707, 2013.

[31] D. J. Rizzo, J. D. White, E. Spedden, M. R. Wiens, D. L. Kaplan, T. J. Atherton and C. Staii, "Neuronal growth as diffusion in an effective potential," *Physical Review E,* vol. 88, pp. 042707, 2013.

[32] S. W. - Moore and M. P. - Sheetz, "- Biophysics of substrate interaction: Influence on neural motility, differentiation, and repair," - *Developmental Neurobiology,* pp. - 1090, .

[33] A. Rajnicek, S. Britland and C. McCaig, "Contact guidance of CNS neurites on grooved quartz: influence of groove dimensions, neuronal age and cell type," *J. Cell. Sci.,* vol. 110 (Pt 23), pp. 2905-2913, Dec, 1997.